DEVELOPMENT OF ELECTROCHEMICAL ZnSe QUANTUM DOTS BIOSENSORS FOR LOW-LEVEL DETECTION OF 17β-ESTRADIOL ESTROGENIC ENDOCRINE DISRUPTING COMPOUND

Abongile Nwabisa Jijana, BSc Honours (*Cum Laude*)

Student number: 2505749

This thesis is submitted in fulfilment of the requirements for the degree of

MAGISTER SCIENTIAE

in the Department of Chemistry, Faculty of Science, University of the Western Cape

Supervisor

Professor Emanuel Iwuoha

November 2010

KEYWORDS

Electrochemical biosensors

Cytochrome P450-3A4 (CYP3A4)

Horseradish peroxidase (HRP)

ZnSe quantum dots

Conducting polymers

Cyclic voltammetry (CV)

Differential-pulse voltammetry (DPV)

17β- estradiol

17α-ethnylestradiol

Estrogenic Endocrine Disrupting Compounds (e-EDC)

Michaelis Menten constant

Hydroxylation

ABSTRACT

The main thesis hub was on development of two electrochemical biosensors for the determination of 17β-estradiol: an estrogenic endocrine disrupting compound. Endocronology have significantly shown that the endocrine disruptors contribute tremendously to health problems encountered by living species today, problems such as breast cancer, reproductive abnormalities, a decline in male population most significant to aquatic vertebrates, reduced fertility and other infinite abnormalities recurring in the reproductive system of mostly male species. The first biosensor developed for the detection of 17β-estradiol endocrine disrupting compound; consisted of an electro-active polymeric 3-mercaptoprorionic acid capped zinc selenide quantum dots cross linked to horseradish peroxidase (HRP) enzyme as a bio-recognition element. The second biosensor developed was comprised of cysteamine self assembled to gold electrode, with 3-mercaptopropionic acid capped zinc selenide quantum dots cross linked to cytochrome P450-3A4 (CYP3A4) enzyme in the presence of 1-ethyl-3-(3-dimethylaminopropyl)carbodiimide hydrochloride and succinimide. The supporting materials used for each of the biosensing systems were immobilized onto a gold disk electrode (AuE) of area: 0.021 cm^2. The supporting materials used for both biosensors showed good electrochemical, optical, physical and chemical properties when studied by various characterisation methods. The size of 3-mercaptopropionic acid capped zinc selenide quantum dots (MPA-ZnSe-QDs), used as support material for the biosensors were about 4.7 nm, these quantum dots also exhibited good photo-absorption properties with an ultraviolet-visible (UV-Vis) photo absorption band occurring at 375 nm associated with low band gap energy of 3.4 eV. The other support material which contained polyaniline (PANI), i.e. PANI:MPA-ZnSe-QDs composite, used to produce one of the biosensor systems was characterized by excellent electrochemistry, enhanced electron transfer kinetics and photo electronic properties exhibiting two absorption bands at 275 nm and 375 nm indicating formation of composite exhibiting properties of both MPA-ZnSe-QDs and PANI. A first biosensor which was fabricated using the support material PANI:MPA-ZnSe-QDs composite and the enzyme HRP, defined as AuE/PANI:MPA-ZnSe-QDs/HRP biosensor for 17β-estradiol exhibited a detection limit

of 2.05 x10^{-8} g L^{-1} and the Michaelis Menten constant K_m^{app} = 0.073 mM. The second biosensor AuE/Cystm/MPA-ZnSe-QDs/CYP3A4 for 17β-estradiol had a detection limit = 2.8 x 10^{-8} g L^{-1} and Michaelis Menten constant K_m^{app} = 0.056 mM. Both detection limits obtained for the biosensors were lower than the recently reported detection limits for 17β-estradiol using similar biosensor platforms in the absence of any enzyme molecule, indicating the use of cytochrome P450-3A4 and horseradish peroxidase enzymes immobilised on the biosensor platforms played a vital role in substrate recognition, accuracy and selectivity.

DECLARATION

I declare that "*Development of electrochemical ZnSe quantum dot- biosensors for low-level detection of 17β-estradiol estrogenic endocrine disrupting compound." is* my own work, that has not been submitted before for any degree or examination in any other university, and that all sources I have used or quoted have been indicated and acknowledged as complete references.

Abongile Nwabisa Jijana 2010

Signed.....

AKNOWLEDGEMENT

I want to first thank the almighty God for being with me all the way to this day, giving me strength and light where everything seemed so dark and continuously be with me unnoticeable. To my parents for your support I know it was not easy for you at times, but thank you for everything you always been my strength and the pillar.

Supervisor: A special thanks to my supervisor, Prof. Emmanuel Iwuoha, for believing in me and guiding me throughout the duration of this project. My thanks also go to the whole the SensorLab researchers. I would also like to acknowledge National Research Foundation (NRF) for awarding me an MSc Innovation Scholarship.

LIST OF PUBLICATIONS

Peter M. Ndangili, **Abongile N. Jijana**, Priscilla G.L Baker and Emmanuel I. Iwuoha, 3-Mercaptopropionic acid capped ZnSe quantum dot-Cytochrome P450-3A4 enzyme biosensor for 17β-estradiol, *Journal of electroanalytical Chemistry*, doi:10.1016/j.jelechem.2010.12.029.

LIST OF ABBREVIATIONS

EDC - Endocrine disrupting compounds

eEDC - Estrogenic endocrine disrupting compounds

CYP3A4 - Cytochrome P450-3A4 enzyme

HRP – Horseradish Peroxidase enzyme

MPA - 3-mercaptopropionic acid

ZnSe-QDs – zinc selenide quantum dots

UV-Vis – Ultraviolet – visible spectrophotometry

AuE - Gold electrode

Cystm – Cysteamine

PANi/PANI – Polyaniline

EE2 – 17α-ethnylestradiol

E2 - 17β-estradiol

PBS – Phosphate buffer solution

SAM - Self assembled monolayer

FT-IR - Fourier Transformation Infrared spectroscopy

CV - Cyclic voltammetry

OSWV - Osteryoung square-wave voltammetry

DPV – Differential-pulse voltammetry

EDS and EDAX – Energy dispersive X-ray spectrometry

SEM – Scanning electron microscopy

TEM - Transmission electron microscopy

SPGE - Screen printed gold electrode

SPCE - Screen printed carbon electrode

EDAC/NHS - 1-ethyl-3-(3-dimethylaminopropyl) carbodiimide hydrochloride / N-hydroxysuccinimide

V_{max} - Maximum rate of formation of products

K_m^{app} - Michaelis Menten constant

D_L - Detection limit

ΔE_p - Change in peak potential

E_{pa} - Anodic peak potential

E_{pc} - Cathodic peak potential

i_{pc} - Cathodic peak current

i_{pa} - anodic peak current

R_{ct} – Charge transfer resistance

LIST OF FIGURES

TABLE OF CONTENT

UNIVERSITY of the
WESTERN CAPE

CHAPTER 1

1.1 INTRODUCTION

Introduction to the research project

Reduced fertility, alteration of male to female ratios, reproductive abnormalities, early puberty, brain and behaviour problems, impairment of the reproductive systems and numerous endocrine related cancerous problems are major health issues the whole world facing has been facing over the past years. These major effects have been reported in many medical, analytical and pharmaceutical publications [1], to be due to the exposure and accumulation of endocrine disrupting compounds in the living organism's body system [2-5]. Most wastewater treatment plants have been designed to filter these estrogenic disruptors up to a certain concentration level [6]. Water had been defined as the ultimate carrier of many pollutants and other hazardous substances which includes exogenous endocrine disruptors, making the effects of estrogenic endocrine disrupting compounds, prominent to aquatic vertebrates. A recent study on biological effect and potency of generally estradiol done on minnows fatheads (aquatic species) has shown that the lowest observable effective concentration (LOEC) of 17β-estradiol to cause vitellognin: a derivative found in egg yolk of a female was about 75 ng L^{-1} for 17β-estradiol and about 25 ng L^{-1} for 17α-estradiol which was shockingly applicable not only to female species but also male minnows [7]. Nano-material especially quantum dots continue to pose interesting physical, electronic and chemical properties because of their small size, size tuneable band gaps and the feasibility to surface modify them with a variety of capping agents for desired property or application [8-9] which makes them enormously popular for a variety of applications such as in: optical devices [10], bio-labelling [11], biosensing [12] and recently these small semiconductors nanomaterials have been used for improvement of properties in existing light emitting diode devices; to improve features such as brightness and fluorescence [13]. Recent assays developed so far comprising of quantum dots have paid attention on the fact these nanomaterials pose good fluorescence properties [14], in fluorescence the biosensor's capability of

quenching the photoluminescence intensity meditated by the quantum dots is monitored as a quantity of analyte gets introduced in the biosensor solution media, resulting into a photon signal. The produced photoluminescence intensity is proportional to the substrate concentration added. Few publications exist whereby other properties such as electronic properties of the quantum dots gets utilised for variety of applications, for example in recent publication by Zhang and co-workers [15], zinc sulphide (ZnS) quantum dots have been successfully used in electrochemical biosensor for uric acid, and on a recent publication by Zhao and co-workers, the authors concentrated on fabrication of an electrochemical biosensor using new type graphene quantum dots [16]. The ability of being able to modify the surface of quantum dots by different types of ligand such as amino, thiol, sulphonic and phosphoric ligand [14] for the purpose of making them biocompatible. This process has allowed growth in applications of these nanomaterials in biological systems and bioassays both in vitro and in vivo [17-19].

In this work, two different enzymes i.e. cytochrome P450-3A4 (CYP3A4) and horseradish peroxidase (HRP) have been used as bio-recognition elements for the development of two electrochemical enzyme based biosensors. The water soluble zinc selenide (ZnSe) quantum dots capped with 3-meraptopropionic acid: a carboxylic acid group derivative, which makes the surface of the quantum dots biocompatible, have been used not only as electron mediator materials for the biosensor but also acted as anchor for bio-molecule attachment for improved stability of the enzyme onto the gold electrode used as a transducer. The 3-mercaptopropionic acid capped (MPA) ZnSe quantum dots were further modified with polyaniline (PANI) conducting polymer resulting in the formation of the composite PANI:MPA-ZnSe-QDs, which was used as second type support material for one of the biosensor systems. Most developed electrochemical HRP enzyme based biosensor, utilising the polymer: PANI had shown not only good electrochemical properties [20] but also good chemical stability. The next paragraph gives summary of how the project objectives were accomplished:

- Chemical synthesis of 3-mercaptopropionic acid capped zinc selenide quantum dots (MPA-ZnSe-QDs).
- Characterisation of the MPA-ZnSe-QDs using ultraviolet-visible spectrometry (UV-Vis), Transmission Electron Microscopy (TEM), Fourier Transform Infrared spectrometry (FT-IR) and Cyclic voltammetry (CV).
- Fabrication and characterization of the composite PANI:MPA-ZnSe-QDs.
- Development of the first biosensor AuE/PANI:MPA-ZnSe-QDs/HRP and its application for quantitative determination of different concentrations of 17β-estradiol.
- Effective studies involving stability, selectivity, linearity and study of interferences.
- The Figure 1-1 gives a summary of approach to development of the first biosensor systems: AuE/PANI:MPA-ZnSe-QDs/HRP.

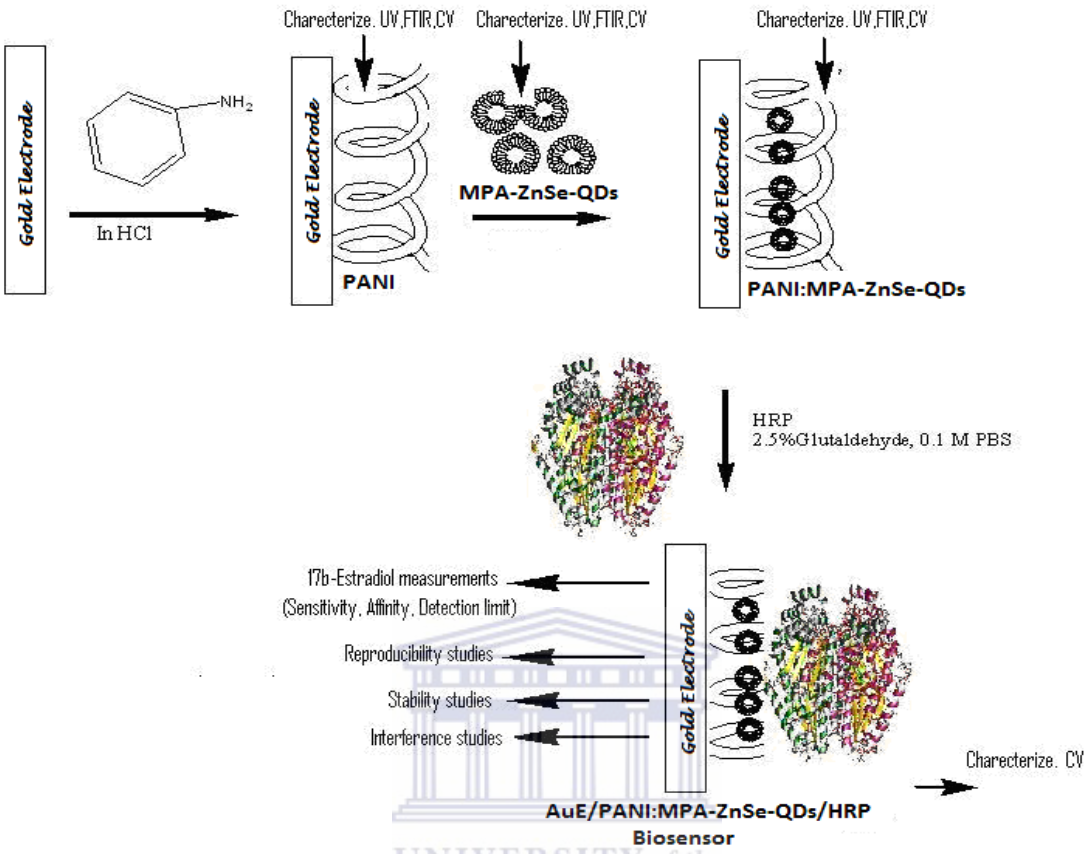

Figure 1-1: Summary to development AuE/PANI:MPA-ZnSe-QDs/HRP biosensor for 17β-estradiol.

Development of the second biosensing system involved the following phases:

- Surface modification of the gold electrode with cysteamine ($SH\text{-}CH_2\text{-}CH_2\text{-}NH_2$), resulting in the formation of a self assembled monolayer (SAM) onto a gold electrode by affinity covalent attachment of the thiol group directly onto the surface of the electrode [21-22].
- Further modification of cysteamine (Cystm) modified gold electrode with 3-mercaptopropionic acid capped ZnSe quantum dots in the presence of a carbdomide and succinimide cross linking agents.
- Incorporation of the enzyme CYP3A4 onto cysteamine and 3-mercaptopropionic acid capped zinc selenide quantum dots modified gold electrode resulting in AuE/Cystm/MPA-ZnSe-QDs/CYP3A4 biosensor.

- Characterisation of the developed biosensor by CV, SEM and FT-IR respectively.

The following scheme gives a summary of the phases and approach to development of AuE/Cystm/MPA-ZnSe-QDs/CYP3A4 second biosensor system.

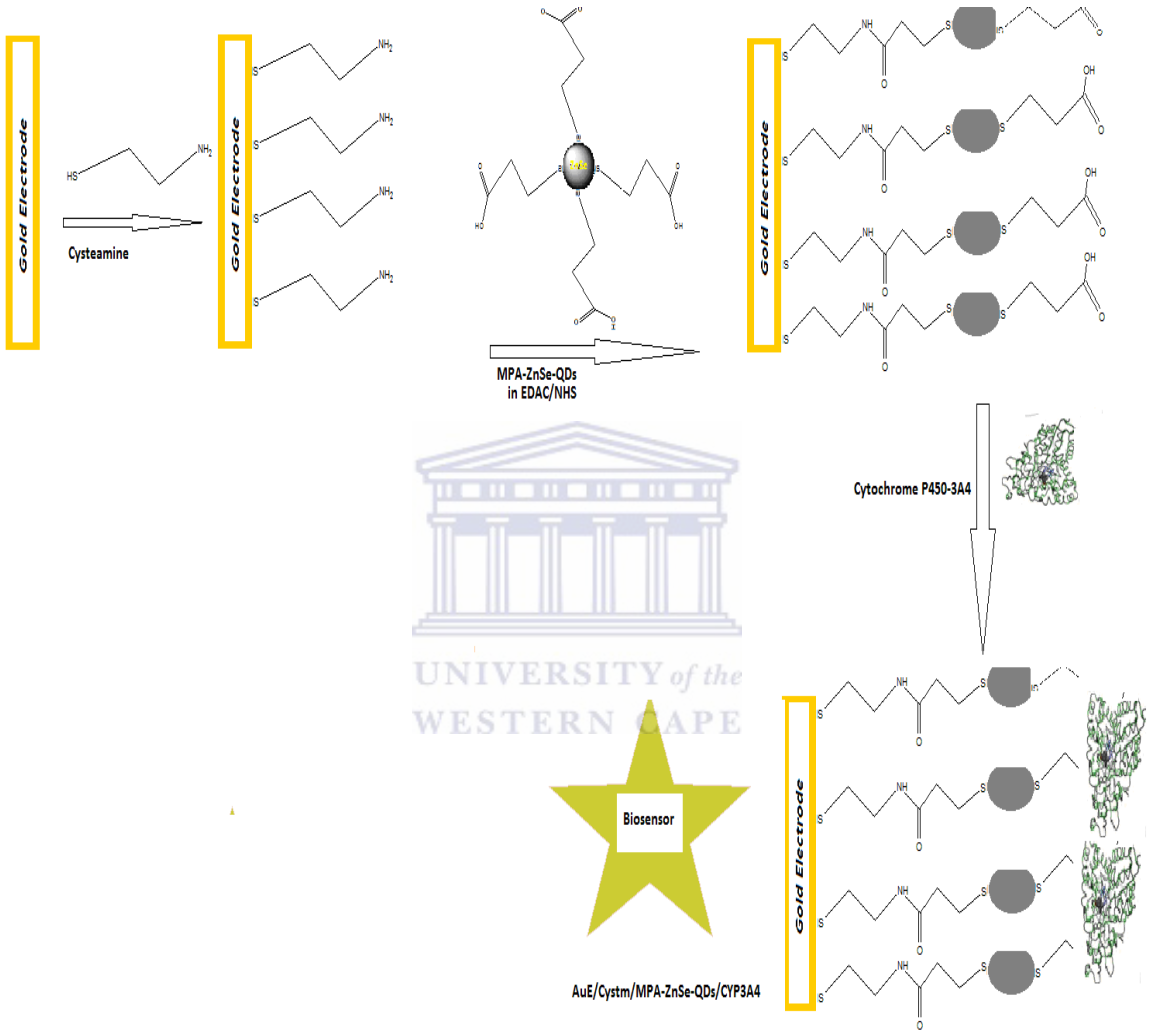

Figure 1-2: Summary to development AuE/Cystm/MPA-ZnSe-QDs/CYP3A4 biosensor for 17β-estradiol.

The developed electrochemical enzyme based biosensors showed good selectivity, accuracy and good chemical stabilities and catalytic activity towards the substrate 17β-estradiol.

LIRATURE REVIEW

CHAPTER 2

2.1 LITERACTURE REVIEW

Chapter Review

The chapter gives a brief survey on the literature covered during the project based on the research topic hypothesis. It covers concepts, biosensor: theory and types, a brief introduction to endocrine disrupting compound; classification and types, an insight on supporting materials used in fabrication of the biosensor, this included materials; conducting polymers, quantum dots: properties, types and applications. The chapter also covers a brief survey on enzymes, enzyme kinetics, enzyme types, enzyme classification and applications.

2.1.1 The endocrine system

The endocrine system consists of series of glands that secrete hormones together with the associated receptors that responds to these hormones. Hormones function as chemical messengers that travel through the body's bloodstream and fluids. Although these hormones travel throughout the body, they only respond to a certain stimuli associated with a specific receptor at which it binds to [1, 5]. The major function of the endocrine system is regulation of all biological processes that occur in body system throughout every organism's life cycle. Female ovaries, male testes, pituitary gland and adrenal glands are major components of the endocrine system. Estrogens are a series of female hormones secreted primarily in the ovaries and small amount are produced in the adrenal glands. Testosterone and other androgens are male hormones produced in the testes of male organisms [23].

2.1.2 Endocrine disrupting compounds

The endocrine disrupting compounds are known to be chemical or exogenous compounds that disrupt or interfere with synthesis, secretion, binding, action of natural hormones in the endocrine system, which is responsible for homeostasis, growth and development of most organisms, a definition which was given by United State Environmental Protecting

agency in 1997 [24].The disruption of the endocrine system occurs in two major ways, chemical species may mimic or fake the natural hormone, thus deceiving the body into over and under stimulation or responses including the under and over production of some natural hormone thus resulting in disruption [5]. Potential endocrine disrupting compounds may include; hormones (natural or synthetic), plant constituents, pesticides, heavy metals and commercial plasticizers [25]. These endocrine disruptors are considered to be disruptors not only by their chemical nature but rather, they are defined by their biological effect [3]. Environment and health effects that these endocrine disruptors cause vary according to type, nature and source of the disruptor, with common effects being reduced fertility, male and female reproductive abnormalities, reduced sperm counts, reduced male to female ratio, menstrual problems, cancer (e.g. breast cancer) and other changes in the hormone levels produced in body [1, 26-27]. The endocrine disrupting compounds pose major health risks to the ecosystem and are a major contribution to population imbalances such as a decline in male organisms most significantly observed in aquatic vertebrates.

2.1.2.1 Estrogenic endocrine disrupting compounds

These classes of endocrine disruptors are divided into two categories; natural female hormones (i.e. natural estrogens) and synthetic estrogens. 17α-ethnylestradiol (EE2) is a major ingredient to most commercial available contraceptives used today [25, 28-29]. The mechanism for its metabolism and how it functions in the body system of a diagnosed patient might be that it suppresses or kills the natural hormones produced during a woman's life cycle or during pregnancy, resulting in the limited amount of hormones produced or secreted in the body, thus at a later stage eliminate pregnancy. Figure 2-1 shows the structures of four well known examples of estrogenic endocrine disruptors; estriol, estrone and 17β-estradiol and 17α-ethnylestradiol:

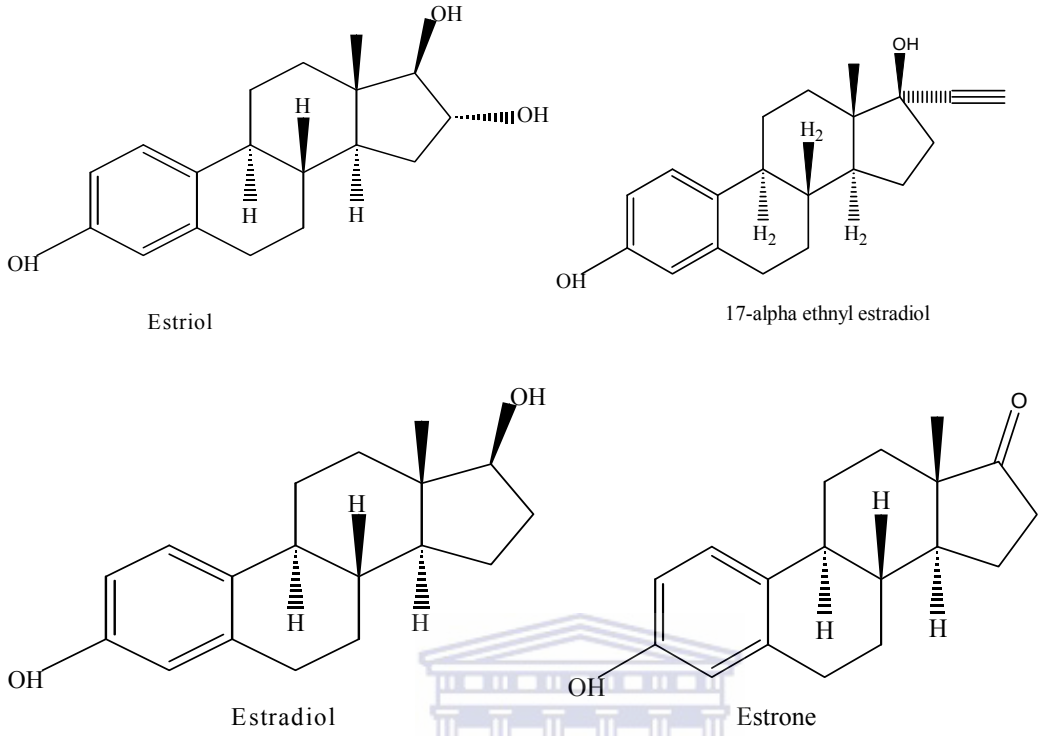

Figure 2-1: Shows four main examples of estrogenic endocrine disruptors (e-EDC), 17β-estradiol, estriol, estrone and synthetic estrogen 17α-ethynylestradiol.

Although these estrogens are required in the reproductive life cycles of female species, if high concentration persists in the body, they pose negative effects like, breast cancers, ovarian cancers, and excessive exposure to male organism can be identified by effects like, change in sexual behaviour, impaired reproductive system and low sperm counts [1, 27, 30]. Studies have indicated that the most vulnerable species to estrogenic endocrine disruptors are aquatic vertebrates such fish, turtles and frogs. The estrogens are released into the environment through wastewater treatment plants as discharges from domestic sewage systems and surface non point sources: rivers, dams etc [4, 31-32]. The elimination of the estrogenic endocrine disruptors, then depend on plant treatment and recovery cleaning methods [2-4, 33] and necessarily might be the population around the area which contribute to wastewater. It is thus of outmost importance to monitor the levels of these compounds in municipal wastewater treatment plants [3-4], so as to know exactly their fate, transport and origin, so as find plant treatment methods capable of

filtering or removing these estrogenic endocrine disruptors, as they pose major effect to the surrounding environment and to aquatic life.

2.1.2.2 Hydroxylation reaction

In chemistry point of view hydroxylation is chemical reaction that introduces a hydroxyl (OH) group into an organic compounds [34-35]. In biochemistry these types of reactions are often known to be induced or facilitated by hydroxylases or monooxygenase which are enzymes, and often require molecular oxygen (O_2) [35-36]. This type of reaction has been considered to be a very important reaction in detoxification in a sense that during the reaction, a lipophilic compound gets converted into a water soluble alcohol derivative that is easily excreted by the body [36]. According to chemical principles the reaction actually involves the conversion of a CH group into a COH group, meaning the reaction is oxidative in nature because oxygen gets introduced into a typical compound (i.e. oxygenation). For biological processes the reaction is mostly initiated by Cytochrome P450 enzymes and usually requires molecular oxygen and iron as a catalyst (the iron is present in Cytochrome P450 enzymes) or NADPH. Most steroid and steroid derived compounds such as 17β-estradiol in study undergo hydroxylation reaction in position, 3, 4, 6, 11, 16, 17, 21 during natural production of hormones or steriodgenesis and the reaction are said to be dependent on the type of cytochrome P450 enzyme involved [36-37]. The hydroxylation reaction is a major reaction that predominately occurs during synthesis of androgens from cholesterol, and biosynthesis of estrogens [37-38]. The numbering system of steroids had been discussed in the next paragraph.

2.1.2.3 17β-estradiol and associated compounds

17β-estradiol is a steroid derivative compound that serves as a main component of female reproductive cycles and functions as the dominant female hormone along with estriol estrone [39]. Estradiols are mainly produced in the ovaries, and smaller amounts are can also be produced by the adrenal glands and other organs. 17β-estradiol is known to have greater disrupting potency as compared the two other, estrogenic endocrine disruptors because it tends to bind to most hormonical receptor sites in the body [40] of most

mammalian species [29, 32, 40]. Numbering system of an estradiol derivative was shown in Figure 2-2:

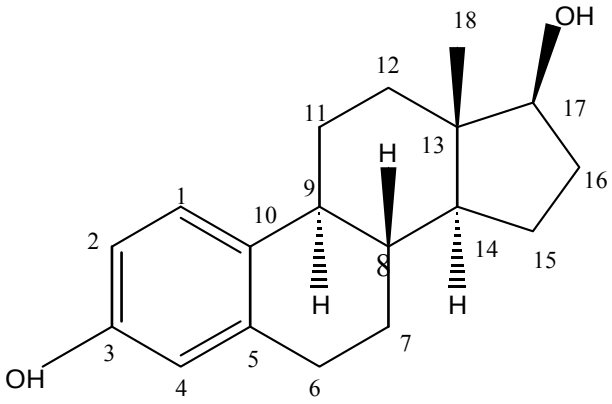

Figure 2-2: The structure of 17β-estradiol.

Most reactions of estradiol derived compounds occur at either carbon 3, 11, 16 or carbon 17 (see Figure 2-2) of the main backbone structure [41]. Below is an example of a reaction of estradiol, this reaction has been discussed by Wash and co-workers [41] to be catalysed by a cytochrome P450 enzyme.

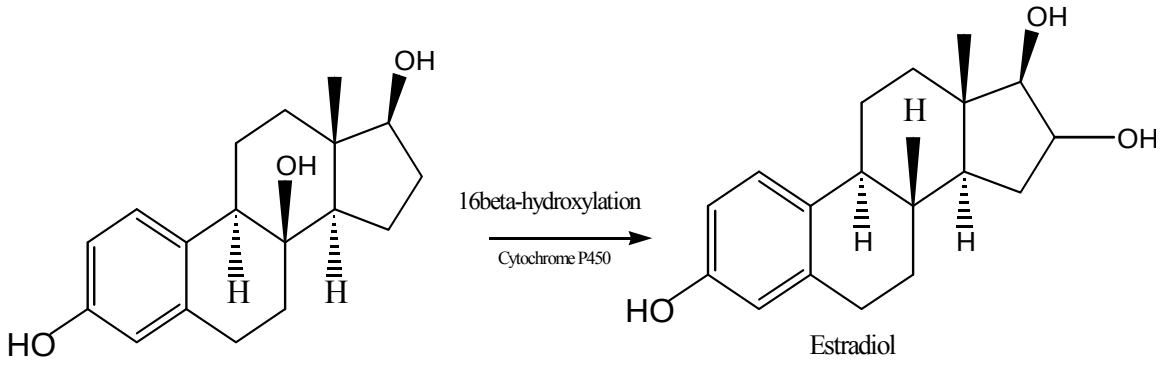

Figure 2-3: Hydroxylation reaction of 17β-estradiol by cytochrome P450 enzyme.

Similar structured cholesterol derived compound show similar reactions when catalysed by cytochrome P450 enzymes, with an introduction of a hydroxyl group to the compound to form a hydroxyl-, di-hydroxyl or a tri-hydroxyl compound [30, 42]. Estradiol can also undergo hydroxylation at other carbon positions depending on the type of cytochrome P450 enzyme involved.

Seventeen beta estradiol (17β-estradiol) has been defined as one of the major estrogenic endocrine disrupting compound having higher disrupting potency compared to estriol and estrone [42]. The allowed concentration values for major endocrine disruptors have been reported by Marie Deborde and co-workers [43], to be at roughly micro gram per litre range, which varies from organism to organism and no exact values reported so far describing precise levels for susceptible different organisms including human beings. Estradiol and other estrogens exert their effect by travelling through the bloodstream and interacting with cells of target tissues. The main target tissues of 17β-estradiol include the uterus, breast tissues, and bone, heart, liver, and brain tissues [44]. Fortunately many methods, such as high performance liquid chromatography, mass spectrometer, immuno-absorbent assays, amongst others have been developed and successfully utilised for determination of 17β-estradiol (E2). A recent report on determination of estrogens using plasma liquid chromatography coupled to mass spectrometry has shown detection limits of approximately; 3.8 x 10^{-8} g L^{-1}, 3.4 x 10^{-8} g L^{-1} and 78.6 x 10^{-8} g L^{-1} for estrone (E1), 17β-estradiol (E2) and estriol (E3) respectively [25, 45]. The limitations to these existing techniques are issues such, high detection limits, complexity and less ease of operation with most significant disadvantages being cost defective [46]. So far, less attention has been paid off: in improvement these technologies or providing new techniques which will limit at least one or more disadvantages encountered by the existing techniques [47].

2.1.3 Biosensor

2.1.3.1 Historical and theoretical survey

Biosensors have found a promising future and recent developments in biosensor technology have grown tremendously, and for the past few years have witnessed many promising applications such as in drug therapies, monitoring, delivery, health care industries, security sectors, food industries and their applications in ongoing researches for clinical monitoring of effectiveness of newly developed bio-active compounds such as drugs [46, 48-49]. A biosensor is defined as the device or system incorporated with one or more bio-recognition elements such as enzymes, antibodies, antigens, immunogenes, living cells, tissues etc [20, 50] attached into a solid support, cell or a gel

matrix, used to detect the presence of chemical or biological compounds in a solution or a gas phase**.** The concept of biosensors was introduced by Clark and Lyons in 1962 [50]. When an analyte become in contact with surface of the bio-receptor which usually contains immobilized enzymes, micro organisms, a product forms which is recognized in the transducer; the transducer (electrochemical, optical or piezoelectric transducer) converts the interaction into a quantifiable signal [51]. The signal then gets organized and processed then printed onto a display. Figure 2-4 gives a summary of main components of a typical biosensor.

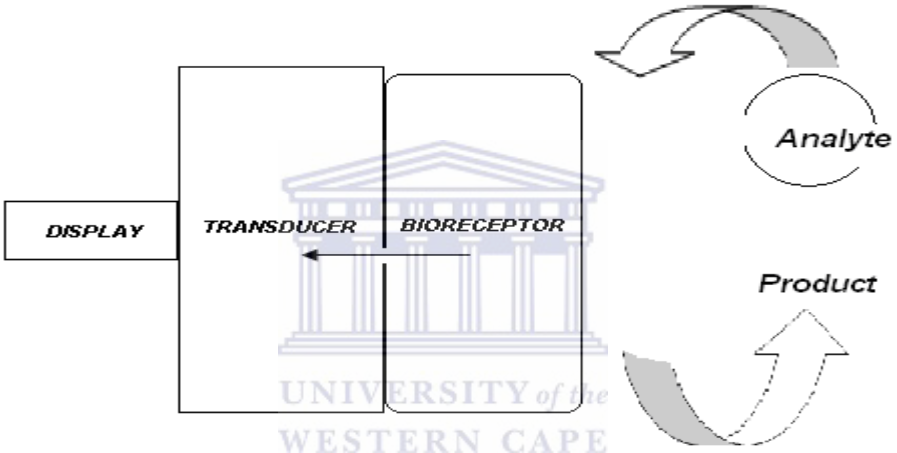

Figure 2-4: A Scheme illustrating main components of the biosensor and the interaction with a typical analyte molecule.

The Bio receptor is the core part of the biosensor that serves the purpose of selective recognition of the presence of an analyte in either a solution or a reaction vessel. *The Transducer:* has a main function of converting the changes experienced by the bio-receptor due to the interaction with the analyte, into a quantifiable signal which is always proportional to the amount of analyte introduced in a reaction vessel or solution. *Mediator* is a low molecular weight compound used to attain the equilibrium between the enzyme and the transducer [52].

2.1.3.2 Classification and types of biosensors

Biosensors differ due to the difference in either a bio-receptor or transducer, from immuno-based biosensors to enzyme-based biosensors and DNA based biosensors [46]. Upon interaction of the bio-receptor with the analyte a signal is generated, the type of signal generated varies due to changes attained by either the bio-receptor or analyte, the changes may include light changes, electronic property variations, heat changes, mass changes etc. Listed, are well known different types of biosensors: electrochemical biosensor, piezoelectric biosensor, immuno-absorbent enzyme biosensor, photo luminescence biosensor and DNA based biosensors [53-54].

2.1.3.3 Enzyme based electrochemical biosensors

Electrochemical enzyme based biosensor converts biological/chemical reduction or oxidation catalytic reactions into quantifiable electric signal. The principle of this type of biosensor is dependent on the properties exhibited by enzymes, described mechanistically in view that an analyte specifically binds to an enzyme that is known to be specific to one type of substrate reaction or a compound (old Key-Lock model), however the enzyme in most cases induces itself around a substrate and brings it closely to its active site [52], the interaction of an enzyme causes a fluctuation of charges that causes ionic moieties to generate electro-static potential, current and voltage signal in both the enzyme and the electrolyte solution, the signal is then channelled throughout the mediator material sandwiched in-between the bio-receptor (i.e. enzyme) and direct surface of the transducer (i.e. an electrode), where a change or interaction is converted into either current, voltage depending on the input signal, when a potential is applied, the output current signal is monitored and vice-versa.

2.1.4 Enzymes

2.1.4.1 General information

Enzymes are low molecular weight biological proteins/ molecules, able to catalyse a series of well known, chemical and biochemical reactions. These biological catalysts have high activity, specificity and efficiency [35, 55]. The enzyme operates by binding a substrate to its central core (i.e. active site) fitting to the most favourable orientation like a key and a lock, resulting into formation of an enzyme-substrate complex [56]. New bonds are formed and broken due to this interaction and products are then released to the surrounding media. Enzymes are sensitive to high temperatures and pH and may denature or loose their activity at such unfavourable conditions. The optimal pH of enzymes used in this study have been reported by many authors to be 7.0, 7.4 for HRP and CYP 3A4 respectively. In this study the most favourable conditions of these two enzymes were achieved firstly by keeping the enzymes in ionic phosphate buffer solution at low temperatures, typically at -4ºC and performing all experiments involving the enzyme moieties in phosphate buffer solutions of appropriate pH to maximise effects like stability and in order avoid denature of these enzyme for maximum functionality.

2.1.4.2 Enzyme Kinetics

Kinetics of enzymes involves conjecture studies of catalytic reactions of enzymes. The concept of enzyme kinetics is easily depicted by the Michaelis-Menten model, named after Leonora Michaelis and Maud Menten, who introduced this concept in early 1900. The model describes the rates of catalytic reactions that are irreversible, and assumes the concentrations of substrate is related to the initial rate of reaction [41, 57]. A brief summary illustrating mechanism and rate of reactions, when a typical substrate molecule interacts with the enzyme is shown in the next equations:

Mechanisms: $E + S \xrightarrow{K1} ES$ Equation 2.1-1

$ES \xrightarrow{K2} E + P$ Equation 2.1-2

Overall reaction: $E + S \rightarrow E + P$ Equation 2.1-3

In these equations, it is assumed that the rate of formation of the enzyme substrate complex ES is irreversible and thus the rate of reactions can be defined as:

Rate of formation of the product: $d\left(\frac{[P]}{t}\right) = K_2\,[ES]$ Equation 2.1-4

Rate of formation of [ES]: $d\left(\frac{[ES]}{t}\right) = K_1[E][S] - K_2[ES]$ Equation 2.1-5

Where [P] is the concentration of product, [S] concentration of substrate and [ES] is the concentration of enzyme-substrate complex. At steady state it is assumed that the concentration of [ES] remains constant as [E] and [S] changes and the rate determining step (i.e. Rate of formation V of the product) is given by:

$$V = \frac{V_{max}[S]}{[S] + K_m^{app}}$$ Equation 2.1-6

The $V = \frac{V_{max}[S]}{[S] + K_m^{app}}$ Equation 2.1-6 is the Michaelis Menten equation.

The parameter V_{max} describes the maximum velocity of molecules and K_m^{app} is the Michaelis Menten constant of its value gives the catalytic potential of the enzyme to substrate. The constant K_m^{app} can also be used to predict the rate of reaction catalysed by the enzyme. The Michaelis Menten constant gives a good approximation of the catalytic activity of the enzyme to a specific substrate.

2.1.4.3 Classification and type of enzymes

Enzymes are classified according to the type of reactions they catalyse. Some enzymes are categorised by the type of co-factors they contain. A co-factor is the non protein chemical compound or moiety that is required by the enzyme for its activities. These co-factors includes; FAD (Flavin Adenine Dinucleotide), TPP (thiamine pyrophosphate), Coenzyme A, NAD^+ (Nicotinamide Adenine Dinucleotide phosphate), ATP in some case the co-enzymes may include metals ions: for example zinc, iron, copper and magnesium ions. Below is the list of different enzymes, classified according to the type of reactions they catalyse [41, 57]:

2.1.4.3.1 Isomerases: Catalyses the geometric and structural changes caused by intermolecular oxidation or reduction within a molecule. Example: recemase, epimase, cis-trans isomerase.

2.1.4.3.2 Lyases: Catalyses the cleavage of C-C , C-O , C-N bonds and double bonds. Examples include: b-synthese, decarboxylase.

2.1.4.3.3 Hydrolyases: Catalyses the hydrolytic cleavage of C-C, C-O, C-N bond including the phosphoric anhydrous bonds. Examples include: carboxylic ester hydrolase, typothophan ester hydrolase.

2.1.4.3.4 Ligases: These type of enzymes catalyses the reactions involving the combination of two or more reacting molecules that are coupled by hydrolysis. Example: synthase.

2.1.4.3.5 Transferases: Catalyses reactions involving the transfer of one group to the other most common group being methyl. Examples: methyl transferase, hydroxyl transferase and formyl transferase.

2.1.4.3.6 Oxidoreductases: These enzyme catalyses the oxidation and reduction reactions as the name implies, examples of well known types of these enzymes include: Cytochromes P450 and Peroxidases, and can be categorised into monooxygenases and reductases. Oxidoreductase enzymes have attracted

many biochemists due to their property of being able to reduce or oxidise a series of reaction and have found their wide application in biosensing technology, drug therapies and other fields of research including biomedical technology, genetic engineering etc [58-59].

2.1.4.3.6.1 Types of Oxidoreductases

2.1.4.3.6.1.1 Horseradish peroxidase (HRP) Enzyme

Hydrogen peroxidase is plant derived enzyme that has an α-helical 3D complex structure with hemi active site [52, 58, 60]. This enzyme consists of single polypeptide chain with 308 amino acid residues. The active site of this enzyme consists of an iron centre surrounded by protoporphyrin ring (IX) type [61-62]. Almost all the catalytic reactions involving the enzymes occur at its active site or relatively close to it. A typical structure of the active site of horseradish peroxidase enzyme active site was illustrated in Figure 2-5:

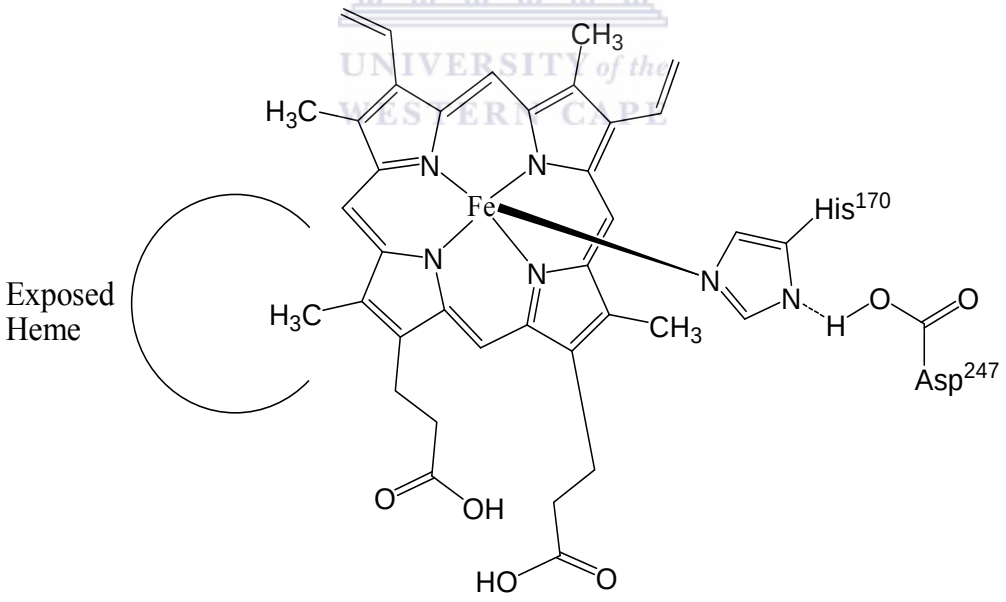

Figure 2-5: Structure of the hemi active site of Horseradish peroxidase (HRP) enzyme.

The histidine (His) and aspartic acid (Asp) are amino acid derivatives. The Asp 247 carboxylate side chain, conjugated to the hemi iron centre helps to control the imadizolate

character of His 170 derivative [58]. The purpose of His 170a derivative is to stabilise the five co-ordinated iron centre of enzyme when it binds to its associated substrate preferable H_2O_2. The aromatic substrates of horseradish peroxidase are said to be only oxidised at an exposed side of the enzyme [63-64].

2.1.4.3.6.1.2 Cytochrome P450

Cytochrome P450's are well known microsomal monooxygenase enzymes responsible for metabolism of most hormones, drugs and other exogenous compounds. The Cytochrome P450 enzymes are found in different parts of the body but large concentrations do exists in the liver cells and endoplasmic reticulum [65-66]. The CYP450 enzymes are also referred to as hemi proteins, hemi meaning they have an iron (Fe^{3+}) centre which is consider, as being the active site [41]. The hemi centre of the cytochrome P450 enzyme is also surrounded by protoporphyrin IX ring similar to HRP enzyme; the protoporphyrin ring consists with 4 nitrogen derived ligand and an extra 5th ligand which is a cystein (Cyst) amino acid residue, directly attached to the centre making the iron centre a five co-ordinated system [57]. Shown in Figure 2-6 is a typical structure of the active site of cytochrome P450:

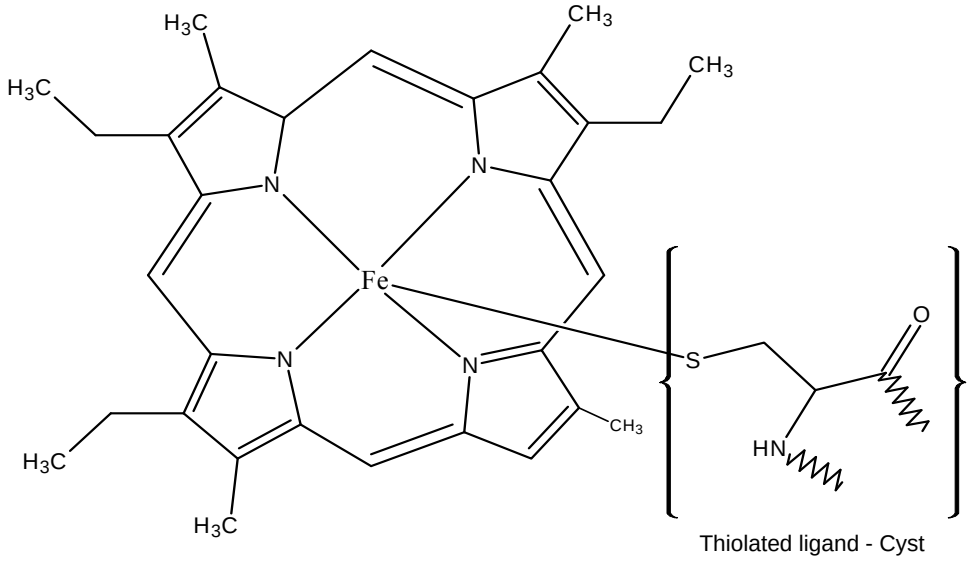

Figure 2-6: Structure of the hemi active site of a typical cytochrome P450 enzyme.

The cystein (Cyst) derivative attached to the iron centre of the enzyme is a type of an amino acid. Cytochrome P450 enzyme have an α-helical structure just like any other enzymes with a series of amino and carboxylic groups associated with them [67]. Another important factor about these types of enzymes is that they are also associated with the presence of reducible complex $NADP^+$ embed on its helical structure. $NADP^+$ also participates in oxidation and reversible reduction of some of its substrates. Most cytochrome P450 enzymes are known to be the major hydroxylase enzymes that metabolise most steroids at different positions depending on the type of cytochrome P450 enzyme involved [68]. These cytochrome P450 enzymes are involved in biosynthesis of steroids and bile acids. Examples of a series of cytochrome P450 enzyme substrate are listed: Testosterone (a male hormone), Verapimil (a pharmaceutical drug), Quinidine, Aldirine (a drug), Estrone (female hormone) and amongst most of drugs and hormone. The scheme illustrating the reactions catalysed by Cytochrome P450 enzymes was shown next in Figure 2-7:

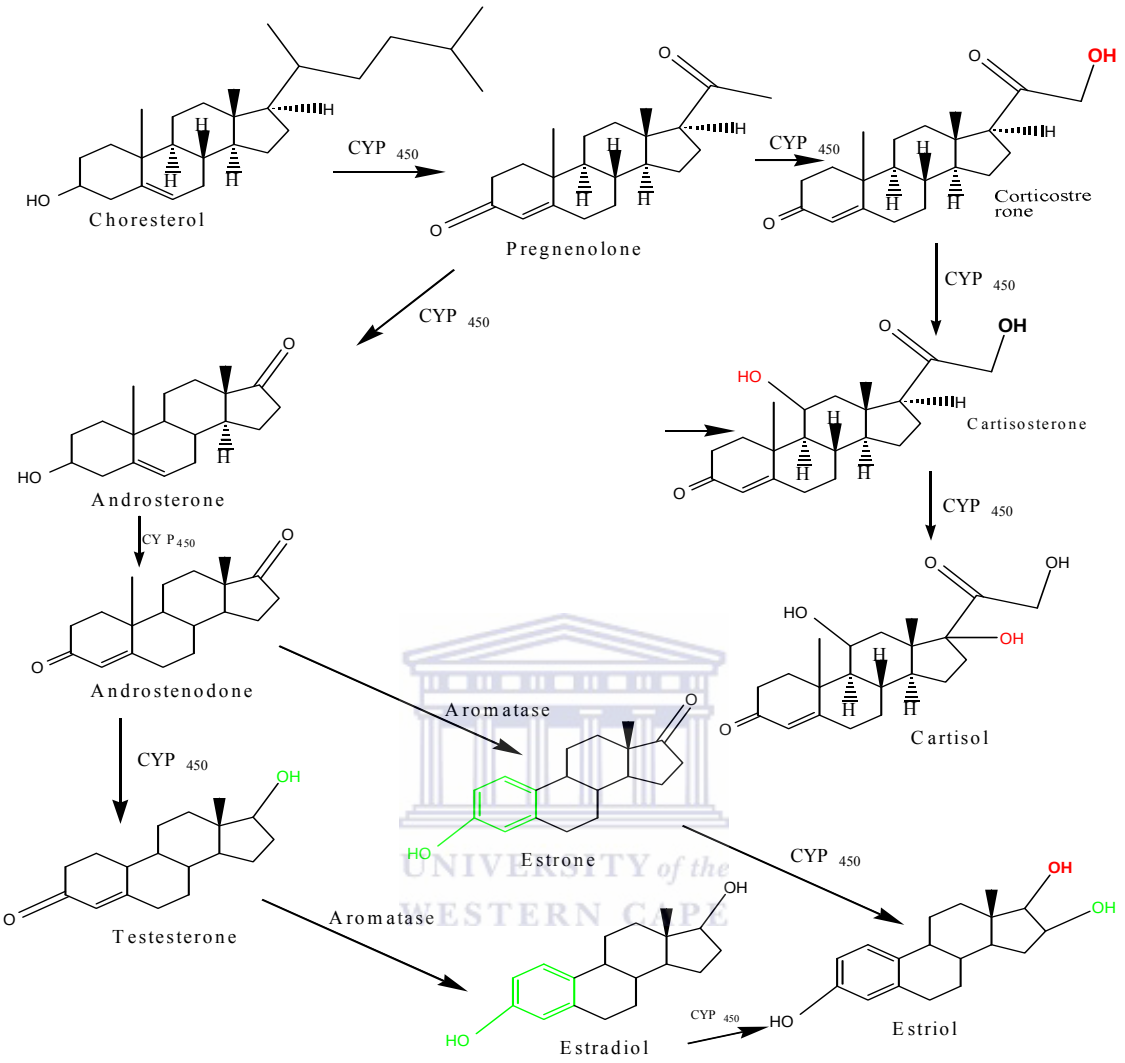

Figure 2-7: Steriodgenisis cycle catalysed by Cytochrome P450 enzymes.

The common mechanisms of these catalytic reactions by cytochrome P450 enzyme involves 5 major steps [69]:

- Substrate binding occurs at its hemi centre (Fe^{3+}).
- One electron reduction by iron by NADPH co-factors of cytochrome reductase.
- Reaction of the ferrous iron with oxygen to form FeO_2 an unstable form.
- This results in oxidation of the substrate with preference to be (loss of hydrogen).

- Lastly the products get released to the surrounding medium.

The next reactions show two typical reaction mechanisms occurring during catalytic metabolism of 17β-estradiol by cytochrome P450 enzyme [30, 70]:

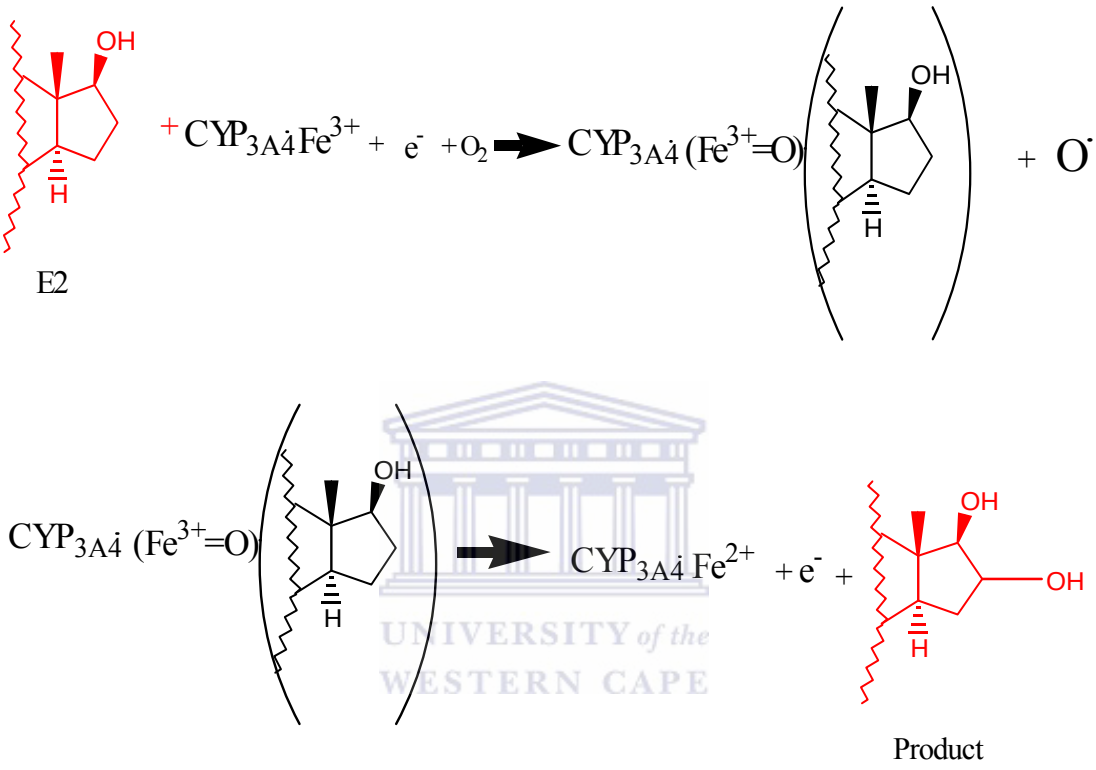

Figure 2-8: Catalytic reaction mechanism occurring during 16beta-hydroxylation of 17β-estadiol by Cytochrome P450-3A4 enzyme.

2.1.4.3.6.1.2.1 Cytochrome P450 (CYP3A4)

The CYP3A4 enzyme is the isoform of cytochrome P450 enzymes, and is a monooxygenase enzyme responsible for the breakdown of many bioactive compounds such food supplements, drugs, medication and pollutants [65, 71] and considered to be the most abundant cytochrome P450 found in the liver as reported by Hendricks an co-workers [65, 72]. The cytochrome P450 enzymes exist in wide variety of form with many different families, and there is an encoding abbreviation used to differentiate one cytochrome P450 from the other. In CYP 3A4, the CYP stands for cytochrome P450, because these enzymes absorb ultraviolet-visible light at wavelength of 450 nm , the 3

stands for family 3, A stands out for subfamily A and 4 stands for isoform 4, other isoforms of cytochrome P450 enzymes include CYP1A2, CYP1A1, CYP3A5,CYP1D2 [67] etc. Cytochrome P450-3A4 is also known to be a major metabolite and the most versatile cytochrome enzyme found in the liver amongst other cytochrome P450's. These characteristics have prompted the use of this type of enzyme for pharmacological studies and in toxicology, for study of newly developed drug, and drug monitoring and therapy, in recent publication by Nicollete and co-workers [72], the authors used this type of enzyme in fabrication of a biosensor for a drug metabolite Verapimil one of the substrates of CYP3A4.

In this project, the CYP3A4 enzyme was used as a bio-receptor element in the developed electrochemical enzyme based biosensors for 17β-estradiol. The 17β-estradiol compound under study is one of the major substrates of cytochrome P450-3A4. It was proposed that during this catalytic reaction of 17β-estradiol by cytochrome P450 enzyme, the 17β-estradiol gets converted into a tri-alcohol moiety with utilisation of the cytochrome P450 active site responsible for this catalytic reaction.

2.1.5 Immobilised enzymes: Properties and modes of immobilisation

An immobilised enzyme is described as a typical enzyme whose motion is restricted to only a small or limited space [73]. The enzyme is immobilised into a solid support, usually in the form of a gel or film. Enzymes attached to solid supports have major advantages [73] such as repetitive use of single batch of enzymes, enzymes are also stabilised extensively by binding, and the enzyme can be easy separated from its associated products. Immobilised enzymes are either selected on the bases of either their bio-chemical or kinetic properties and for ease of control over properties such as stability, temperature and pH, as the enzymes differ in terms of stability and sensitivity and are subsistence to certain environmental conditions. The choice of enzymes immobilised into a solid support is then dependent properties exhibited by the support material, the application and enzyme solution media or the working conditions. In electrochemistry the concept of enzyme immobilisation is used in order to bring the enzyme moiety closely to the electrode surface for adequate electron transfer reactions resulting from catalytic

reaction initiated by a particular choice of enzyme and substrate under investigation. In this project the HRP and CYP3A4 enzymes will be immobilised onto an electrode surface in the presence of electron mediators used to channel the movement of electrons generated by the interaction of the enzyme with its substrate to the electrode surface as the support material and catalytic platform. The concept of enzyme immobilisation in the presence of the electron mediator was utilised in order to have a controlled movement of electrons that would lead to faster substrate to enzyme current responses.

2.1.5.1 Modes of enzyme immobilization:

There are about four well known method of immobilising an enzyme onto a solid support, a gel or a membrane. The four methods have been described:

2.1.5.1.1 Adsorption method

In this method a solid support is incubated into a solution consisting of an enzyme at an appropriate pH, ionic strength. The enzyme physical absorbs on the surface of solid support.

2.1.5.1.2 Covalent linkage

In this method a minimal amount of enzyme is used, a substrate or support initially activated with a thiol group or ammonia group or carboxylated group is crosslinked with an enzyme by means of a cross linking agent such as glutaldehyde and carbdomide compound. This method provides a good stability of enzyme onto the solid support.

2.1.5.1.3 Entrapment

In this method an enzyme is mobilised with a ceramic gel such as acryl amide gel or a membrane by means of introducing a stirring effect to localise the enzyme thorough out the membrane or gel, for faster reaction and stability of the enzyme onto the support.

2.1.5.1.4 Cross linking

The method is similar to previously described method; covalent linkage because it involves the covalent bonding between the enzyme and the solid support by means of a cross linking agent, this methods is known to be the most stable method.

2.1.6 Supporting Material

In this context the supporting materials refer to mediator materials, used in this study for the fabrication of the biosensor: this included materials ZnSe-QDs and polymer-PANI. A mediator had been defined in 2.1.3.3 as the material used to attain equilibrium between the electrode surface and the enzyme. In order to choose a required support material for the application in electrochemical biosensor technology, a major requirement is the production of an optimal electrode that responds well to its given application. As discussed previously in electrochemistry, one studies oxidation and reduction reactions happening at the surface of an electrode, a critical aspects such as physical stability, rate of electron transfer and product sensitivity, electron conduction of material onto the electrode surface and other critical aspects. This means that cost and lifetime of material have to be considered when choosing an adequate supporting material for any electrochemical enzyme biosensor platform. The next paragraphs highlight the supporting materials that were used during fabrication of the developed biosensors during this project and have been discussed thereof.

2.1.6.1 Quantum dots

Quantum Dots (QDs) are semiconductors nanomaterials that have a size diameter between 2-10 nm. Quantum dots have narrow tunable band gap (i.e. minimal energy needed to excite electrons from the ground state to its exited state) as described by Walling and co-workers. [11]. A single quantum dot is excited the same manner as any other type of conductor; by absorbing minimal amount of energy that cause a single dot to jump form ground state to exited state, once in the excited state it experiences the instability and goes back to its ground state and the transition from the exited state to the ground state results in the emission of light. Due to their small size, these quantum dots exhibit unique properties like, electrical, magnetic, optical and chemical properties [74-75]. Current applications of QDs include: their uses in light emitting diode devices, lasers, in biological labelling, sensors, bioassays etc. Use of quantum dots as bio-labellers have attracted many researchers all over the world, for their use in targeting cancers, tumours and diagnosis, and seem to be the promising approach for diagnosing and targeting most known incurable cancers and tumours, both in vitro and vivo [74-76].

2.1.6.1.1 Types of quantum dots

Quantum dots are mostly compromised of the listed combinations of group numbers as depicted in the periodic table of elements:

Group (II-VI) (example, cadmium selenide, cadmium sulphide and cadmium tellunide).

Group (IV-VI) (examples, lead sulphide, lead telenide, tin telenide)

Group (III-V) (examples, Indium phosphate)

Other types of quantum dot include, the use of transition metal such as zinc together with group IV non metals for example, zinc sulphide and zinc selenide quantum dots. Quantum dots are synthesized by simple methods such as colloidal synthesis, shell growth aqueous solubilization and their synthesis can be achieved both at ambient room temperature and very high temperatures ranging from 25 $^{\circ}$C to about 400 $^{\circ}$C [19, 77]. Many quantum dots based optical biosensors have been developed over the past decades utilising the advantage that these nanomaterials exhibit good photo electronic properties [77-78]. These types of biosensors are referred to as photoluminescence biosensors, the principle of these biosensors is that after interaction of the substrate with bio-molecule immobilised onto the biosensor in the presence of quantum dots, the interaction causes the quenching of photoluminescence of the quantum dots. The photoluminescence intensity then decreases and many parameters can be determined such as detection limit and biosensor efficiency. Examples of recent photoluminescence biosensors that has been fabricated using quantum dot include, an enzyme biosensor incorporated with CdSe quantum dots for glucose detection that was reported by Li and co-workers [19] and a biosensor fabricated using CdSe/ZnS clusters that was reported by Chuan Liang and co-workers [79]. The photoluminescence biosensors use the principle of quenching of photoluminescence intensity related to the amount of substrate introduced in the reaction media [79]. Very few publications exist where other properties such as electronic properties of these quantum dots are taken into advantage for application in devices such as sensors or biosensors.

2.1.6.1.2 Other Quantum Dots applications: In solar cells

Quantum dots are widely used in photovoltaic devices: the operational procedure of a typical voltaic cell that utilises quantum dots, begins in the p-n junction: the sunlight excites the electrons creating an electron hole pair, these electrons then conjugate or accumulates and shutter on other side of the conductor resulting in generation of electricity [76, 80].

2.1.6.2 Conducting Polymers

A conductive polymer is an electro-active polymer that is able to conduct electrons at the same time stores energy in its backbone. A first conducting polymer was developed by Natal and co-workers as the black powder derivative which was later proven to be semi-conductive with a conductivity of up to 7 $x10^{-3}$ S m^{-1} [20]. The development of this polymer led to researchers taking the development further by studying the effect of polymer doping with either an oxidising or a reducing agent that was later proven to increase the conductivity of polymers tremendously [13, 81]. Conductive polymers are well known to be very good charge carriers and energy storage materials because of their long chain flexible backbone. The energy storage mechanism of the conducting polymers was explained by the fact that these polymers were able to lower their energy by altering their bonds which caused the production of energy of up to 1.5 eV making it a higher energy semiconductor [82-83]. A conducting polymer transfers charges by first losing a single electron from one of its bonds and localising it throughout its polymer chain [84].

2.1.6.2.1 Applications and types of conducting polymers

Applications of conducting polymers include their use as electrostatic materials, conducting adhesives, artificial nerves, optical capacitors and in chemical and bio sensing [82]. A type of polymer to be used for a specific application depends on three main factors stability, conductivity, and processing. The next Table 2-1 gives a list of properties of most common polymers categorised according to stability, processing and conductivity.

Table 2-1: Different types of polymers with their conductivity and stabilities. [85]

Polymer	Conductivity ($\Omega^{-1}cm^2$)	Stability	Processing
Polyaceteylene	10^3-10^5	Poor	Poor
Polyphenylene	10^3	Poor	limited
Polyphenylene Sulphide	10^2	Poor	Excellent
Poly(p-phenylene vinyllene)	10^3	Poor	limited
Polyaniline	10	Good	Good

This study focuses on the use of polyaniline as a dopant for water soluble ZnSe quantum dots. From the above table polyaniline shows not only good stability but also a reasonable conductivity and ease of processing compared to the other related polymer types.

2.1.6.2.1.1 Polyaniline and its synthesis

Polyaniline is a type of conjugated polymer which falls under the class of polymers known as flexible rod polymers (these type polymers can be converted into conducting polymers by doping with a good oxidising agent) [81, 86]. This type of polymer is known to have very good electrical conductivity and good chemical and environmental stability [82]. Polyaniline exists in three base forms: leucoemaradine (fully reduced state), emeraldine (a neutral state) and pernigraniline (fully oxidised form), these base forms describes the intermediate oxidation states of polyaniline [84, 87]. Polyaniline can be

synthesised by a series of methods: chemical synthesis with ammonium persulfate in the presence of hydrochloric acid, a second method is electro-polymerization in acid media, hydrochloric acid or sulphuric acid, both these method includes the use of monomer aniline as the base precursor [81]. The simplest method of synthesis of polyaniline is the electrochemical polymerization of aniline, however only suitable for small scale applications and very limited for large scale synthesis [20, 88].

Electrochemical method (i.e. cyclic voltammetry) synthesis of Polyaniline (PANI): This methods involved electro-deposition of a polymer layers by applying or scanning the potential across the three electrode system, fitted in a glass cell containing a solution of a monomer derivative. In this study the monomer was aniline in the presence of a solvent 1 M HCl [82]. As the potential is scanned through, layers of polymers deposit onto the working electrode surface. After the synthesis is complete, a polymer can be dispersed in an appropriate solvent for further applications and uses. Polyaniline exists in three base forms differing in the oxidation states as described above [81-82]. The figures: Figure 2-9, Figure 2-10 and Figure 2-11 show the structures associated with three base forms of polyaniline, Luecoemaraldine, pernigraniline and emaraldine respectively [82, 89].

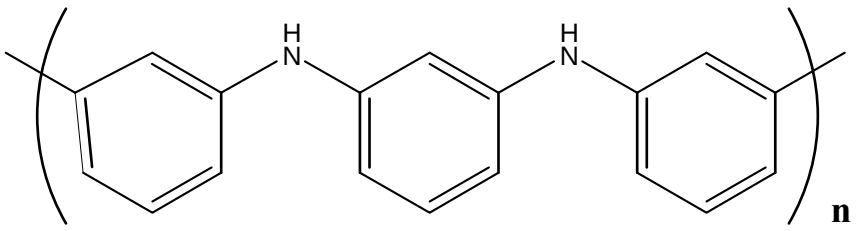

Figure 2-9: Pernigraniline base of PANI.

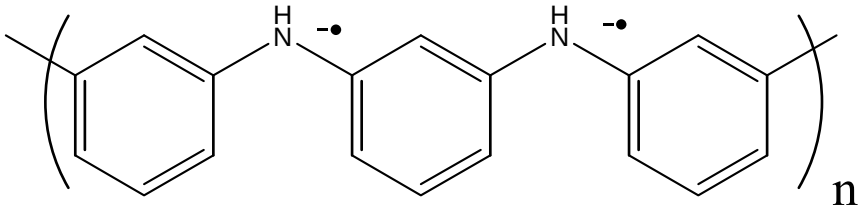

Figure 2-10: Luecoemaraldine base of PANI.

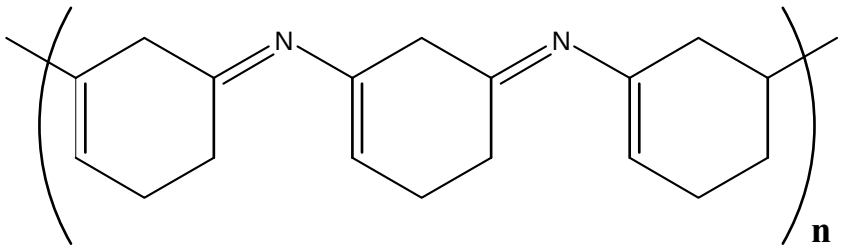

Figure 2-11: Emaraldine base of PANI.

2.1.6.3 Quantum Dot-Polymer Composites

A composite is defined an engineered or chemically prepared material made from two or more constituent materials with significant different physical or chemical properties, which remain separate at microscopic level within the finished material [88, 90]. The combination of the two or more different constituent material allows the composite to exhibit new properties which are in between and pose mixed properties of constituent material used [83-84]. Composite material are the widely used material in many industries such as paint, glass manufacturing industries, automotive industries, coating and in electronics, with most common types of composites made of polymers combined with other polymers, with small traces of metals and other materials in purpose of distributing and manipulating properties such as mechanical properties, electrical properties, thermodynamic properties and chemical properties [91]. The process of polymer to quantum dots system, involves embedding the quantum dots onto a complex polymer chain [83]. There are well known several techniques that are in use already for preparation of quantum dot-polymer composites, these methods includes surface passivation, chain end attachment and layer by layer assembly [13, 83]. Some of the applications require that the quantum dots to have certain surface characteristics such as hydrophilic or hydrophobic thus would require surface modification. Recently quantum dots have been successfully combined with polymers for application in photo-electronics devices and other applications [84, 88]. Thus by successfully combination of quantum dots with polymer one intrinsically design a polymer-quantum dots architect material with combinations of conductivity, chemical stability, mechanical stability posed by polymers together with electronic, photo-electronic properties and biocompatibility posed

by the quantum dots [84, 92-93]. During this project a new type of composite: PANI:MPA-ZnSe-QDs was developed and successfully characterised by techniques such as Ultraviolet –Visible spectrophotometry (UV-Vis), Cyclic Voltammetry (CV), Fourier Transform Infrared spectrometry (FT-IR) and Transmission Electron Microscopy (TEM), in order to interrogate the new characteristics exhibited by combination of these two materials. This newly composite material was successfully used as the electron mediator for one the biosensors developed during this project. The design of the polymer- quantum dots composite was a similar approach to one method recently reported composite by Tomcizaka and co-workers by embedding the quantum onto the polymer chain [93].

2.1.7 Characterization Techniques

2.1.7.1 Electrochemical techniques

Voltammetry is an analytical technique based on the measurements of current flowing through a dipped electrode into a solution containing an electro-active species while applying a potential, a frequency, a current etc depending on the choice of mode. A typical voltametric cell consists of a reference electrode, a platinum electrode and a working electrode: a working electrode has a little surface area in order to have a minimal quick and accurate potential imposed by electric circuit [94]. The technique is known to be the versatile technique for research and allows for studies of many electrochemical and or bio-electrochemical reactions i.e. reactions involving the transfer of electrons between reactants and products. Voltammetry is widely used in investigation studies of many physical properties of material for their applications in devices such as electric resistors, capacitors, transistors, sensors etc.

Fundamental Electrochemical reactions: Suppose that a working electrode is dipped into a solution consisting an electro-active species or compound A_{ox} (oxidised) that can be reduced to species A_{red} at a known potential (V), the following reaction applies [94]:

$$A_{ox} + ne^- \rightarrow A_{red}$$

The fundamental aspect of electrochemistry is that the reactions occur at an electrode surface based on the chemical changes resulting from the flow of ionic species from the

electrolyte solution to the surface of the electrode. The next illustration Figure 2-12, show the inter-phases occurring at an electrode/ solution system.

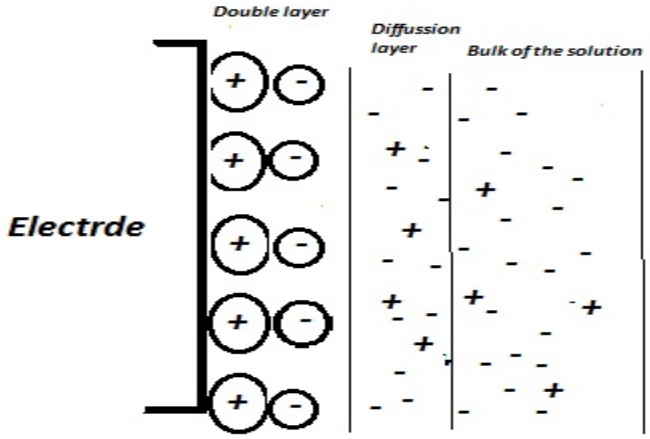

Figure 2-12: Illustrates the interfaces that describes the electrode/solution system at a positively charge electrode.

There are three mechanisms of which the electro-active species can move form the bulk of the solution to the electrode surface where the main electrochemical reaction occurs.

Convection: describes the movement of electro-active species under the effect of mechanical force or pressure imposed into the solution.

Migration: describes the movement of ions by an electric field created due to charge difference i.e. force of attraction and repulsive forces.

Diffusion: described the movement of electro-active species or charges in solution due to concentration gradient from the region of high concentration (solution) to a region of lower concentration (electrode surface). The initial stage of the electron transfer reaction starts by introduction of an electro-active species into the *electrolyte solution/supporting electrolyte*. The supporting electrolyte surrounds the electrode with constant charge, reducing the electro-static attraction [73, 94]. The supporting electrolyte must exhibit properties like: be chemically inert and must have low ionic conductivity and low electric

resistance, to minimise capacitive current due to growth of diffusion layer caused by high solution concentrations.

2.1.7.1.1 Cyclic voltammetry

The principle of cyclic voltammetry involves varying the times and applied potential to an electrode immersed into an electrolyte solution consisting of a certain concentration or volume of species/compound under the study. This records the current to potential curves and these curves indicates the potentials of which the reduction-oxidation (redox) processes occur [94]. The magnitude of current generated by a faradic process (current generated by interaction of the electrode surface with the electro-active species) is proportional to the concentration of the active species present in the solution. Cyclic voltammetry can be used to define the reversibility and irreversibility of electrochemical reactions. The Figure 2-13 illustrates the cyclic voltamograms of a reversible redox reaction.

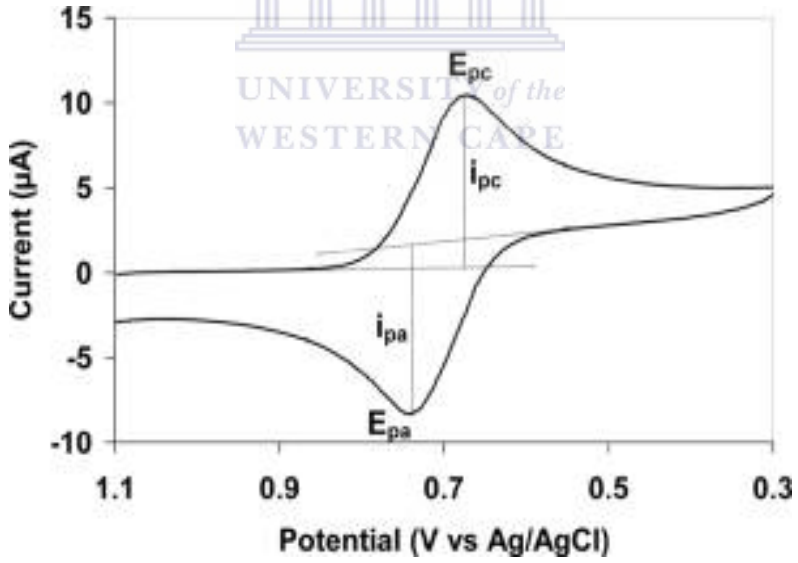

Figure 2-13: A typical cyclic voltammogram of a reversible reduction-oxidation reaction.

Parameter i_{pc} is the cathodic peak current at cathodic peak potential, E_{pc} resulting from a typical reduction of a species, i_{pa}, anodic peak current on the other hand describes the oxidation of typical species at an anodic peak potential, $E_{pa.}$ A *reversible reaction* is

observed by appearance of both oxidation and reduction peaks. The *irreversible electrochemical process* is observed by appearance of only a reduction peak [94]. A quasi-reversible process is the transition between that of a reversible process and irreversible process. One of the important equations in electrochemistry is what is describes as Randle Sevcik equation, this equation describes the boundary conditions of a Nersian process (reversible process) and the reactions occurring at the electrode surface. Randle Sevcik equation [94] is given by:

$$i_p = 0.4463nFA\left[\frac{nF}{RT}\right]^{1/2} C_0^* D_0^{1/2} \nu^{1/2} \qquad \text{Equation 2.1-7}$$

Where i_p = {Peak Current in A}, n = 1 {number of electrons}, F = 96485 C mol^{-1} {Faradays Constant}, A = 0.0201 cm^2 {geometric area of the electrode}, R = 8.314 J mol^{-1} K^{-1} {Gas Constant}, T = 298.15 K{absolute Temperature} and ν = {Scan Rate in V s^{-1}}.The equation above gives an estimation of a number of parameters such as the number of electrons (n) involved that can also be calculated as follows: $\Delta E = \frac{59}{n}$ (for a reversible processes).

2.1.7.1.2 Square-wave voltammetry and Differential-pulse voltammetry

The square-wave and differential-pulse voltametric technique are similar to cyclic voltammetry, but are much more sensitive than cyclic voltammetry [94]. A series of voltametric techniques such as cyclic voltammetry, square-wave voltammetry, differential-pulse voltammetry and time base (amperometry) have been used in this study, for electrochemical characterisation of different films immobilised onto a gold electrode surface films such as : MPA-ZnSe-QDs, PANI:MPA-ZnSe-QDs, and the AuE/ PANI:MPA-ZnSe-QDs biosensor.

2.1.7.2 Scanning electron microscopy

An electron microscopy introduces a beam of very energetic electrons that penetrates deep down the object at very fine defined scale by using a series of objective lenses [95]. In summary, the process starts when an electronic gun usually situated at the top

compartment of the instrument produces a series of electrons , the produced electrons are then condensed into an objective lenses controlled by a coarse current probe. The purpose of these lenses is to minimise the amount of current flowing. A beam of electrons is then channelled into a thin, tight coherent beam. Secondary objective lenses (situated at close approximate to the sample/ specimen) scans the coherent beam and directs it to the sample, when the beam of electrons then strikes the sample the interaction is sent to an electronic detector that maps and produces the image of the sample [95-96]. Electron microscopic techniques give brief; the information such as the surface morphology, topography and particle sizes of material in one dimensional (1D), two dimensional (2D) and 3 dimensional (3D). These amazing electronic spectroscopic features have initiated many researches involving development of new material, study of existing material because of the ability of these techniques to look at even the electronic states of all sorts of material, up to a size diameter nanometre ($x10^{-9}$) [96]. The scientists often used these techniques to investigate the shape, volume, cracks and voids with sets of materials. In this study the technique was used to study a series of material such as: the MPA-ZnSe-QDs, and PANI:MPA-ZnSe QDs composite.

2.1.7.3 Ultraviolet - Visible spectrophotometry (UV-Vis)

The principle of ultra violet spectrophotometer is that it uses light in the UV-Vis region of the spectrometer or in the ranges near infrared to excite the sample, where upon the sample absorbs some of the light. The absorption of light in the visible range affects the perceived colour of chemical species involved [97]. When a particular substance absorbs this light it undergo an electron transition whereby; a valence electron gets excited form ground state to excited state (i.e. from lower energy to higher energy). These electronic transitions can provide the properties of substances such as structure and colour and energy associated with each transition.

Beer-Lambered Law is used for estimation of concentration of light absorbing species as the light passes through it and is given by:

$$A = -\log_{10}\left(I_0 / I\right) = \varepsilon.c.L \qquad \text{Equation 2.1-8}$$

The equation describes the absorbance of light is directly proportional to the concentration of the absorbing species. The parameter A = describes the absorbance, I_0 = is the intensity of incident light, I = is the intensity of the transmitted light, ε = is the molar absorptivity and L = is the path length. A good estimation of energy resulting from these electronic transitions can be determined by Plank's law:

$$\Delta E = h\nu = h\left(\frac{c}{\lambda_{max}}\right) \qquad \text{Equation 2.1-9}$$

Where E = is the energy of light, h = 6.626 x10^{-34} J s^{-1} is Planks constant, ν = frequency of light, c = 3.0x10^{8} m s^{-1} is the speed of light and λ_{max} = maximum wavelength (nm).

The far most known transition is from HOMO to LUMO with the states listed:

$$\sigma \rightarrow \sigma^*$$
$$\pi \rightarrow \pi^*$$
$$n \rightarrow \sigma^*$$
$$n \rightarrow \pi^*$$

The * describes the excited state σ, Π, and n describes the type of orbital involved. The UV-Vis is the complementary technique to fluorescence. In fluorescence instrumentation the detector measures the emission of light from substance, as it looses energy and transits from excited state to ground state. Both these instrumentation techniques can be used to study a series of compounds and substances for transition metals, organic complexes and charge transfer complexes [97-98].

2.1.7.4 Fourier Transform infrared Spectroscopy(FT-IR)

The name infrared (IR) comes from the fact that the instrumentation utilises the infrared radiation to excite a particular molecule or compound [98]. The principle of the technique is that, the molecule get excited to a higher energy state by absorption of IR radiation, a

particular molecule only absorbs certain frequencies of IR radiation , which are associated with changes in the energy that occurs during absorption. The difference in radiation frequencies of a particular molecule or compound, results into either stretching or bending frequencies of the molecule. The energy of the absorbed IR radiation increases the amplitude of vibrational motion of bonds in a molecule or compound in study. Only bond with appropriate dipole moment have an ability of absorbing IR radiation [98-99]. The FT-IR is a widely used technique for determination of structural features of unknown compounds [99]. In this study the FT-IR had been used for the study of structural properties of newly developed MPA-ZnSe quantum dots together with the composite PANI:MPA-ZnSe-QDs and other associated molecules used throughout the study.

EXPERIMENTAL SECTION

CHAPTER 3

3.1 EXPERIMENTAL SECTION

Chapter review

Briefly the chapter elaborates firstly on the listing of chemicals and instrumentation used during the project; the chapter also include preparation procedures of different electrolyte solutions and buffer solutions as used for biosensor's applications and characterization. Secondly the chapter emphasises on synthesis and characterisation of MPA-ZnSe-QDs, preparation of polyaniline dopped 3-mercaptopropionic acid zinc selenide quantum dots (PANI:MPA-ZnSe-QDs) composite, characterization and applications of the biosensors AuE/PANI:MPA-ZnSe-QDs/HRP and AuE/Cystm/MPA-ZnSe-QDs/CYP3A4, and preparation procedure for analyte 17β-estradiol, 17α-ethnylestradiol and estrone. This experimental section also includes the procedure for preparation of samples for characterisation.

3.1.1 Chemicals and Instrumentation

3.1.1.1 Chemicals

All chemicals used in this study were of analytical grade and purchased from Sigma Aldrich, this include sodium dihydrogen phosphate, disodium hydrogen phosphate, zinc nitrate hexahydrate (99%) , selenium powder 99% purity, sodium borohydride, 3-mercaptopropionic acid (MPA), sodium hydroxide, aniline, hydrochloric acid, potassium hexaferricynide, potassium hexaferrocynite, horseradish peroxidase (EC 1.11.1.7) , bovine serum albumin (BSA), 50% glutaldehyde, 17β-estadiol, 17α-ethylestradiol, estrone, hydrogen peroxide (30%) , genetically engineered cytochrome P450-3A4 (CYP3A4), purified from a full length human CYP3A4 (EC 1.14.14.1) cDNA clone and over expressed in *Escherichia coli* cells, consisting of only the terminal oxidase (hemi domain), cysteamine, N-hydroxysuccinimide (NHS), 1-ethyl-3-(3-dimethylaminopropyl) carbodiimide hydrochloride (EDAC) as the coupling agent, Ethyl diaminetetraacetic acid (EDTA), DL- Dithietol (DTT), absolute ethanol. The 0.1 M phosphate buffer solutions (PBS) of pH 7.4 and 7.0 were prepared from sodium dihydrogen phosphate, disodium hydrogen phosphate in double distilled water filtered by Millipore ^{TM} filtering system.

3.1.1.2 Instrumentation

All electrochemical experiments were carried using a BAS100W integrated and automated electrochemical work station from Bio Analytical Systems (BAS), Lafayette, USA. All voltammograms of cyclic voltammetry and square-wave voltammetry differential-pulse voltammetry and steady state amperometry, were recorded with a computer interfaced to the BAS 100W electrochemical workstation. A 10 mL electrochemical cell with a conventional three electrode set up was used. The electrodes used in the study were: (1) Gold working electrode (A = 0.0201 cm^2) from BAS (2) platinum wire, from Sigma Aldrich, acted as a counter electrode and (3) Ag/AgCl (3 M NaCl) from BAS was the reference electrode. Transmission electron microscopy (TEM) analysis of materials dispersed and spread on a copper coated TEM grid, were done using a Tecnai G2 F20X-Twin MAT 200 kV Field Emission Transmission Electron Microscope from FEI (Eindhoven, Netherlands). Screen printed gold electrodes (Ref. 220AT) and Screen printed carbon electrode with a surface area of 0.1257 cm^2; from Dropsens, Spain were used as working electrodes to prepare samples for SEM analysis The SEM images were taken using Hitachi Model X-650 Scanning Electron Micro analyser from Tokyo, Japan coupled to Energy Dispersive X-ray Analyser. Alumina micro polish and polishing pads were obtained from Buehler, IL, USA and were used for polishing the gold electrode before any modification. All FT-IR spectra were recorded on PerkinElmer spectrum 100, FT-IR spectrometer on a NaCl pill. The FT-IR spectrum analysis was done on liquid samples of MPA-ZnSe-QDs, PANI and PANI:MPA-ZnSe-QDs films respectively the films were placed in between two NaCl plates of about 2.5 cm diameter, and FT-IR spectrum was recorded from a frequency range of 4000 cm^{-1} to 750 cm^{-1}.

3.1.2 Synthesis and Preparation procedures

3.1.2.1 Synthesis of 3-mercaptopropionic acid capped ZnSe quantum dots

Zinc selenide quantum dots were prepared by the same approach described by F. Zhang and co-workers [15] with some modification, where 0.03 g of zinc nitrate hydrous salt was dissolved in water followed by addition of 69.9 µL mercaptopropionic acid, the pH

of the resulting solution was then adjusted to 12.54 using 0.1 M sodium hydroxide (NaOH), this solution was then bubbled under nitrogen for 2 hours at 25 °C. After which, a solution containing 0.02 M selenium ions (i.e. prepared by chemical reduction of 0.2 mmol sellium powder by equivalent molar sodium borohydride ($NaBH_4$) under nitrogen gas for a maximum period of 1 hr, in the presence of 10 ml of water) was introduced drop wise until a bright yellow solution was obtained indicating a slow formation of MPA capped zinc selenide quantum dots. The resulting 3-mercaptopropionic acid capped ZnSe quantum dot solution (MPA-ZnSe-QDs) was then transferred in the refrigerator at -20 °C for 5 min to quench size escalation. The water soluble MPA-ZnSe-QDs solution was finally kept in room temperature in the dark until used. The MPA-ZnSe-QDs prepared were stable for period of 3 days.

3.1.2.2 Preparation of polyaniline (PANI)

A gold disk electrode of area 0.0201 cm^2 was pre-cleansed by polishing the electrode surface with 3 alumina slurries of particle sizes (0.03, 0.5 and 0.03 μm) respectively in glassy polishing pads for a minimum time of 5 min on each pad. After polishing, the electrode was ultra-sonicated for about 15 min, with double distilled water and absolute ethanol respectively to remove any possible absorbed alumina crystals on the electrode surface; this was followed by re-rinsing the electrode again with double distilled water. The electro-polymerisation was achieved by potential scanning a cleansed gold electrode from the potential E = 1100 mV to E = -200 mV at a scan rate of 100 mV s^{-1}, over 20 scans or 10 cycles from positive to negative potentials, in a pre-argon degassed 4 ml solution containing: 0.1 M aniline and 1 M HCl. The potential was scanned until stable thin layers of PANI gradually deposited onto the surface of the gold electrode, visually identified by a change in colour of the gold electrode surface to a greenish appearance. The PANI modified gold electrode was then washed with double distilled water to remove any residues of aniline and HCl that might have been loosely adsorbed onto the modified electrode surface. The greenish poly-aniline films deposited onto the gold electrode surface were then dispersed in trace amount of methanol and kept in a small 1 ml glass vial until used at 25 ºC.

3.1.2.3 Preparation of PANI:MPA-ZnSe-QDs composite

A gold disk electrode of 0.0201 cm^2 was pre-cleansed by the method described in 3.1.2.2. Cyclic voltammetry was then run from a potential E = 1100 mV to E = -200 mV at a scan rate of 100 mV s^{-1} over 20 scans or 10 cycles, in a pre-argon degassed 4 ml solution containing: 0.1 M aniline solution, 1 M HCl and 40 µL MPA-ZnSe-QDs. The resulting PANI:MPA-ZnSe-QDs modified gold electrode was then washed with double distilled water to remove residues of aniline and MPA-ZnSe-QDs that might have been loosely attached onto the modified electrode. The PANI:MPA-ZnSe-QDs modified gold electrode was then used for further electrochemical characterization as it has been discussed in the next chapters, different ratios of PANI and MPA-ZnSe-QDs were also prepared by the same method described.

3.1.2.4 Preparation of the HRP enzyme stock solution

The 0.1 µM HRP enzyme stock solution was prepared by dissolving 3 mg of HRP in a 0.03 mg μL^{-1} BSA solution (prepared by dissolving 4 mg of BSA in 120 µL of 0.1 M PBS, pH 7.0). This enzyme stock solution was the stirred gently for about 1 min and stored in the refrigerator at -4 $^{\circ}C$.

3.1.2.5 Preparation AuE/PANI:MPA-ZnSe-QDs/HRP biosensor for 17 β-estradiol i.e. the first biosensing system for the detection of 17β-estradiol

A clean gold electrode was pre-cleansed by the same procedure described in 3.1.2.2. The electro deposition of PANI:MPA-ZnSe-QDs composite onto gold electrode was achieved by the same exact procedure described in paragraph 3.1.2.3, scanning from a potential E = 1100 mV to E = -200 mV over 10 cycles at a scan rate of 100 mV s^{-1} in the solution containing 92 µL of 0.1 M aniline and 36 µL of MPA-ZnSe-QDs. After electro polymerisation and deposition of PANI:MPA-ZnSe-QDs film onto gold electrode, the modified electrode was then washed with double distilled water to remove possible unbound residues of aniline, MPA-ZnSe-QDs and HCl. The PANI:MPA-ZnSe-QDs modified gold electrode was then allowed to dry under nitrogen fume for about 2 hours after which 0.1 µM HRP enzyme stock solution was drop coated onto the polymeric zinc selenide quantum dots modified gold electrode resulting onto a film of HRP/PANI:MPA-

ZnSe-QDs deposited onto gold electrode. The final enzyme modified electrode was then allowed to dry for 4 hours at room temperature 25 ºC. The AuE/PANI:MPA-ZnSe-QDs /HRP has been defined in this context as the first biosensing system. The resulting AuE/PANI:MPA-ZnSe-QDs/HRP biosensor was then characterised electrochemically in phosphate buffer solution i.e. 0.1 M PBS of pH 7.0 for investigation of the electrochemical behaviour and electron transfer kinetics. After characterization, the biosensor AuE/PANI:MPA-ZnSe-QDs/HRP was used for quantitative determination of different concentrations of 17β-estradiol. The biosensor was then stored at 4 °C in 0.1 M PBS of pH 7.4 when not in use.

3.1.2.6 Preparation of AuE/Cystm/MPA-ZnSe-QDs/CYP3A4 biosensor i.e. the second developed biosensing system for the detection of 17β-estradiol

This second biosensor developed during this study was prepared by the following procedure: A new gold electrode was polished with 1, 0.5 and 0.03 μm alumina slurries in glassy polishing pads, minimum for 5 min on each pad, after polishing, the electrode was ultra-sonicated for about 15 min, with distilled water and absolute ethanol respectively to remove any possible absorbed alumina crystals on the electrode surface and rinsed carefully with distilled water. The above procedure resulted into a clean gold electrode. The clean Au electrode was then immersed into a solution containing 0.02 M cysteamine for 24 hours in the dark at room temperature, this resulted in a self assembled monolayer onto the gold electrode as described by Karolien and co-workers, 2008 [22], the electrode was then rinsed carefully with distilled water to remove any unbound cysteamine molecules. The cysteamine modified gold electrode was then immersed into solution containing 3-mercaptopropionic acid capped zinc selenide quantum dots in the presence of 0.1 M EDAC/NHS (1-ethyl-3-(3-dimethylaminopropyl) carbodiimide hydrochloride / N-hydroxysuccinimide) cross-linking agent (1:1) solution for 2 h, which then resulted in an MPA-ZnSe-QDs/Cystm film onto gold electrode. This modified gold electrode was allowed to dry for 2 hours in the dark. A 1 μM CYP3A4 enzyme stock solution (i.e. prepared by injecting of 9.1 μL suspension of CYP3A4 into a solution containing, 20 mM PBS of pH 7.4, 0.1 M EDAC, 0.1 M NHS, 0.02 mM EDTA and 1 mM DTT, stored in the refrigerator at -20 °C) was then drop coated onto the

AuE/Cystm/MPA-ZnSe-QDs electrode, the resulting CYP3A4 modified electrode was then allowed to dry for 3 hours at 4 °C. After the modification of the CYP3A4 enzyme, the final enzyme modified gold electrode was then defined as the biosensor AuE/Cystm/MPA-ZnSe-QDs/CYP3A4. The biosensor was then stored at 4 °C in 0.1 M PBS, pH 7.4 when not in use. This biosensor was then used for determination of different concentrations of 17β-estradiol.

3.1.2.7 Preparation of 17β-estradiol, estrone and 17α-ethynylestradiol standard solutions

The 0.001 M 17β-estradiol, estrone and 17α-ethynylestradiol standard solutions were prepared by dissolving the required compound in a 25/75 (ratio by volume) of absolute ethanol and 0.1 M PBS of the appropriate pH depending on the type of biosensor used. The solution was then sonicated for 30 min. The prepared solution samples were then stored at 4 °C for a day before use. The samples were again stored at the same temperature when not in use. The described preparation method for 17β-estradiol, estrone and 17α-ethynylestradiol was the same method discussed by Song and co-workers [47, 100].

RESULTS AND DISCUSSION

CHAPTER 4

4.1 RESULTS AND DISCUSSION

4.1.1 Characterization of MPA-ZnSe-QDs and PANI:MPA-ZnSe-QDs Composite

4.1.1.1 Optical studies of MPA-ZnSe-QDs and PANI:MPA-ZnSe-QDs composite

4.1.1.1.1 Optical studies of MPA-ZnSe-QDs

The absorption spectra of MPA-ZnSe-QDs was recorded from wavelength of 250 nm to 600 nm at bandwidth of 2 nm. The Figure 4-1 shows the absorption characteristics of MPA-ZnSe-QDs, used as support material for the biosensor systems developed.

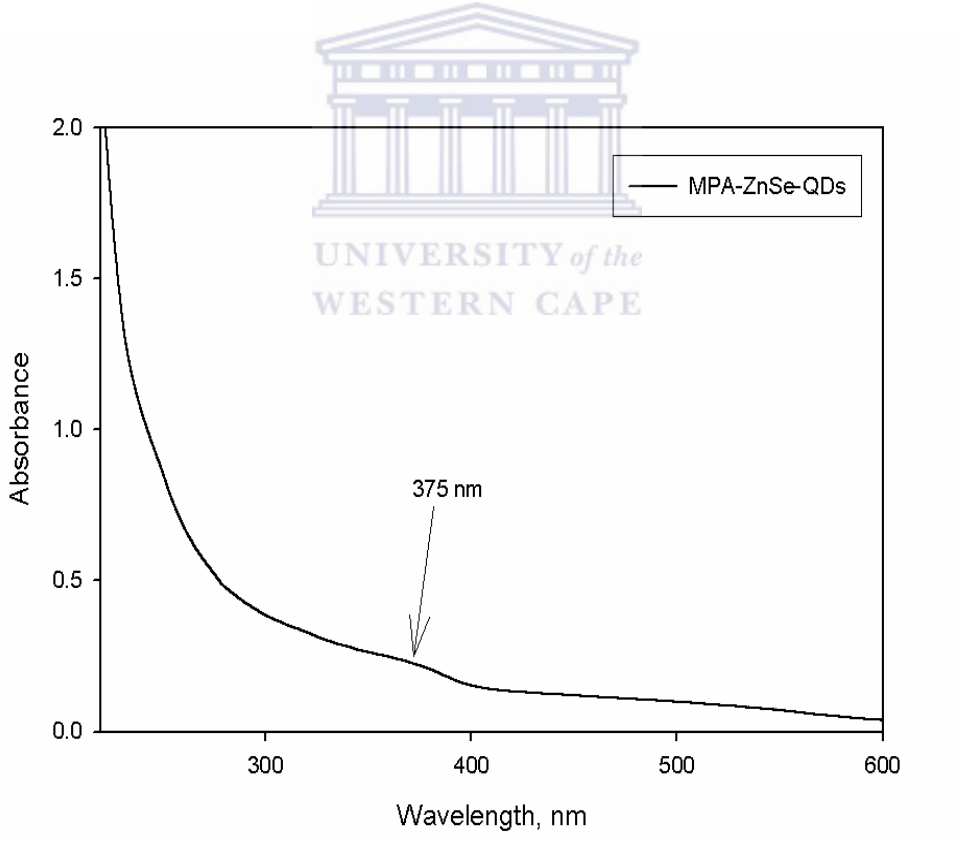

Figure 4-1: The UV-Vis absorption of MPA-ZnSe-QDs.

The MPA-ZnSe-QDs in Figure 4-1 showed a very broad weak absorption peak at 375 nm. This peak was deduced to be associated with electrons transition of d valence

electrons from Zn to Zn^* exited state. The energy associated with the deduced electronic transition was estimated by Plank's Law given by $\Delta E = h\nu = h\left(\frac{c}{\lambda_{max}}\right)$ Equation 4.1-1:

$$\Delta E = h\nu = h\left(\frac{c}{\lambda_{max}}\right) \qquad \text{Equation 4.1-1}$$

The change in energy of the absorbed light by MPA-ZnSe-QDs as interpolated from the UV-Vis absorption band was found to be 5.304 x 10^{-19} J. The absorption band at 375 nm was associated with the band gap energy of 3.4 eV [8] . The particle size of the quantum dots associated with this band gap energy from UV-Vis absorption spectra was estimated using the effective mass approximation model according to $E_g = \frac{h^2}{8a^2}\left(\frac{1}{m_e} + \frac{1}{m_h}\right)$ Equation 4.1-2 [8, 12]:

$$E_g = \frac{h^2}{8a^2}\left(\frac{1}{m_e} + \frac{1}{m_h}\right) \qquad \text{Equation 4.1-2}$$

Where E_g is the band gap (eV), a = is the particle size, h = is the planks constant, m_e is the mass of an electron = $0.17m_o$, m_h is mass of the hole = $1.44m_o$ (m_o = 9.1095 x 10^{-31} kg, is the mass of a stationary electron). The size of MPA-ZnSe-QDs estimated using the approximation was found to be 4.70 nm.

4.1.1.1.2 Optical studies of PANI:MPA-ZnSe-QDs composite

The UV-Vis spectrometry was used to study the electro-photonic properties of the composite PANI:MPA-ZnSe-QDs used as the support material for one of the developed biosensors. The UV-Vis studies of PANI: MPA ZnSe-QDs composite were recorded form the wavelength of 200 - 450 nm at a bandwidth of 2 nm.

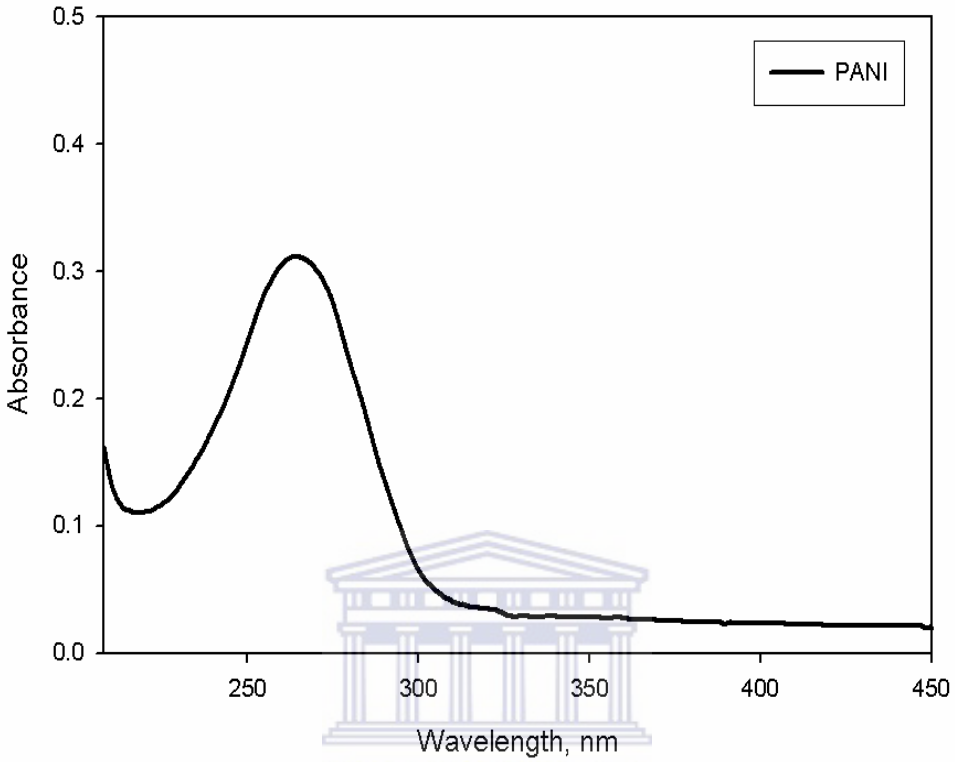

Figure 4-2: The UV-Vis absorption spectra of PANI.

The study was first done on PANI. The UV-Vis absorption characteristic of PANI (Figure 4-2) was an appearance of an intense absorption peak at wavelength of 275 nm, indicating the capability of PANI being able to absorb UV-Vis light at low wavelengths. The appearance of the peak at 275 nm for PANI indicated that the PANI itself was a photo-electronic conductor and exhibited some properties of the metals, thus a good conductor of electrons and a good light absorbing material The energy associated with the absorbed light of PANI at maximum wavelength was estimated using

Equation 4.1-2 and was found to be 7.956×10^{-19} J, slightly higher than that obtained for MPA-ZnSe-QDs which was 5.304×10^{-19} J. The slight difference in the obtained energies of absorbed light, for both MPA-ZnSe-QDs and PANI indicated that within the PANI:MPA-ZnSe-QDs composite, one of the material can be used to maximise or minimise the absorbed energy, by the forming a composite using different

ratios of one of the materials, which could results in switchable UV-Vis absorption energy properties.

Figure 4-3 shows the UV-Vis absorption by PANI:MPA-ZnSe-QDs composite with varying ratios of PANI to MPA-ZnSe-QDs and the influence of the ratios on absorbance intensity and wavelength.

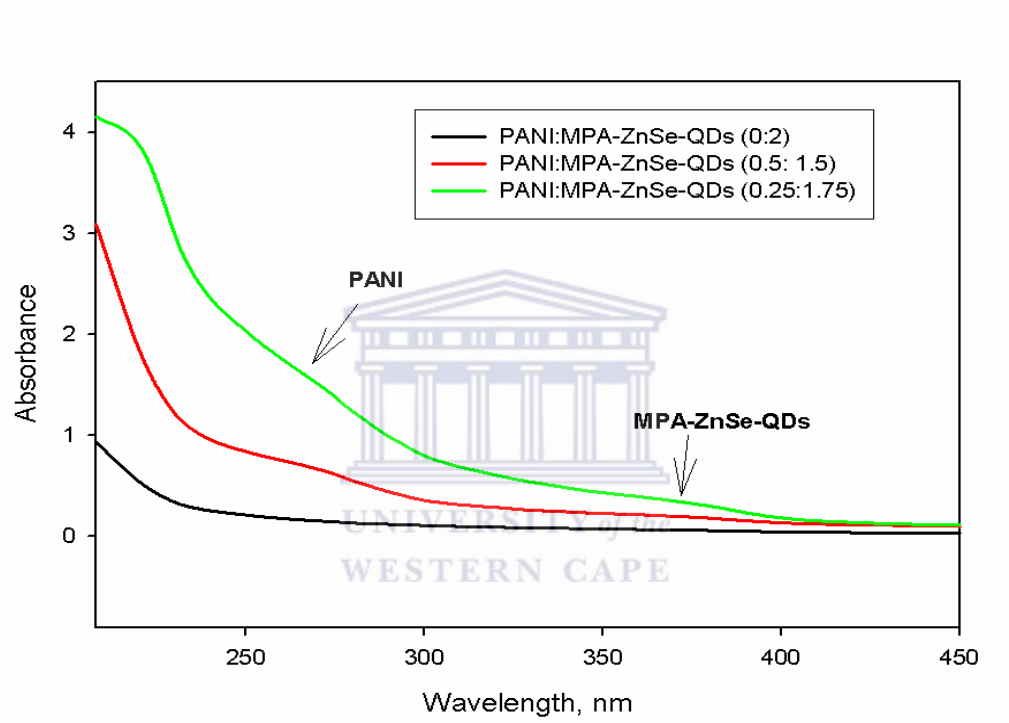

Figure 4-3: UV-Vis absorption of PANI:MPA-ZnSe-QDs.

In Figure 4-3, it was observed the composite (PANI:MPA-ZnSe-QDs), showed two broad absorption bands at wavelength of 275 nm, indicating the presence of PANI and the band at wavelength = 375 nm was an indication of presence of MPA-ZnSe-QDs within the composite. The occurrence of both for PANI and MPA-ZnSe-QDs within the composite indicated the formation of a very strongly composite that has photo-electronic properties between that of semiconducting MPA-ZnSe-QDs and PANI [88, 100].

4.1.1.2 Spectroscopy studies of MPA-ZnSe-QDs and PANI:MPA-ZnSe-QDs

4.1.1.2.1 Spectroscopy studies of MPA-ZnSe-QDs

The FT-IR analysis was done on liquid samples of MPA-ZnSe-QDs that were placed in between two NaCl plates. The FT-IR was operated from a wave number 4000 cm^{-1} to 750 cm^{-1}. The study was done to examine the structural and chemical properties of MPA ZnSe-QDs. The FT-IR spectrum of MPA-ZnSe-QDs (Figure 4-4), showed only four visible peaks comprised of three stretching frequencies at 3400 cm^{-1} , 2098 cm^{-1} and 1401 cm^{-1} and one band at fingerprint region which was 767 cm^{-1}.

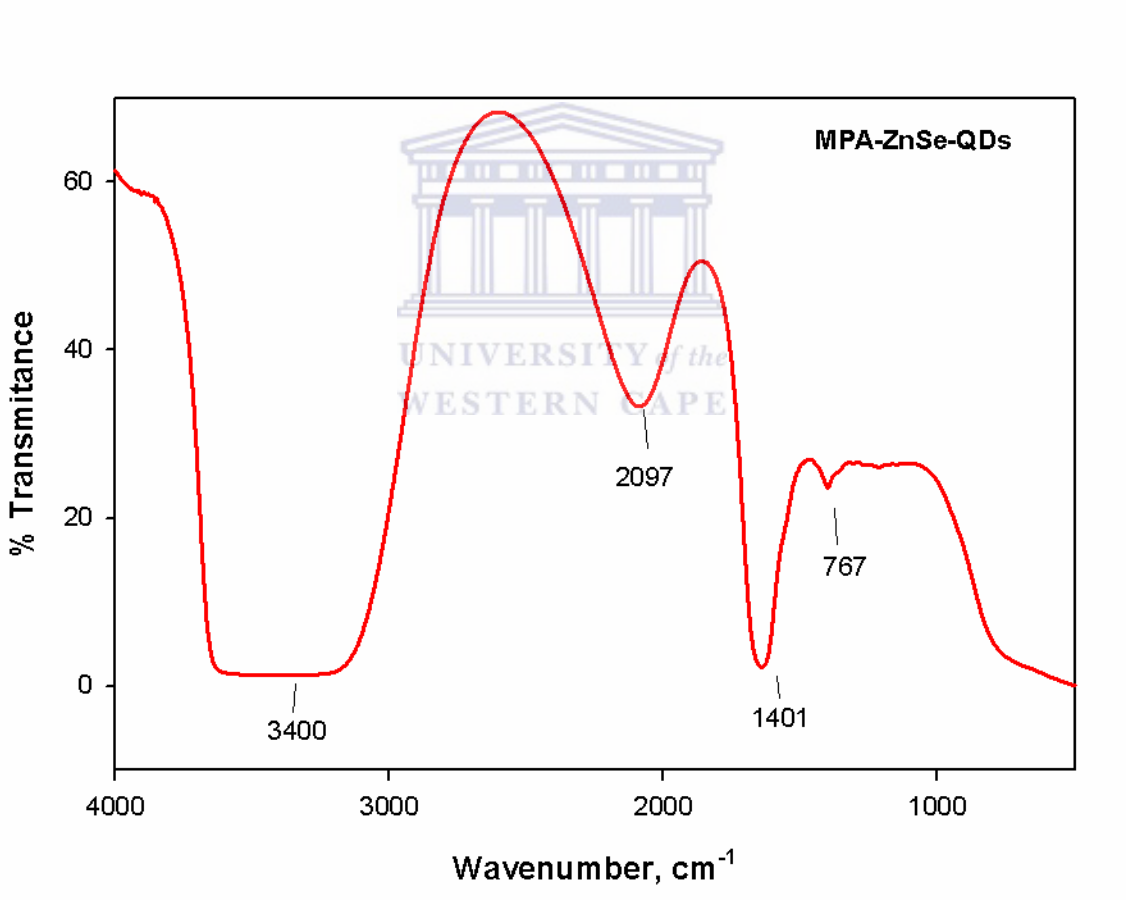

Figure 4-4: FT-IR spectrum of MPA-ZnSe-QDs.

From the spectrum in Figure 4-4, a typical structure of a single MPA-ZnSe quantum dot was suggested:

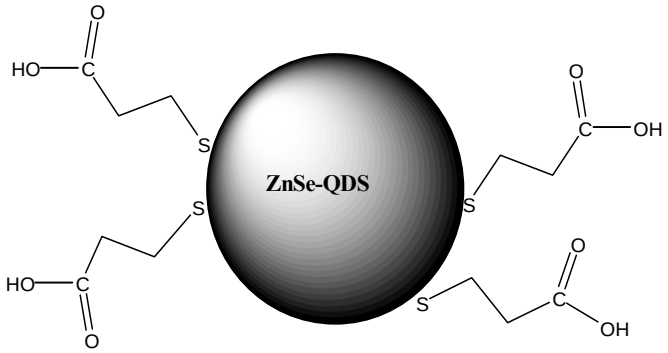

Figure 4-5: Illustration of a single MPA-ZnSe-QD.

The proposed structure of a single quantum dot was shown in Figure 4-5. The band at 1401 cm^{-1} was deduced to be due to C-C single bond of the 3-mercaptopropionic acid capping agent of the MPA-ZnSe-QDs, the weak band at 767 cm^{-1} was deduced to be caused by wagging of the same single bond, which occasionally occurs at fingerprint region of the spectrum. However, the peak at 2097 cm^{-1} might have been due to $\bar{\nu}(C=O)$ from the terminal carboxylic group [99] of the 3-mercaptopripionic acid capping of the ZnSe quantum dots in study, a broad peak at 3400 cm^{-1} might have been a resultant of $\bar{\nu}(OH)$ from the OH group of carboxylic acid derivative from the 3-mercaptopropionic acid capping agent, and unbound OH groups from water that was present during synthesis. The absence of a CH stretching frequency at 2850 cm^{-1} to 3000 cm^{-1} might have been either due the CH being concealed in the internal core of the quantum dots or the peak was predominated by the presence of the access amount of water within the MPA-ZnSe-QDs solution.

4.1.1.2.2 The spectroscopy studies of PANI:MPA-ZnSe-QDs composite

The spectroscopy of PANI:MPA-ZnSe-QDs composite (Figure 4-6) was studied using FT-IR to investigate the chemical bond properties of the newly formed composite.

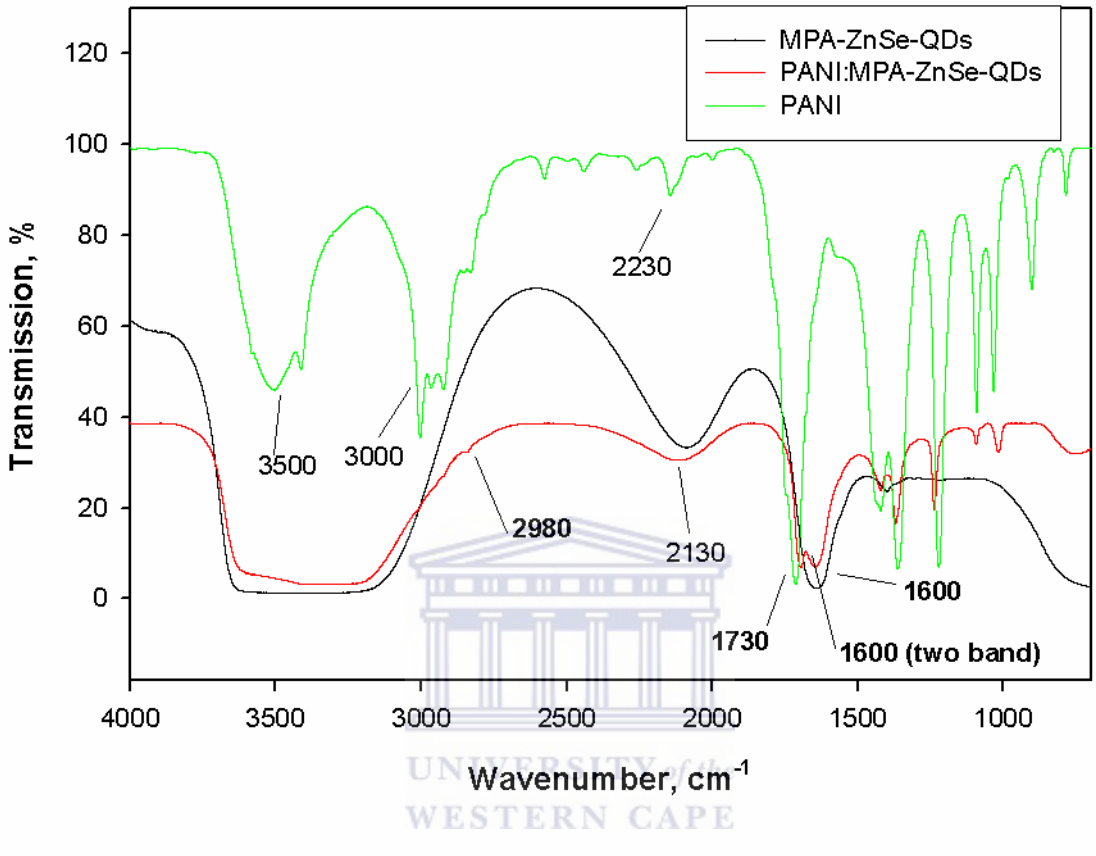

Figure 4-6: FT-IR spectrum of PANI, PANI:MPA-ZnSe-QDs and MPA-ZnSe-QDs**.**

In Figure 4-6; the very weak band at a stretching frequency: $\nu = 2980.02\ cm^{-1}$ observed for the PANI:MPA-ZnSe-QDs composite (red) was deduced to be the characteristic band of tertiary amine. This band might have been possibly resulted from the weak reaction of free carboxylic group (-COOH) in MPA-ZnSe-QDs and a neucleophilic nitrogen group ($N^{\cdot}$) of the emaraldine derivative PANI chain, illustrated by chain reaction in Figure 4-7. However the reaction might have been happening in partial parts of the exposed nitrogen groups of the polymer chain as illustrated in Figure 4-7.

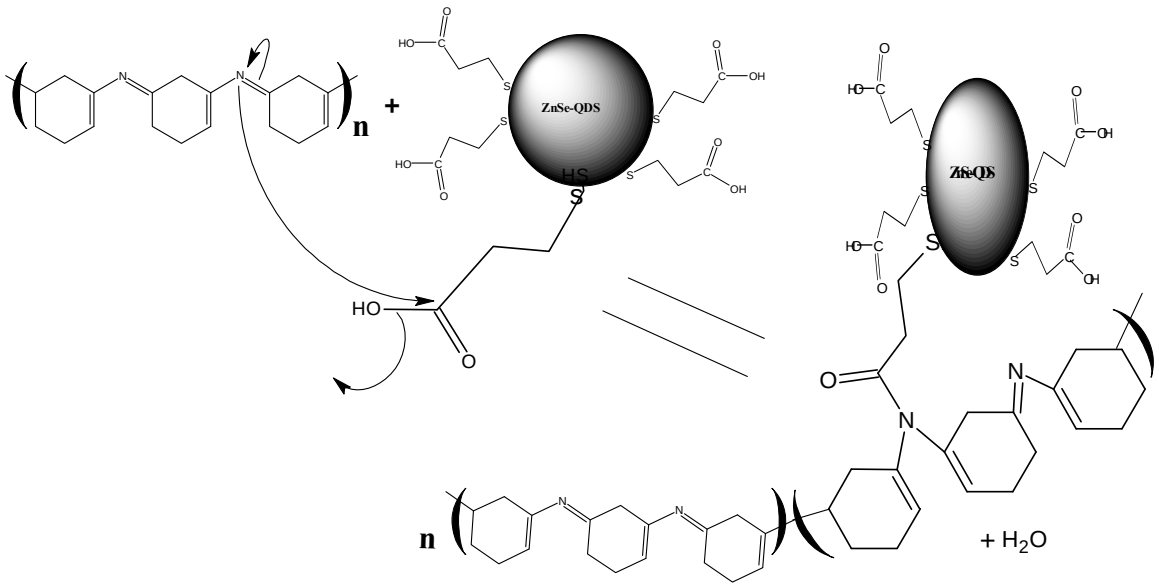

Figure 4-7: Represents a proposed reaction suspected to be occurring at the PANI bridges with carboxylic acid terminated MPA-ZnSe-QDs.

The postulated reaction of ZnSe-CH_2COOH groups (carboxylic groups of MPA-ZnSe-QDs) with. N-PANI (nucleophilic nitrogen of a tertiary amine from the emaraldine derivative of PANI) was also supported by an occurrence of an absorption peak at ν = 1600 cm^{-1} (shown in red in Figure 4-6) with two bands indicating a carbonyl group from an ester derivative [98]. The proposed chemical reaction was assumed to be the conversion of a carboxylic acid (-COOH) to an ester derivative (-CON). This observations might have indicated that the mercaptopropionic acid capped zince selenide quantum dots in this study might not had only physically embed themselves onto the polymer:PANI, also some of these quantum dots molecules chemically reacted with PANI resulting in the formation of an even much more stable composite PANI: MPA-ZnSe-QDs.

4.1.1.3 Microscopy studies of MPA ZnSe-QDs and PANI:MPA-ZnSe-QDs composite

4.1.1.3.1 Microscopy studies of MPA ZnSe-QDs

The microscopy of 3-mercaptopropionic acid capped zinc selenide quantum dots was studied using transmission electron microscopy (TEM). The method was used to study the shape and size of the MPA-ZnSe quantum dots used as support material for the biosensors developed.

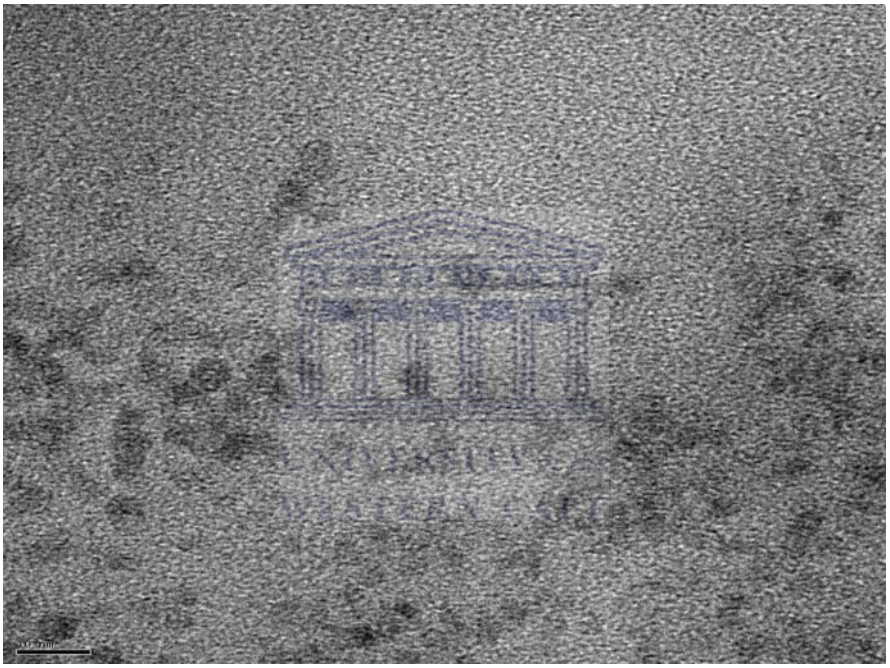

Scale: 10 nm:

Figure 4-8: The TEM images of MPA-ZnSe-QDs.

The size of the synthesised 3-mercaptopropionic acid capped zinc selenide quantum dots were found to be about 4.5 nm and mono dispersed with minimal aggregation as indicated by the TEM image in Figure 4-8. The dark spots were deduced to be ZnSe quantum dots. These nearly mono dispersed quantum dots exhibited the shape and appearance similar to what was reported by Kumar and co-workers [8] as quantum dots, synthesised by similar chemical method, which exhibit the Wurtzite shape [8].

The energy dispersive spectroscopy (EDS) spectrum was recorded using an EDAX microanalyser and detector. The MPA-ZnSe-QDs films were deposited onto screen printed carbon electrodes. The EDS spectrum of the MPA-ZnSe-QDs obtained was shown in Figure 4-9.

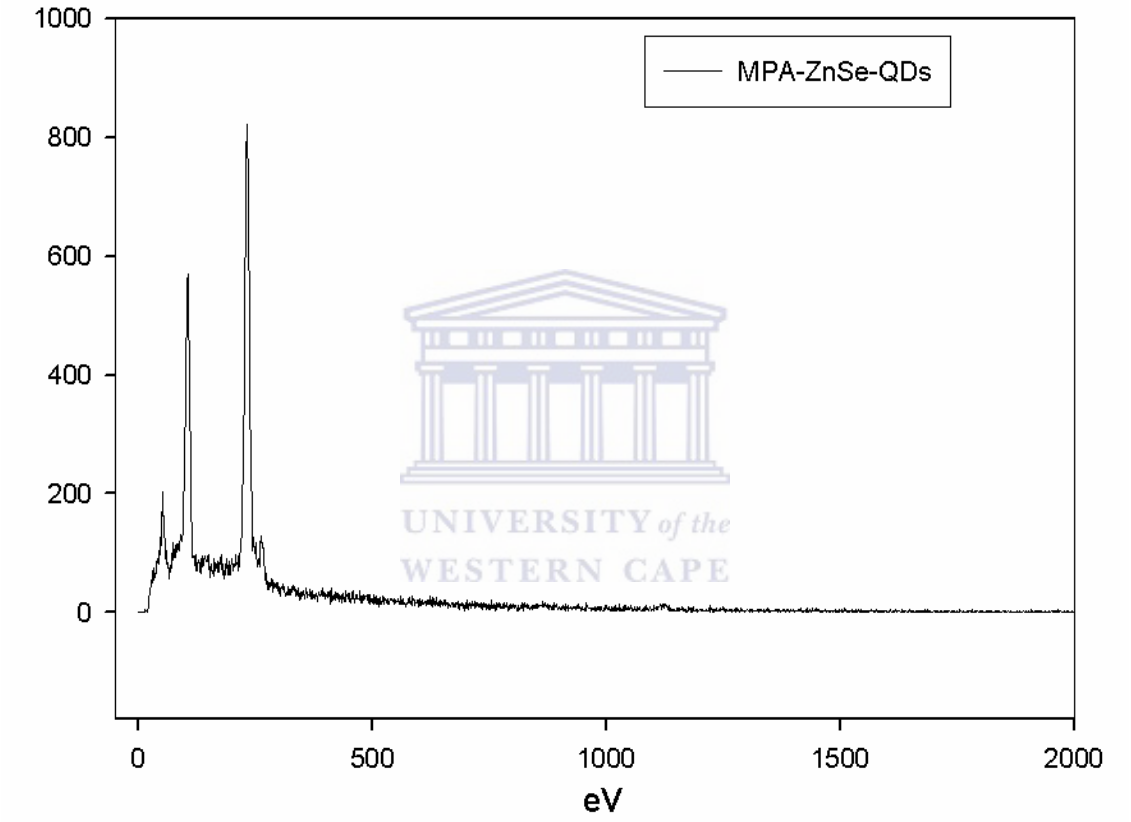

Figure 4-9: The EDAX spectrum of MPA-ZnSe-QDs.

In Figure 4-9, the EDS pattern of MPA-ZnSe-QDs showed major peaks occurring at different energies for carbon (C), oxygen (O), sodium (Na) , sulphur (S) , zinc (Zn) and selenide (Se) elements present at a screen printed carbon electrode surface. The EDS spectra could be explained as follows; the C, O and S peaks were caused by 3-mercaptopropionic acid derivative used as capping agent for ZnSe quantum dots. The high intensity of the peaks obtained for these elements might have been due to the fact that a single ZnSe quantum dot molecule not only capped by a single mercaptopropionic

acid group, but many 3-mercaptopropionic acid groups. The sodium (Na) energy peak was due to presence of sodium ion traces used during synthesis of the MPA-ZnSe-QDs. The appearance of Zn and Se elements at relatively close energies in the EDS spectrum might have gave an indication that the two elements were geometrically oriented close to each other, thus might be a proof of presence of very small traces of ZnSe nanomaterials.

4.1.1.3.2 Microscopy studies of the PANI:MPA-ZnSe-QDs composite

In this following context the SEM was used to study the structural and surface morphology of PANI:MPA-ZnSe-QDs composite. The study was first done on PANI (Figure 4-10).

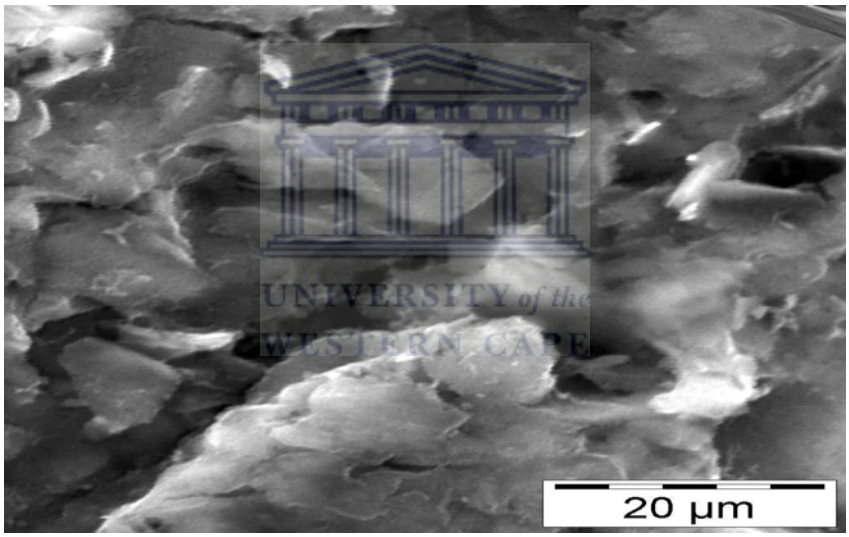

Figure 4-10: The SEM image of PANI on SPCE.

The SEM image of PANI, shown in Figure 4-10 clearly indicated that the PANI had thin layers which were oriented approximately ontop of each other. These layers of PANI flakes exhibited a smooth surface resembling micro sized oval cavities in between them, which would allow for entrapment or adsorption proteins necessary the enzymes within these cavities for much more enhanced stability of the enzyme onto the electrode thus a good support material for application in the biosensor. The SEM images of quantum MPA-ZnSe-QDs; shown in Figure 4-71 in the appendix exhibited charging effect due to quantum dots being highly fluorescent. The charging effect was also observed on the SEM image of the composite: PANI:MPA-ZnSe-QDs showed in Figure 4-72 in the appendix, which was identified to be caused by the presence of quantum dots within the composite. SEM in this case was regarded not to be a good method to study the morphological features of these highly fluorescent charging materials i.e. MPA-ZnSe-QDs and PANI:MPA-ZnSe-QDs, due to blur and poor SEM images produced.

However the TEM characterization technique was used for the study of PANI:MPA-ZnSe-QDs shown in Figure 4-11.

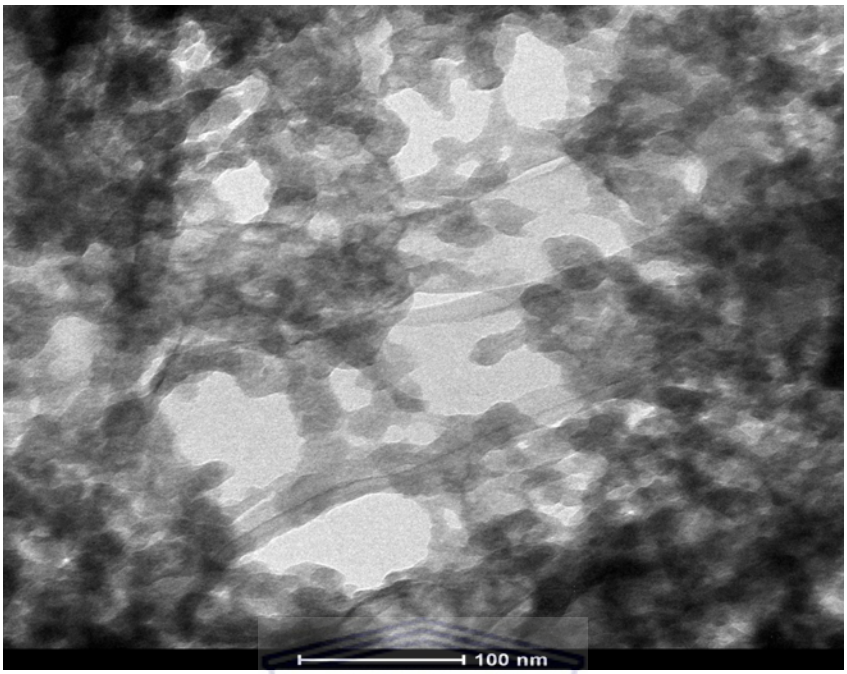

Figure 4-11: The TEM image of PANI:MPA-ZnSe-QDs.

The PANI:MPA-ZnSe-QDs composite exhibited a polymer like clustered chains with bridges connecting one polymer chain to the other. In addition this TEM image was used to estimate the thickness of the a single PANI chain of the composite and was somehow estimated to be about 50 nm measured from the bridges assumed to be PANI chains.

The EDS spectrum of PANI:MPA-ZnSe-QDs shown in Figure 4-12(b), was recorded and compared to the EDS spectra of PANI only shown by Figure 4-12(a), and MPA-ZnSe-QDs only shown by Figure 4-9. The spectra of the composite PANI:MPA-ZnSe-QDs shown in Figure 4-12(b), had lot of other interferences due to impurities present in the material, the spectra also showed the presence of trace amount of Fe, Mg, Na, Ni, but were eliminated and the spectra was redrawn concentrating on the EDS peaks of elements of interest. The PANI spectra; in Figure 4-12(a) showed three expected bands at energies less than 1000 eV, which were the bands of carbon (C), nitrogen (N) and chlorine (Cl).

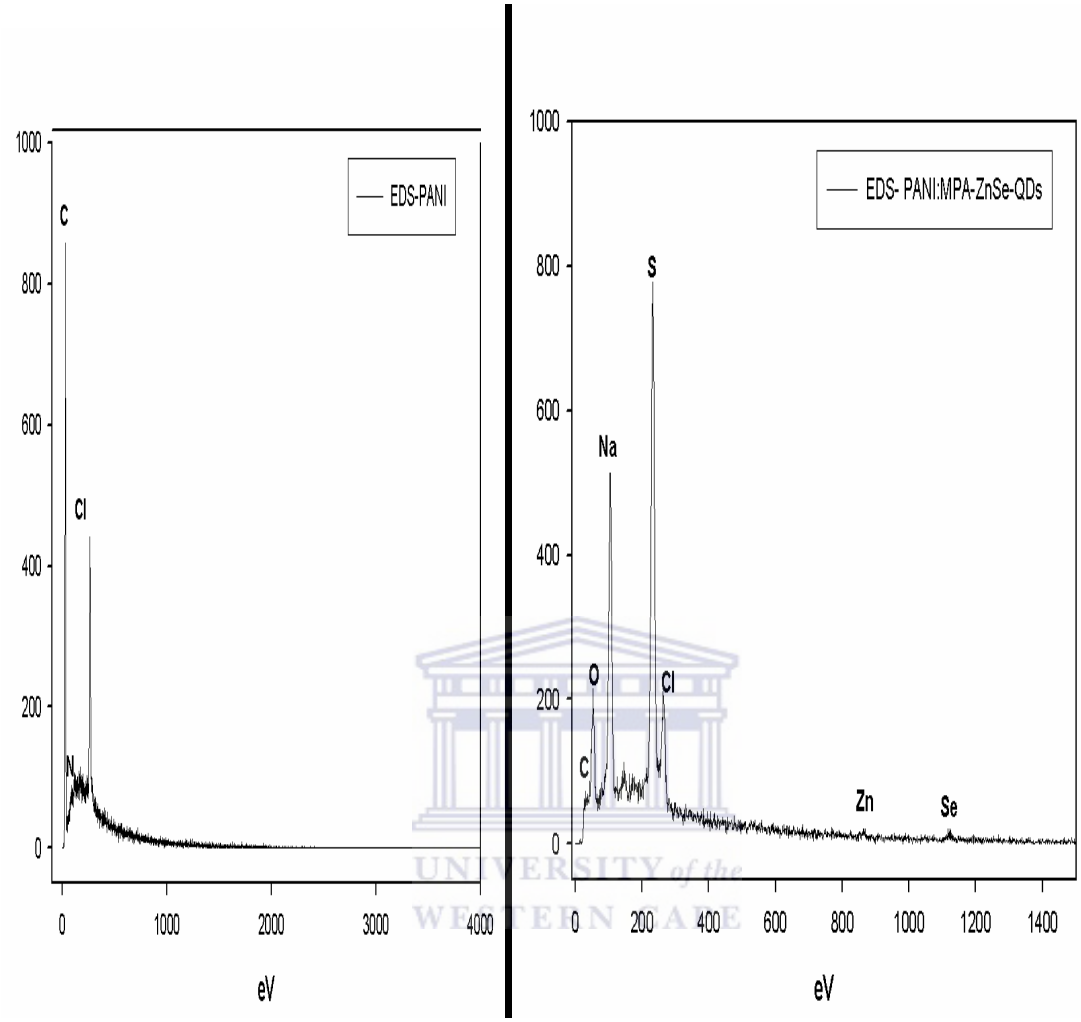

(a) (b)

Figure 4-12 : The EDAX spectrum of (a) PANI, (b) PANI:MPA-ZnSe-QDs.

The structural feature of emaraldine base of PANI shown in Figure 4-13; consists of only carbons, nitrogen and hydrogen as also depicted by the obtained EDS spectra; Figure 4-12(a). The EDS spectra showed an intense peak for chlorine, the chlorine might have been caused by the presence of the un-reacted hydrochloric acid used during the synthesis of PANI.

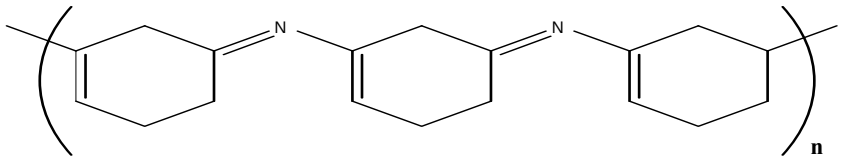

Figure 4-13: Structure of Emaraldine form of PANI

However the EDS spectra of PANI:MPA-ZnSe-QDs composite (Figure 4-12 (b)) showed the peaks for C, N, O, Na, S, Cl, Zn and Se, which were the indication of presence of relative quantities of 3-mercaptopropionic acid capped zinc selenide quantum dots and polyaniline within the newly developed composite.

4.1.1.4 Electrochemical Characterization of PANI:MPA-ZnSe-QDs in $K_3Fe(CN)_6$ and $K_4Fe(CN)_6$

This part of the study was performed using the electrolyte solution containing two different electrolytes $Fe(CN)_6^{3-}$ and $Fe(CN)_6^{4-}$ in 0.1 M PBS. The cyclic voltammetry studies were recorded from a potential scan of E = 1100 mV to E = -200 mV, at a scan rate of 100 m s^{-1} shown in Figure 4-14. For impendence studies, a scan rate of 50 mV s^{-1} was applied over the re-dox couples, at an over potential $E^{o\prime}$ = 200 mV and frequencies ranging from 1 Hz to 100 MHz. shown in

Figure **4-15**. The results were then fitted on Z-plot for determination of charge transfer resistance (R_{ct}).

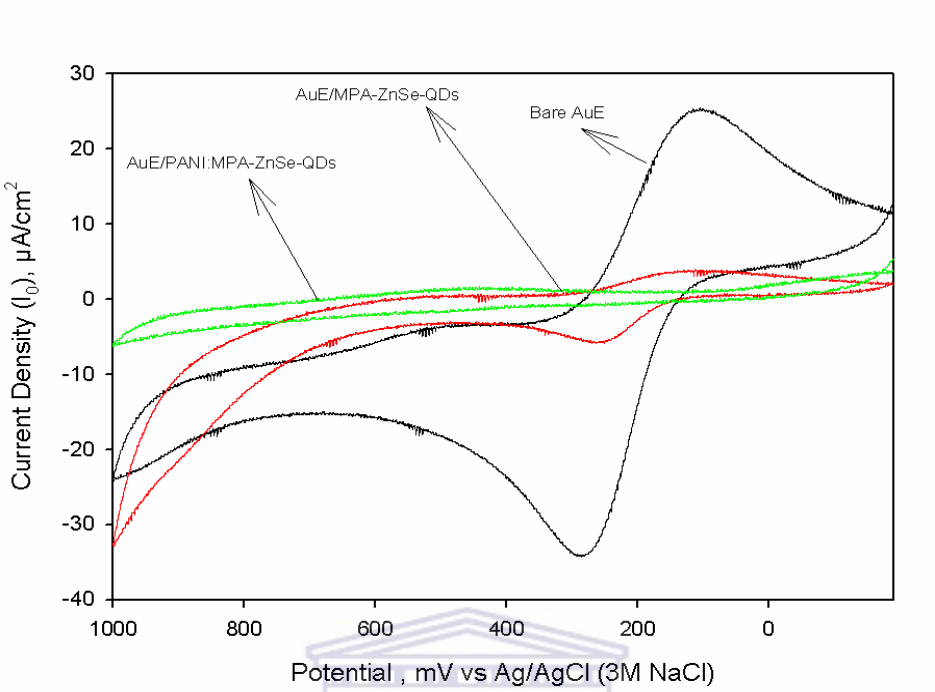

Figure 4-14: Cyclic Voltammograms illustrating the study of PANI:MPA-ZnSe-QDs films deposited onto gold electrode, in $K_3Fe(CN)_6$ and $K_4Fe(CN)_6$ at a scan rate 50 mV s^{-1}.

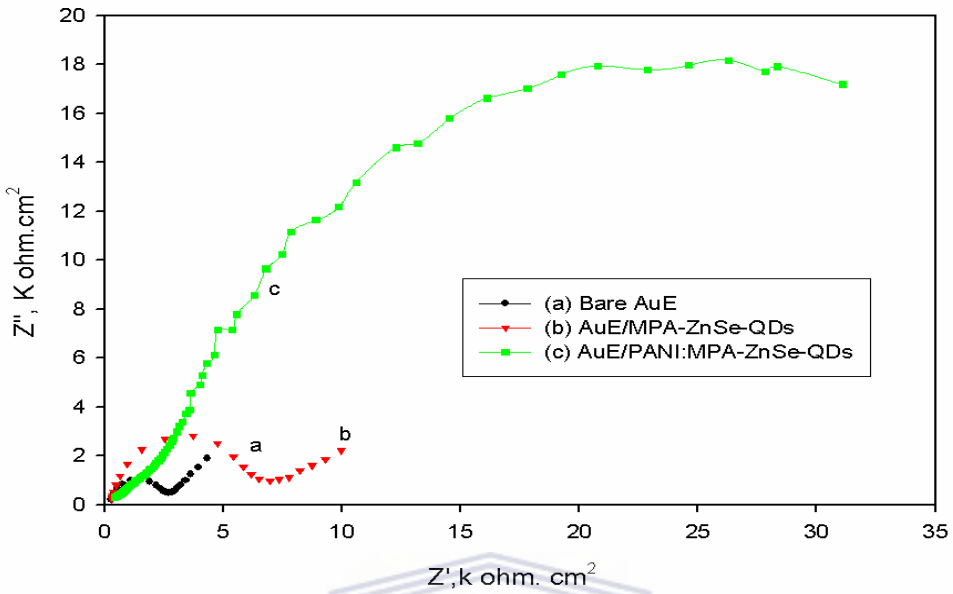

Figure 4-15: Impedance Niquist plots of: AuE/MPA-ZnSe-QDs and PANI:MPA-ZnSe-QDs films onto gold electrode recorded at E°′ = 150 mV in 0.1 M PBS containing $K_3Fe(CN)_6$ and $K_4Fe(CN)_6$.

The electrochemical impedance spectroscopy analysis shown by Figure 4-15, indicated that the bare gold electrode had a greater charge transfer resistance R_{ct} = 333.3 Ω, followed by MPA-ZnSe-QDs modified gold electrode with a charge transfer resistance: R_{ct} = 119 Ω. The PANI:MPA-ZnSe-QDs film modified gold electrode showed a charge resistance of almost 0 Ω. A great charge transfer resistance indicates the susceptibility of the material to charge opposition and depends on charged species on the electrolyte solution and the charge of the film immobilised onto the electrode surface. It was clearly identified that the MPA-ZnSe-QDs had much more great charge susceptibility to the charged materials present in $Fe(CN)^{2+/3+}$ solution than the PANI:MPA-ZnSe-QDs composite. Thus, the PANI:MPA-ZnSe-QDs composite showed much more less resistance to charge transfer in $Fe(CN)^{2+/3+}$ than the pure MPA-ZnSe-QDs thus indicated that the composite PANI:MPA-ZnSe-QDs was better charge conducting material and a better electron conductive than the unmodified MPA-ZnSe-QDs which might be due to presence of the conducting PANI film within the composite.

4.1.1.5 Electrochemical Characterization of PANI:MPA-ZnSe-QDs composite at different scans rates in HCl

The PANI:MPA-ZnSe-QDs film onto gold electrode was studied by cyclic voltammetry at different scan rates from 5-100 mV s^{-1} at a potential range from E = -200 mV to E = 1500 mV in a traditional electrochemical setup consisting of Ag/AgCl as a reference electrode, Pt mesh wire as the counter electrode and a gold disk electrode of area of 0.021 cm^2 as the working electrode, dipped into an acidic solution consisting 1 M HCl. The results shown in Figure 4-16, Figure 4-17 and Figure 4-18, indicated fast reversible and quasi-reversible reactions of three intermediates red-ox couples occurring at over potentials $E^{o\prime}$ = 100 mV, 50 mV and 350 mV for red-ox couples a-a′ (Pernigraniline transition P^+/P), b-b′ (Luecomeradine transition L/L^+) and c-c′ (Emeraldine transition E/E^+) respectively.

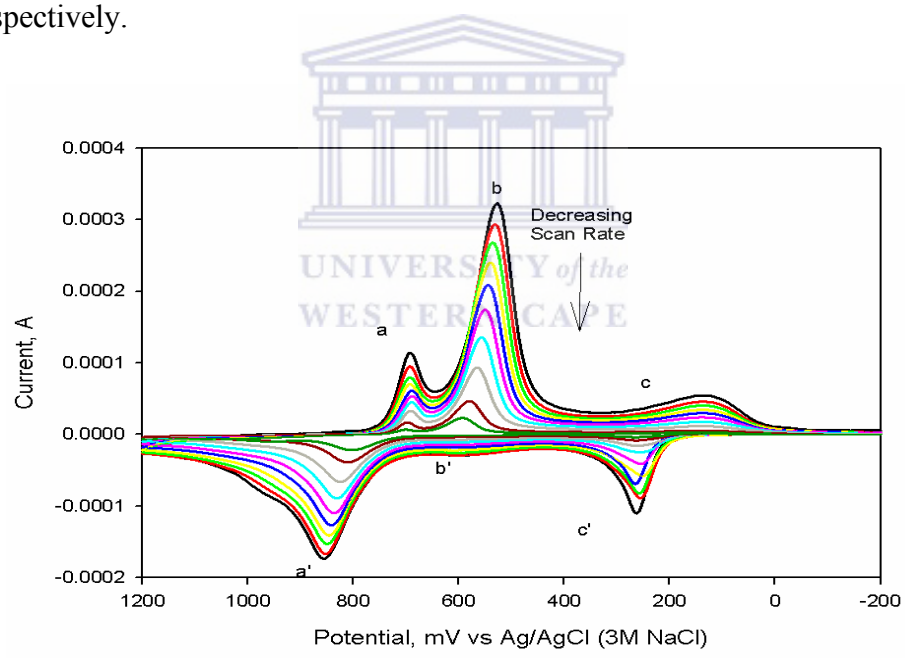

Figure 4-16: Cyclic voltammograms illustrating the electrochemical properties of PANI:MPA-ZnSe-QDs films deposited onto gold electrode in 1 M HCl at scan rates 5-100 mV s^{-1}, for aniline to MPA-ZnSe-QDs ratio of (1:0).

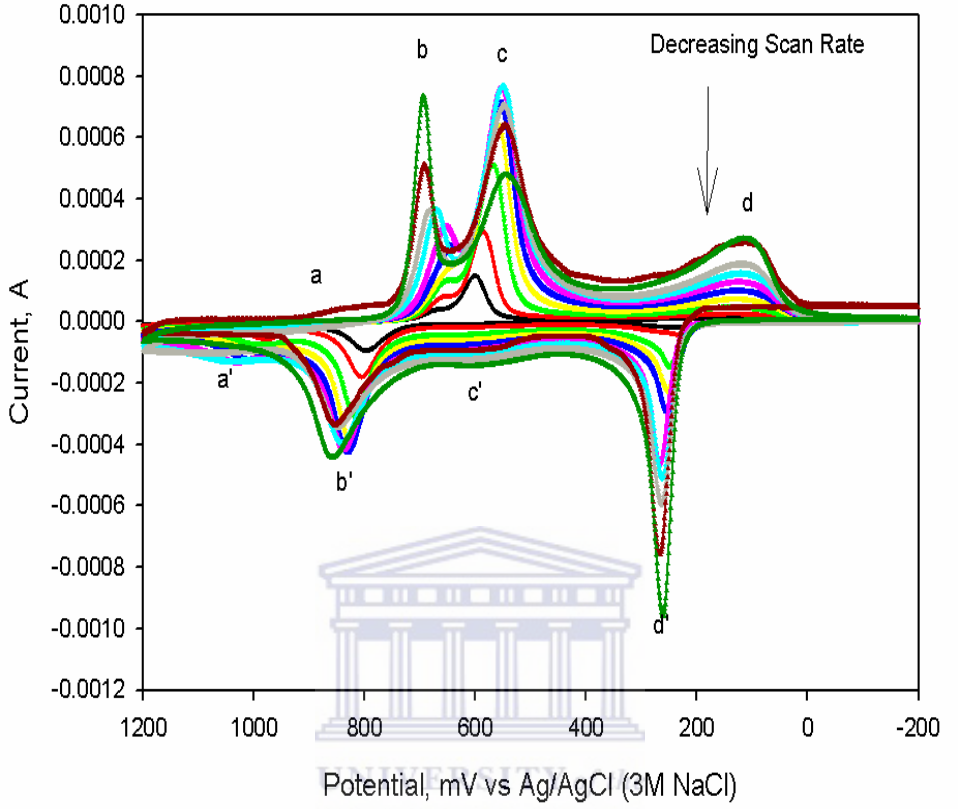

Figure 4-17: Cyclic voltammograms illustrating the electrochemical properties of PANI:MPA-ZnSe-QDs films deposited onto gold electrode in 1 M HCl at scan rates 5-100 mV s^{-1}, for aniline to MPA-ZnSe-QDs ratio of (1:2).

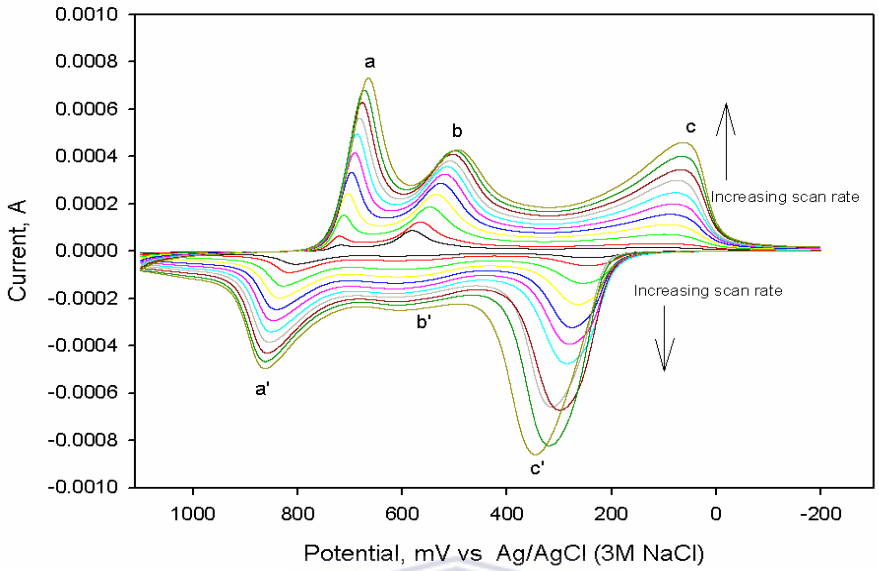

Figure 4-18: Cyclic voltammograms illustrating the electrochemical properties of PANI:MPA-ZnSe-QDs films deposited onto gold electrode in 1 M HCl at scan rates 5-100 mV s^{-1}**,** for aniline to MPA-ZnSe-QDs ratio of (2:1).

Better electrochemical properties of PANI:MPA-ZnSe-QDs composite with minimal overlap of peaks was achieved when the ratio of aniline to MPA-ZnSe-QDs was 2:1 (Figure 4-18) and this ratio had been used throughout the studies involving further electrochemical applications and characterisation of the composite. The obtained cathodic peak currents were; i_{pc} = 0.00005 A, i_{pc} = 0.0001 A and i_{pc} = 0.0002 A for the ratios (1:0) (i.e. Figure 4-16), (1:2) (i.e. Figure 4-17) and (2:1) (i.e. Figure 4-18) of aniline to MPA-ZnSe-QDs respectively with characteristic cathodic peak currents estimated at scan rate of 40 mV s^{-1} at peak c which is known to be the most stable peak indicating a single electron transfer reversible reaction [82, 86].

The electrochemical properties of the PANI:MPA-ZnSe-QDs composite films onto gold electrode were studied using two different approximation equation i.e. Randle Sevcik plot [94] and Brown Anson plot [94] for prediction and approximation of the type of electrochemical reaction controlling factors, whether the electron transfer reaction were controlled by adsorption or diffusion [94]. The study was done for 2:1 ratio of PANI:

MPA-ZnSe-QDs. Diagnosis of the obtained current to potential response peaks of PANI:MPA-ZnSe-QDs composite films in 1 M HCl was achieved by characterization of the linear plots obtained from Brown Anson and Randle Sevcik approximation equations:

- *Brown Anson equation*, for analysis of absorption controlled reactions the equation is given by [94]:

$$i_p = \frac{n^2 F^2 A \Gamma}{4RT} \nu \quad \text{Equation 4.1-3}$$

Where i_p = {Peak Current in A}, n = 1 {number of electrons}, F = 96485 C mol^{-1} {Faradays Constant}, A = 0.0201 cm^2 {geometric area of the electrode}, R = 8.314 J mol^{-1} K^{-1} {Gas Constant}, T = 298.15 K {absolute Temperature} and ν = {Scan Rate in V s^{-1}} and Γ is the surface concentration coverage. Below are the plots of Brown Anson modulation equation obtained at each re-dox couple observed in Figure 4-18.

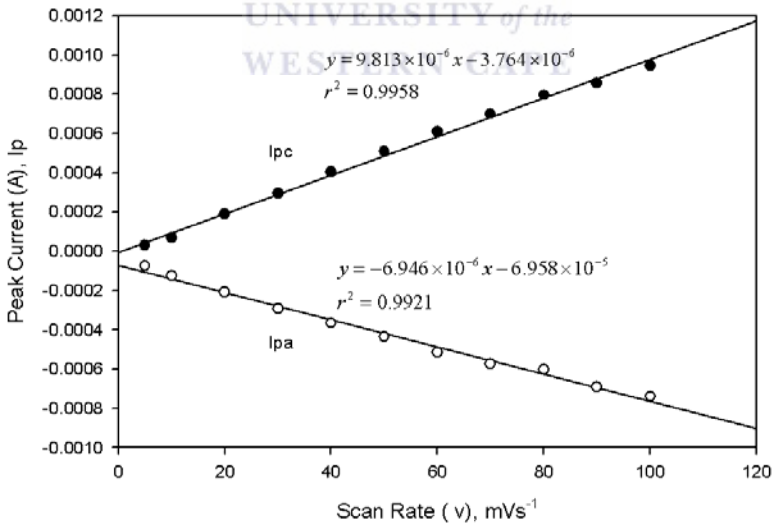

Figure 4-19: Brown Anson plots of PANI:MPA-ZnSe-QDs films deposited on gold electrode estimated at peaks a-a′.

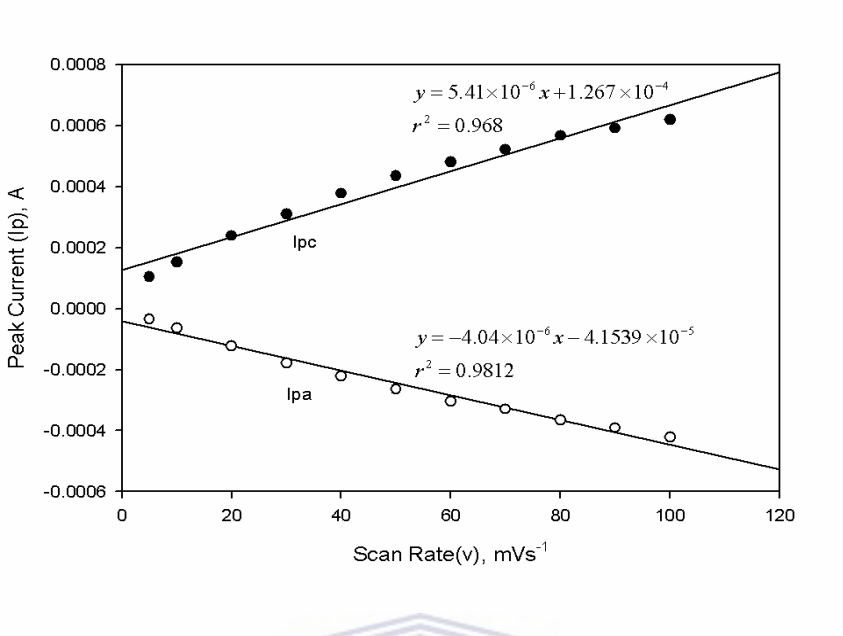

Figure 4-20: Brown Anson plots of PANI:MPA-ZnSe-QDs films deposited on gold electrode estimated at peaks b-b′.

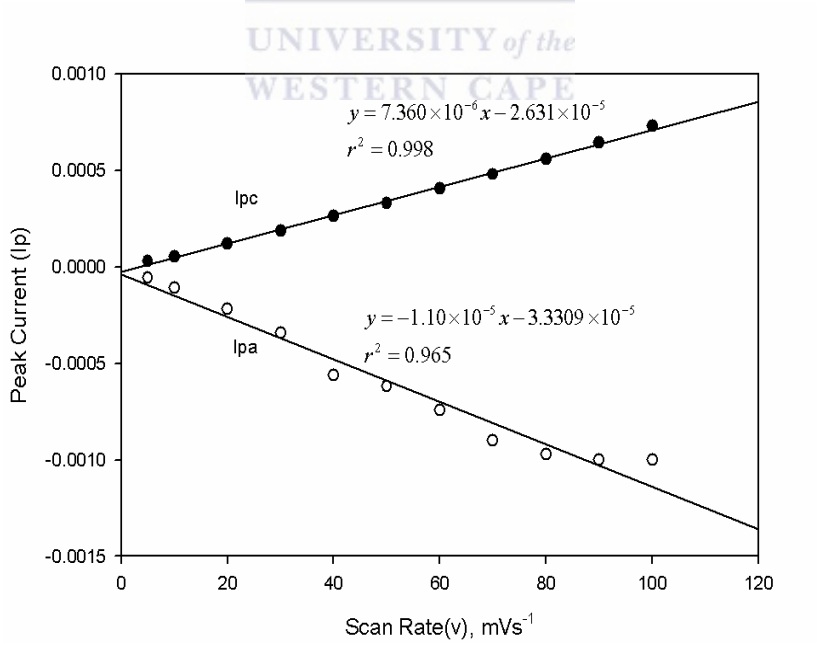

Figure 4-21: Brown Anson plots of PANI:MPA-ZnSe-QDs film deposited on gold electrode estimated at peaks c-c′.

Table 4-1: Characterization of PANI:MPA-ZnSe-QDs composite onto gold electrode in 1 M HCl at different scan Rates.

	a – a´		**b – b´**		**c – c´**	
Plot I_p vs. ν	a	a´	b	b´	c	c´
Slope	$9.813x10^{-6}$	$6.945x10^{-6}$	$5.413x10^{-6}$	$-4.040x10^{-6}$	$7.360x10^{-6}$	$-1.10x10^{-5}$
Intercept	$-3.764x10^{-6}$	$-6.958x10^{-5}$	$1.267x10^{-4}$	$-4.153x10^{-5}$	$-2.630x10^{-5}$	$-3.809x10^{-5}$
R^2	0.996	0.992	0.968	0.981	0.998	0.956
Plot I_p vs. $\sqrt{\nu}$	**a – a´**		**b – b´**		**c –c´**	
	a	a′	b	b′	c	c′
Slope	$1.224x10^{-6}$	$-8.708x10^{-5}$	$6.903x10^{-5}$	$-5.110x10^{-5}$	$9.030x10^{-5}$	$-1.389x10^{-4}$
Intercept	$3.241x10^{-4}$	$1.600x10^{-5}$	$-6.01x10^{-5}$	$9.539x10^{-5}$	$-2.566x10^{-4}$	$3.336x10^{-4}$
R^2	0.984	0.989	0.9981	0.997	0.952	0.976

The linearity of the Brown Anson plots summarised in Table 4-1: i_p vs. ν, confirmed that the radical coupling electron transfer reaction of the PANI:MPA-ZnSe-QDs composite, was somewhat adsorption controlled and the surface concentration Γ of the

adsorbed species was calculated from Brown Anson equation (i.e. Equation 4.1-3) to be Γ = 1.442 x10^{-5} mol cm^{-2} obtained at peak c-c′. The selection of the red-ox couple c-c′ was on the bases that this reduction oxidation electron transition is well known to be a stable reversible one electron transfer transition of PANI reported by Mathebe and co-workers [86], thus would be a good approximation of the whole behaviour of the system PANI:MPA-ZnSe-QDs films modified gold electrode in 1 M HCl. This obtained value for the surface concentration was lower that the surface concentration obtained by Munoz et al. [86] for a similar platform indicating the presence of quantum dots minimised the surface concentration with minimal coverage of the composite material onto gold electrode at the same time exhibiting higher electron conductivity which would result in a application of the composite PANI:MPA-ZnSe-QDs under study as a good and fast electron mediator for use in the biosensors developed.

Randle Sevcik Plot given, for analysis of diffusion controlled reactions [94].

$$i_p = 0.4463nFA\left[\frac{nF}{RT}\right]^{1/2} C_0^* D_0^{1/2} \nu^{1/2} \quad \text{Equation 4.1-4}$$

Where I_p = {Peak Current in A}, n = 1 {number of electrons}, F = 96485 C mol^{-1} {Faradays Constant}, A = 0.0201 cm^2 {geometric area of the electrode}, C_0^* = 0.1 mol dm^{-3} {Concentration of bulk substrate concentration}, R = 8.314 J mol^{-1} K^{-1} {Gas Constant}, T = 298.15 K {absolute Temperature} and ν = {Scan Rate in V s^{-1}} Where the diffusion co-efficient, was found to be D_0 = 1.6810 x 10^{-5} cm^2 s^{-1}. The linear co-efficient R^2 ranging from 0.998-0.999 (shown in Table 4-1) indicated a very good linearity of the Randle Sevcik plots: i_p vs. $\nu^{1/2}$, the linearity of these plots once again confirmed that the reaction was also diffusion controlled. The linearity of the demonstrated by both Brown Anson and Randle Sevcik plots confirmed that the overall catalytic kinetic reaction in the presence of 1 M HCl electrolyte, for the composite, PANI:MPA-ZnSe-QDs modified gold electrode was both diffusion controlled and absorption controlled. In addition to the electrochemical kinetic red-ox reaction on the

composite modified gold electrode being both adsorption and diffusion controlled, a shift in the potential with 10 folds of $\Delta E_{p/2} = 30/n$ with increasing scan rate observed was a clearly indicated that the electron transfer reaction within the PANI:MPA-ZnSe-QDs composites was a quasi-reversible electrochemical first order reaction following reversibility.

4.1.1.6 Comparison of different electrolyte solution used for characterization of PANI: MPA ZnSe QDs, at scan rate 50 mV s^{-1}

The study was done to examine the stability and electrochemical characteristics of the PANI:MPA-ZnSe-QDs composite films, studied in different electrolyte solutions, 5 mM $Fe(CN)^{3+/2+}$ and 1 M HCl both at scan rate $\nu = 50$ mV s^{-1}. The cyclic voltammetry studies were performed from a potential range E = 1100 mV to E = -200 mV, at a scan rate of 50 mV s^{-1}. For the electrolyte solution 5 mM $Fe(CN)^{3+/2+}$, the quasi- reversible red-ox couple was observed with $i_{pc} = 2.10 \times 10^{-9}$ A and $i_{pa} = 1.667 \times 10^{-8}$ A corresponding to $E_{pc} = 100$ mV and $E_{pa} = 200$ mV respectively (at $E^{o\prime} = 150$ mV) , in Figure 4-14. This typical behaviour was also observed when the composite was studied in 1 M HCl with re-ox current peaks occurring almost at the same peak potentials, far most negative potentials Figure 4-18, $E_{pc1} = 100$ mV and $E_{pa1} = 250$ mV ($E^{o\prime} = 175$ mV) but the intensity of current peaks was quite different, with $i_{pc1} = 2.57 \times 10^{-4}$ A and $i_{pa1} = 1.43 \times 10^{-3}$ and additional currents peaks were observed at other potential, which are usually representative of composites with PANI in acidic medium especially hydrochloric acid [89]. The characterizations of the composite in different electrolyte solutions and the obtained kinetic parameters (i.e. for studies in 1 M HCl the over potential was, $E^{o\prime} = 175$ mV and standard rate constant $k^o = 4.352 \times 10^{-6}$ cm^2 s^{-1} and in the case of $Fe(CN)^{3+/2+}$ the parameters were $E^{o\prime} = 150$ mV, $k^o = 3.2 \times 10^{-4}$ cm^2 s^{-1}) and assumed that the transfer co-efficient α was 0.5 for both studies, thereof indicated that the electrochemistry of the composite under study immobilised onto an electrode was dependent on the type of the electrolyte solution used for characterisation, on the bases of the difference in the obtained kinetic electron transfer parameters which might have been also due to the type of electrolyte used and its concentration thereof with characterization of the composite more preferable in HCl.

4.1.1.7 Further Characterization of the PANI:MPA ZnSe-QDs, PANI and MPA-ZnSe-QDs in 1 M HCl

The study was performed in order to identify the difference in the electrochemistry of various films used in fabrication of the composite PANI:MPA-ZnSe-QDs and their behaviour in HCl in order of identification the nature of current peaks generated during the characterization of the composite. The films included PANI, and MPA-ZnSe-QDs and PANI:MPA-ZnSe-QDs. The cyclic voltammetry studies of the different films onto gold electrode were performed at a potential range between E = 1500 mV to E = -200 mV, in the electrolyte solution containing 1 M HCl, at 25 $^{\circ}$C at a scan rate of 50 mV s^{-1}. The obtained cyclic voltammograms were represented by Figure 4-22 and Figure 4-23:

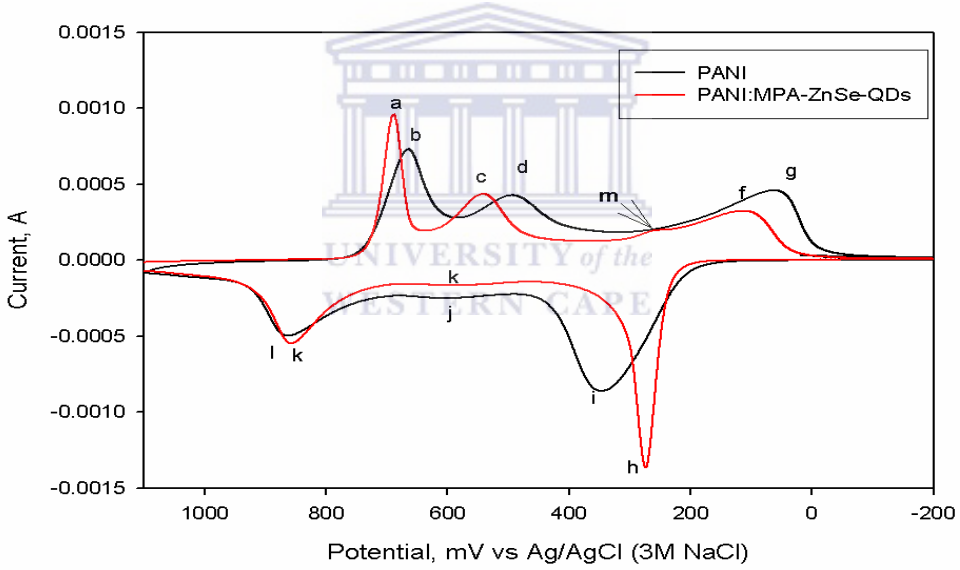

Figure 4-22: Cyclic voltammograms representing the electrochemistry of: PANI and PANI:MPA-ZnSe-QDs in 1 M HCl at scan rate 50 mV s^{-1}, 25 ^{o}C.

The voltammograms in Figure 4-22 were due to the electrochemistry of the PANI and PANI:MPA-ZnSe-QDs films deposited onto a gold disk electrode. The PANI films (black voltammogram) showed three reduction peaks and three oxidation peaks as

expected for the PANI often the j peak is not well pronounced, indicating the presence of a pernigraniline derivative of PANI usually occurring at $E_{pa/pc}$ (k) = 600 mV [89] which was associated with partially reduced and partially oxidised PANI ,thus exhibiting neutrality. The peak f, E_{pc} = 100 mV was a resultant of a fully reduced PANI derivative emaraldine which had been described by Jamade and co-workers, [89] to occur at the potential around E = 100 mV, this derivative has been identified as the oxidation state representing the fully reduced form of PANI emaraldine. Lastly the peak k at E = 800 mV was identified to be associated with the oxidation state of a fully oxidised form of PANI derivative leucomarlnadine. However in the presence of MPA-ZnSe-QDs (red voltammogram) all the peaks exhibited by the normal PANI were observed but there was an appearance of a shoulder current peak identified by m at a potential of E_{pc} = 213 mV, Figure 4-22 directly onto peak f: E_{pc} = 100 mV proportional to g current peak in PANI which did not exhibit a shoulder current peak. The peak was deduced to be occurring due to electronic transfer reaction onto the composite modified gold electrode which might have been generated due to interaction of the electrolyte solution with the MPA-ZnSe-QDs within the composite PANI:MPA ZnSe-QDs. In addition to appearance of the peak m in the composite, the voltammograms for the PANI:MPA-ZnSe-QDs indicated faster electron transfer properties deduced by estimation of the diffusion co-efficient. When comparing the two films onto the gold electrode, the films exhibited slightly different diffusion co-efficient characterised at peaks occurring at far most negative potentials i.e. f-i and g-h , the obtained kinetic parameters, diffusion co-efficient were D_o = 1.538 x 10^{-5} cm^2 s^{-1} and D_o = 1.885x 10^{-5} cm^2 s^{-1} for PANI and PANI:MPA-ZnSe-QDs respectively, indicating that the PANI:MPA-ZnSe-QDs film exhibited a faster electron transfer kinetics when compared to PANI alone. In addition to fast electron transfer kinetics within the composite, a shift in the potential with 10 folds of $\Delta E_{pc/2}$ = 30/n with increasing scan rate was observed, which was an indication that the electron transfer reaction within the PANI:MPA-ZnSe-QDs composites was a very fast quasi-reversible electrochemical first order reaction with k^o = 2.4 x 10^{-4} cm^2 s^{-1} [94]. However when the same characterization was done on MPA-ZnSe-QDs film (shown in Figure 4-23) and

compared to the PANI:MPA-ZnSe-QDs composite both immobilised onto gold the electrode.

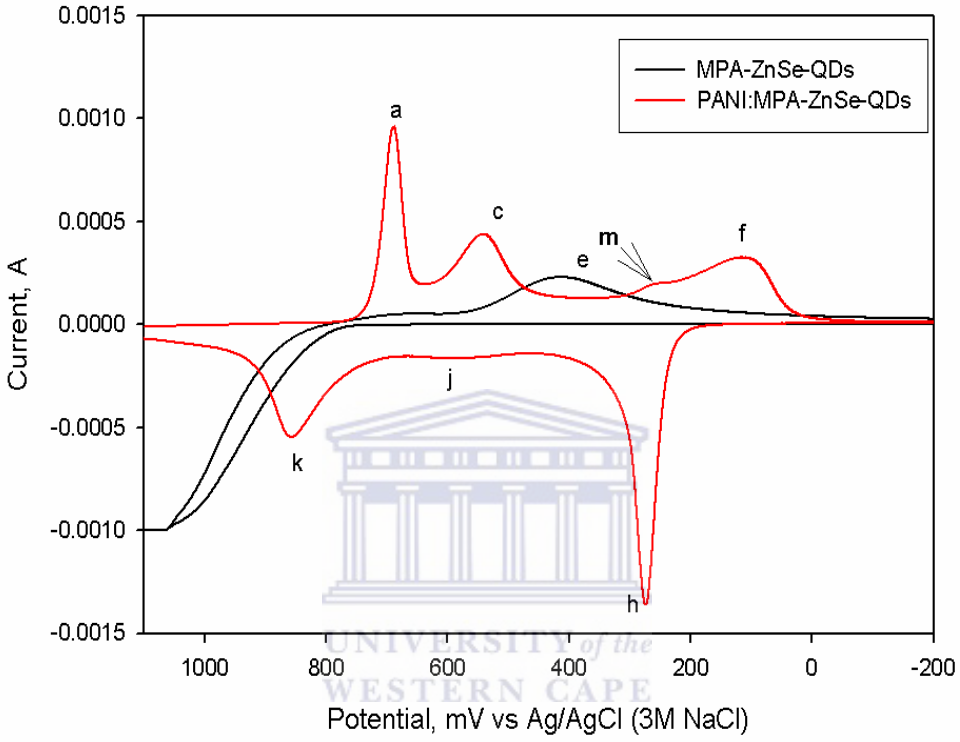

Figure 4-23: Electrochemical characterisation of: MPA-ZnSe-QDs and PANI:MPA-ZnSe-QDs film in 1 M HCl at 50 mV s^{-1}, 25 ºC.

As indicated by Figure 4-23, the MPA-ZnSe-QDs film onto gold the electrode in 1 M HCl (black) exhibited a single reduction peak which occurred at a potential E_{pc} = 420 mV identified by peak labelled e. Thus, the study proved once again that the composite PANI:MPA-ZnSe-QDs composite exhibited electrochemical properties of both PANI and MPA-ZnSe-QDs simultaneously.

4.1.2 Characterization of AuE/PANI:MPA ZnSe-QDs/HRP biosensor

4.1.2.1 Selection of appropriate scan rate for the detection of 17β-estradiol

The motive of this study was to monitor the appropriate scan rate suitable to ensure a maximum response and reasonable stability of HRP/PANI:MPA-ZnSe-QDs biosensor film onto gold electrode. This was performed using three-standard electrode system. The working electrode: was comprised AuE/PANI:MPA-ZnSe-QDs/HRP prepared by the method described in 3.1.2.5, the electrolyte solution was comprised of 0.1 M PBS of pH 7.0 at 25 $^{\circ}$ C in the presence of 0.1 M KCl electro active material. The studies were performed under oxygen free environment by degassing the electrolyte solution for 15 min by a purge of argon gas. The cyclic voltammetry were recorded from a potential of E = -200 mV to E = 1500 mV at scan rate from 5 mV s^{-1} to 100 mV s^{-1}.

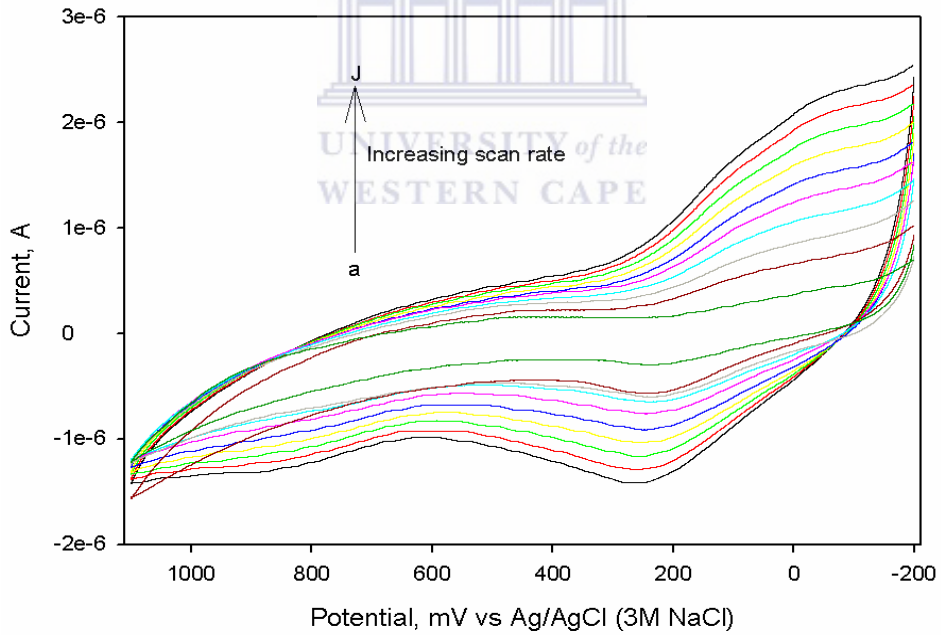

Figure 4-24: Cyclic voltammograms of AuE/PANI:MPA-ZnSe-QDs/HRP biosensor at different scan rates from (a)-(j): 10, 20, 30, 40, 50, 60, 70, 80, 90 and 100 mV s^{-1}respectively in 0.1 M PBS, pH 7.0, 25 $^{\circ}$C.

In Figure 4-24; it was observed that a scan rate of 10-20 mV s^{-1} was low enough to minimize the capacitive current or background and has been used through out the cyclic voltametric studies, performed using AuE/PANI:MPA-ZnSe-QDs/HRP biosensor.

As shown by the voltammograms in Figure 4-24, at higher scan rates the biosensor AuE/ PANI:MPA-ZnSe-QDs/HRP exhibited some electronic properties of the composite PANI:MPA-ZnSe-QDs characterised by the oxidation peak at E_{pa} = 200 mV, that was prominent at a scan rate above 20 mV s^{-1}. In this context it was an indication of electron fouling thus a desire for use of scan rates below 20 mV s^{-1} would be favourable for the studies using this biosensor system to avoid such instance. At higher scan rates three current response peaks (as indicated by the voltammograms in Figure 4-24), were observed with two weak reduction peaks occurring at E_{pc} = 100 mV and E_{pc} = -10 mV and a single oxidation peak occurring at E_{pa} = 200 mV. The reduction peak at E_{pc} = 100 mV was deduced to be resultant of a minimal capacitive current generated by the movement of electro-active species in solution. The cyclic voltammograms due to capacitive currents are usually not well pronounced peaks, because the current generated outside the double layer of the electrode is very minimal and usually not observable [94]. The reduction peak at E_{pc} = -10 mV was deduced to be due to the catalytic current produced by the biosensor, due to the presence of the enzyme, which is common behaviour of enzymes [101]. In this case the outside surface of the biosensor is the enzyme molecule; HRP, which might be the caused by transition of amino acid derivative present closely to this enzymes active site i.e. HRP-COOH + H_2O ➔ HRP-COO^- + H_3O^+ + e^-. Carboxylic acids are very week acids and dissociate readily in water, in relation to the context, during this dissociation process electrons are lost and gain simultaneously by the enzyme and electrolyte solution respectively. The oxidation peak occurring at a potential of E_{pa} = 200mV might have been a resultant of the minimal current generated by interaction of exposed mediator composite films, in the case where the film is thinner. Thus a need of use of thinner material is crucial to avoid such flaws. The peaks were characterised by the use of Randle Sevcik equation (i.e. Equation 4.1-4) for determining the rate at which the species diffuse within the layers of the AuE/PANI:MPA-ZnSe-QDs/HRP biosensor.

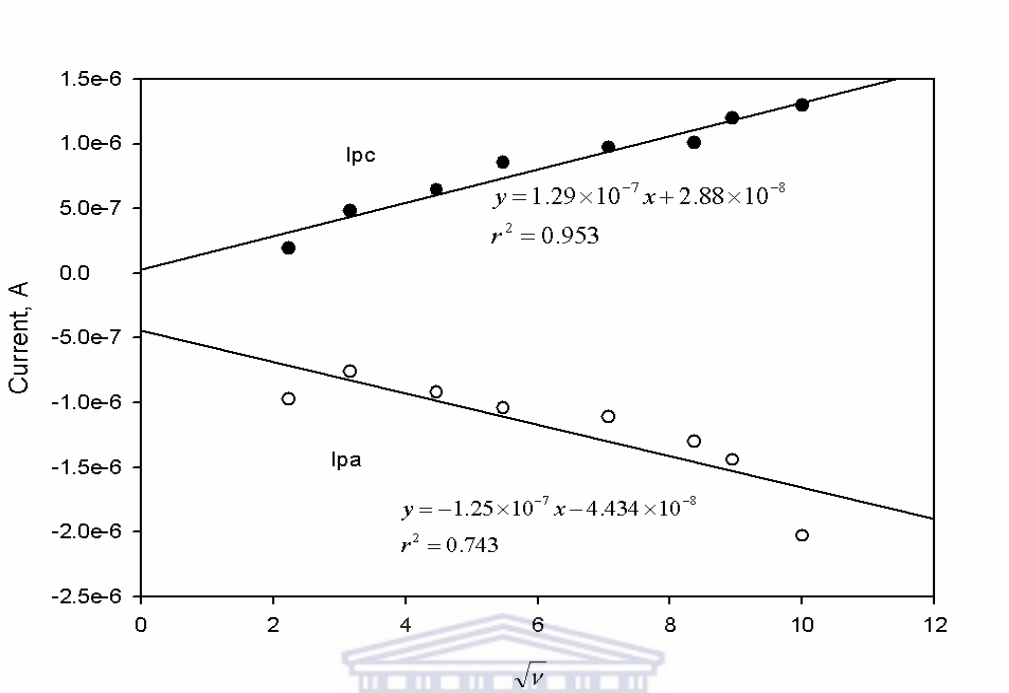

Figure 4-25: Randle Sevcik plots of AuE/PANI:MPA-ZnSe-QDs/HRP biosensor responses studied in 0.1 M PBS, pH 7.0 at different scan rates for determination of the diffusion co-efficient D_0.

The plots in the Figure 4-25 indicated that the reduction reaction that was occurring at E_{pc} = -10 mV was diffusion controlled with correlation co-efficient of R^2 = 0.953 and the diffusion co-efficient was found to be D_o = 1.569 x10^{-5} cm^2 s^{-1}, indicating faster electron transfer kinetics within diffusion layer of the biosensor. However the oxidation current peak occurring at E_{pa} = 200 mV had a correlation co-efficient of R^2 = 0.743 indicating no linearity in the Randle Sevcik plots, an obvious case was that this oxidation reaction that was occurring at that potential; was adsorption controlled rather than diffusion controlled. This could be due to the presence of the polymer PANI:MPA-ZnSe-QDs composite, some of the oxidised electro-active species get adsorbed or trapped within the mediator layer of the biosensor which was a typical electrochemical behaviour of PANI:MPA-ZnSe-QDs composite.

4.1.2.2 Choice of potential window for the quantitative determination of 17β-estradiol

The purpose of this study was to select the appropriate potential range for the determination of 17β-estradiol. The studies were performed under partial oxygen atmosphere achieved by degassing the 0.1 M PBS for at least 5 min only once before the beginning of the experiment. The cyclic voltammograms were recorded first from a very wide potential window of E = 1100 mV to E = -1000mV for the first set of voltammograms and the potential window was changed and minimised to E = 500 mV to E = -600 mV, all the voltammograms were monitored at a scan rate of 20 mV s^{-1}, in 0.1 M PBS, pH 7.0 at different concentrations of 17β-estradiol i.e. 0 µM, and 1.0 µM. The cyclic voltammograms obtained were shown in Figure 4-26.

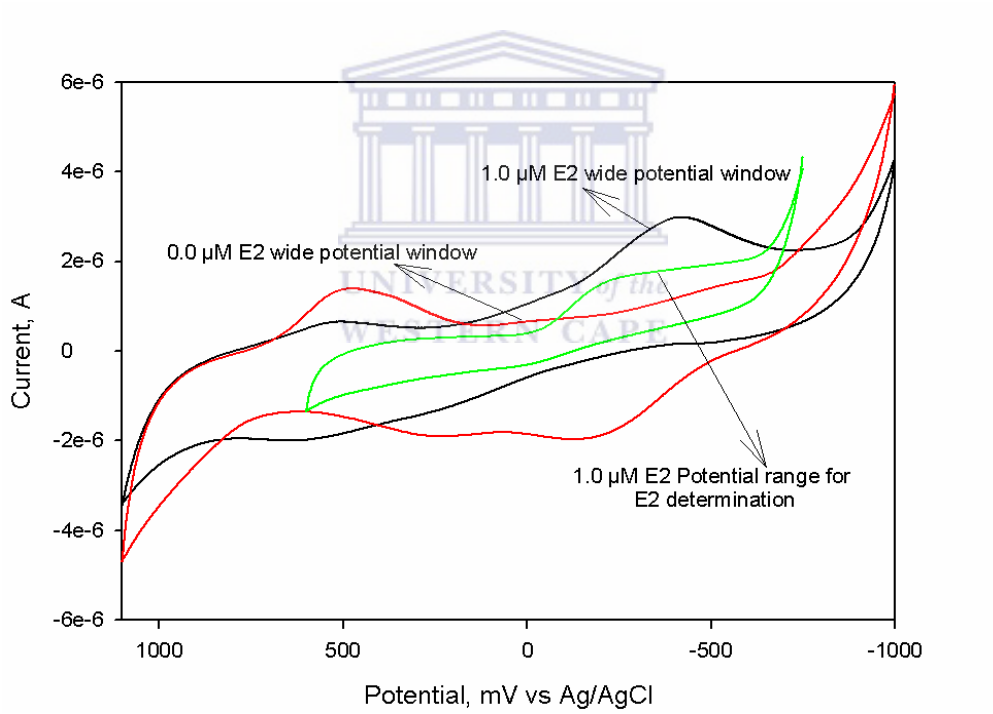

Figure 4-26: Cyclic voltammograms illustrating the selection of the appropriate potential window for 17β-estradiol detection, in 0.1 M PBS pH 7.0, scan rate of 20 mV s^{-1}.

In Figure 4-26, the cyclic voltammogram shown in red and labelled 0.0 µM E2 was the response of the biosensor at zero E2 substrate concentration in 0.1 M PBS recorded at a wide potential range, the current peaks at E_{pc} = 500 mV and E_{pa} = -100 mV might have been due to the background catalytic current of different films immobilised onto the

biosensor surface. However, the most important current peak, after the addition of 1 μM of E2 to 0.1 M PBS (voltammogram shown in black) was a new prominent current peak at potential ; E_{pc} = -350 mV. At this particular potential the reduction might have been due to the electrons being transfered between the biosensor and the analyte (i.e. the substrate E2). This study was done more than two times and the same responses were obtained, a conclusion was made that the E2 detection was occurring at mostly towards the negative potential which is also known to be the working potential range for HRP based biosensor platforms [86]. The potential window was then minimise to a range from E = 550 mV to -600 mV, this potential window was then taken as the appropriate potential range for cyclic voltammetry studies of involving the enzyme biosensors under study.

4.1.2.3 Criticality of PANI:MPA-ZnSe-QDs in the biosensor AuE/PANI:3-MPA-ZnSe-QDs/HRP

The purpose of this part of the study was to investigate the function of what has been referred to in this context as an electron mediator PANI:MPA-ZnSe-QDs composite, in the fabricated AuE/PANI:MPA-ZnSe-QDs/HRP biosensor. Different working electrodes with and without the mediator material were prepared, the working electrode AuE/HRP was prepared by direct immobilisation of HRP enzyme onto gold disk electrode, the electrode was then dried under nitrogen fume for 2 hours. The second electrode AuE/PANI:MPA ZnSe-QDs/HRP biosensor was prepared by the method described previously in 3.1.2.5. The electrolyte solution was comprised of 0.1 M PBS of pH 7.0. All the studies were performed under anaerobic conditions (or in an oxygen free environment) by degassing the electrolyte solution for 15 min, by a purge of argon gas and keeping a blanket of argon on top of the solution throughout the duration of the experiment. The cyclic voltammetry studies were performed at a potential range from E = -750 mV to E = 1500 mV at scan rate of 20 mV s^{-1}.

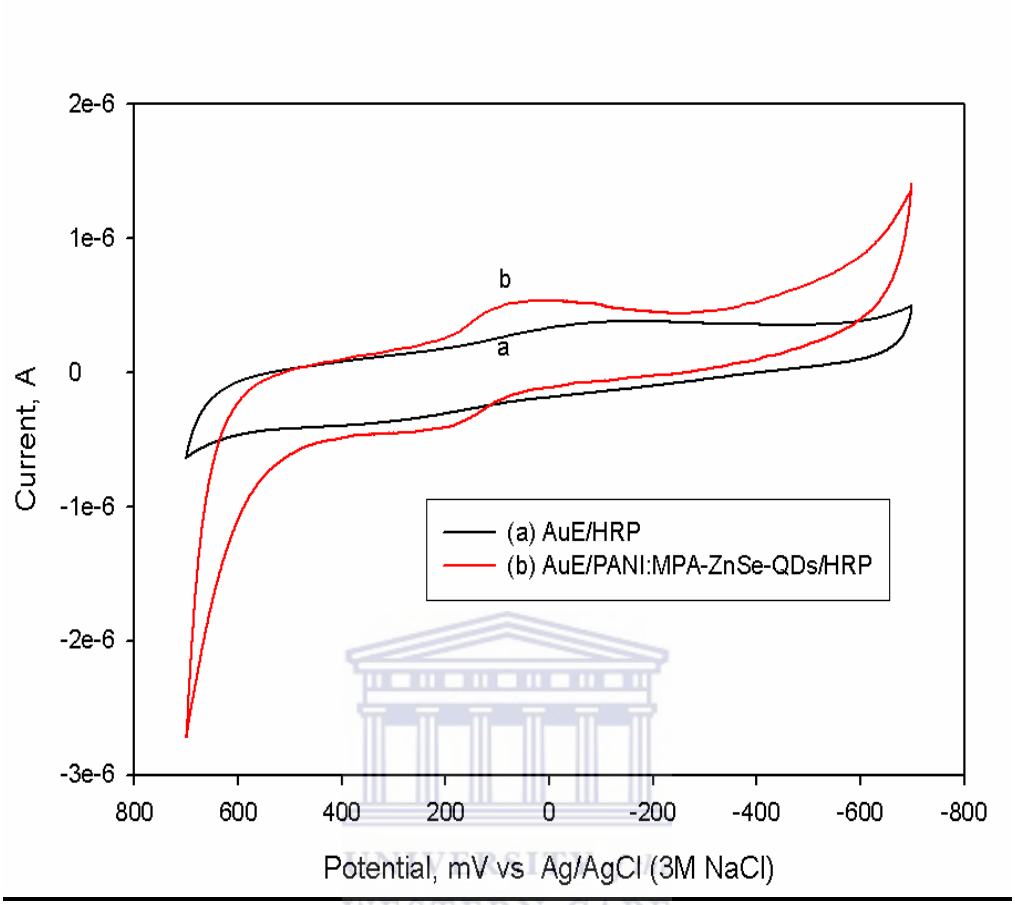

Figure 4-27: Cyclic voltammograms illustrating different films deposited onto gold electrode: (a) AuE/HRP and (b) AuE/PANI:MPA-ZnSe-QDs /HRP in 0.1 M PBS, at pH 7.0, 25 ºC.

From the resultant cyclic voltammograms shown in Figure 4-27, it was observed that the biosensor gave little or no current response for the electrode (a) AuE/HRP in the absence of the mediator. Although a catalytic reaction or the electron transfer reaction is possible between the enzyme and the electro active material within the bulk of the solution, this reaction will occur at a far distant to the electrode surface. The explanation would that the stability of enzyme molecule onto the electrode surface will be not good enough to hold the enzyme in-close proximity to the gold electrode surface (i.e. transducer), thus one would expect low electrochemical reactions, slow enough to be not even observed. In the presence of the mediator PANI:MPA-ZnSe-QDs as indicated in Figure 4-27 by (b) (i.e.

red voltammogram); the biosensor gave very good current response indicating quasi-reversibility response characterised by the presence of a redox couple, with reduction peak occurring at a potential of E_{pc} = 45 mV and an oxidation peak at E_{pa} = 200 mV. The electron transfer reaction was a one electron transfer redox reaction estimated using the obtained peak potential separation which was found to be ΔE_p = 65 mV. These observations clearly indicated that the PANI:MPA-ZnSe-QDs mediator was necessary for speeding up the electron transfers reaction, anchoring the enzyme and creating the equilibrium more closely to the transducer (i.e. gold electrode), and also served the purpose of keeping the bio receptor stable at the electrode surface to prevent a common case of electrode fouling, i.e. discharging of the films immobilised onto electrode surface to the surrounding electrolyte media [73].

4.1.2.4 Electrochemical properties of each of the films immobilised onto the surface of biosensor AuE/ PANI:MPA-ZnSe-QDs/HRP in 0.1 M pH 7.0, phosphate buffer

The study was performed in order to pre-look into the electrochemical properties of different films that were used in fabricating the biosensor AuE/PANI:MPA-ZnSe-QDs/HRP in the presence and absence of the horseradish peroxidase enzyme. Different working electrodes were prepared with and without the HRP enzyme; The working electrode AuE/PANI:MPA-ZnSe-QDs was prepared by the procedure that was described in detail, in 3.1.2.3. The second working electrode described in the context of this research as AuE/ PANI:MPA-ZnSe-QDs/HRP biosensor was prepared by the same exact method described in 3.1.2.5. The electrolyte solution was comprised of 0.1 M PBS of pH 7.0 at 25 °C. The cyclic voltammetry studies were performed under an oxygen free environment by degassing the electrolyte solution for 15 min with a purge of argon gas. The cyclic voltammetry studies were recorded from a potential range; E = -600 mV to E = 1500 mV at scan of 20 mV s^{-1}.

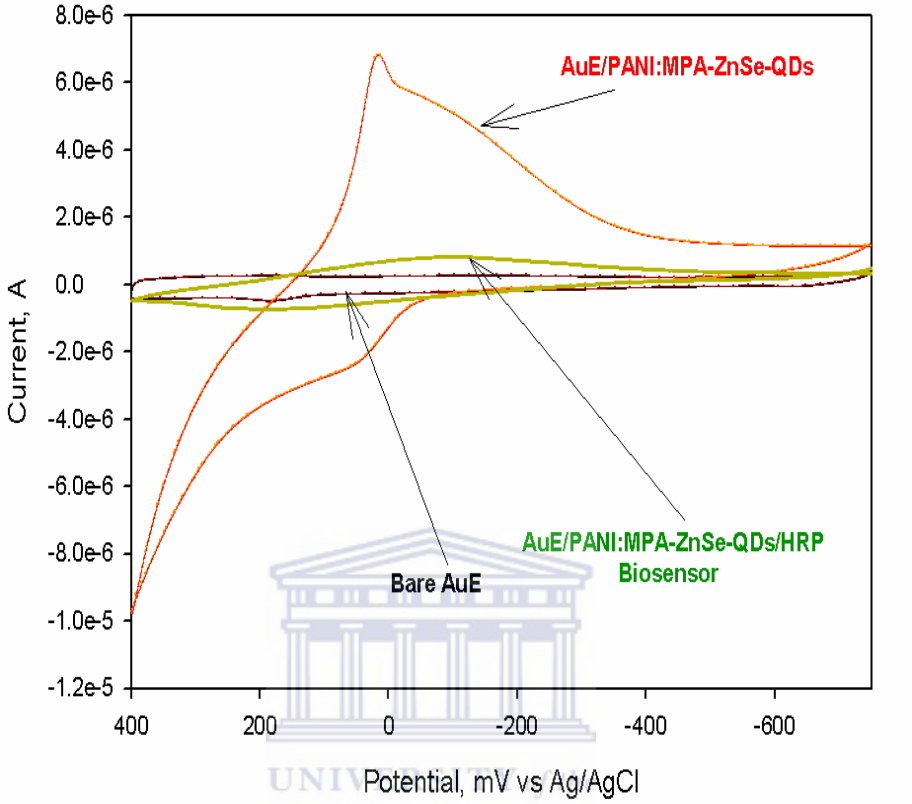

Figure 4-28: Cyclic voltammetry responses of: a) AuE bare b) AuE/PANI:MPA-ZnSe-QDs and c) AuE/PANI:MPA-ZnSe-QDs/HRP electrodes in 0.1 M PBS at a scan rate, 20 mV s^{-1}.

From Figure 4-28, it was observed that the electrodes; AuE and AuE/PANI:MPA-ZnSe-QDs/HRP biosensor gave minimal background current when studied in 0.1 M PBS solution. When the surface of gold electrode was immobilised with the composite PANI:MPA-ZnSe-QDs (shown in Figure 4-28) and studied in 0.1 M PBS, an intense reduction peak at E_{pc} = -7.5 mV, and an oxidation peak at E_{pa} = 50 mV were observed with a peak separation ΔE = 58 mV indicating a one electron transfer reversible electrochemical reaction initiated by the presence of the the composite. The current peaks observed for the AuE/PANI:MPA-ZnSe-QDs electrode indicated that the PANI:MPA-ZnSe-QDs composite was electro-active in 0.1 M PBS and was thus successfully employed as an electron mediator between the bio-recognition element HRP enzyme.

However, when the HRP biosensor was immobilised on top of the PANI:MPA-ZnSe-QDs (i.e. the biosensor AuE/PANI:MPA-ZnSe-QDs/HRP), the redox couple peaks at potentials; E_{pc} = -7.5 mV and E_{pa} = 50 mV disappeared indicating that a new surface or the HRP film was being deposited onto the composite: PANI:MPA-ZnSe-QDs modified gold electrode ,where upon the newly formed electrode with the enzyme was quite not as electro-active phosphate buffer only.

However an additional study was then performed in the presence of concentrations of electro-active species: 17β-estradiol in 0.1 M PBS and then monitored the electrochemical behaviour of each electrode or modified electrode, this study was shown by Figure 4-29.

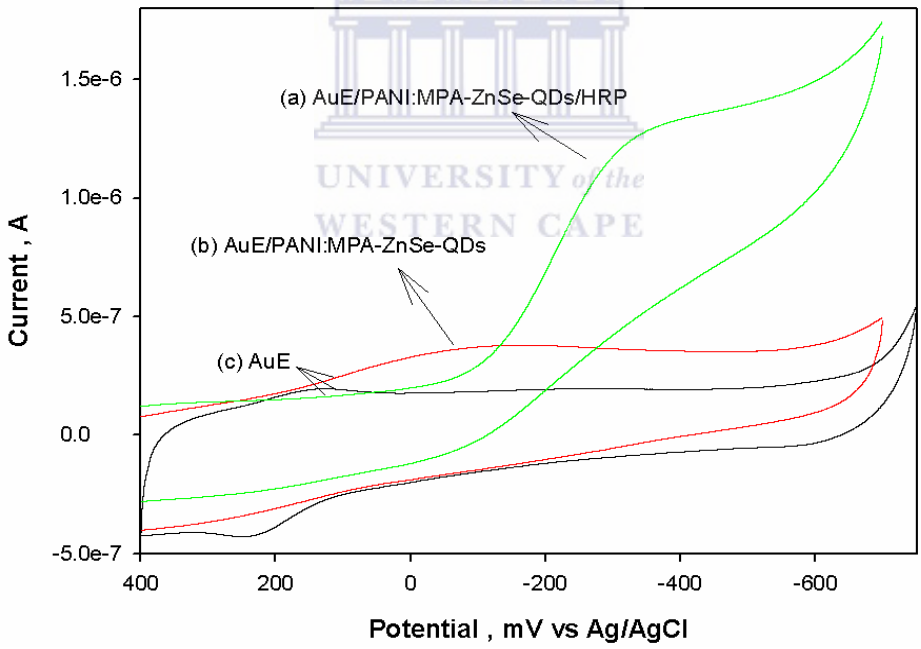

Figure 4-29: Cyclic voltammetry responses of different electrodes (a) AuE/PANI:MPA-ZnSe-QDs/HRP, (b) AuE/PANI:MPA-ZnSe-QDs and (c) bare AuE, in the presence of 17β-estradiol in 0.1 M PBS, pH 7.0.

From Figure 4-29, it was observed that the highest current response in the presence of 2 µM 17β-estradiol (E2) was obtained with the electrode AuE/PANI:MPA-ZnSe-QDs/HRP

defined as the biosensor. The current responses obtained for different films were: for the bare gold electrode AuE; the catalytic current was i_{pc} = 8.653 x 10^{-9} at E_{pc} = 100 mV, for AuE/PANI:MPA-ZnSe-QDs electrode; the catalytic current obtained was i_{pc} = 0.267 x 10^{-7} A at E_{pc} = -100 mV and for the electrode AuE/PANI:MPA-ZnSe-QDs/HRP (i.e. the biosensor); the catalytic current response was i_{pc} = 1.356 x 10^{-6} A at E_{pc} = -210 mV. Thus the current peak that was observed for the biosensor (i.e. AuE/PANI:MPA-ZnSe-QDs/HRP) showed high catalytic current responses as opposed to other electrodes thus preferable the best electrode to be used for the detection of 17β-estradiol (E2).

4.1.2.5 Selection of scan rate for determination of 17β-estradiol (E2) using AuE/PANI:MPA ZnSe-QDs/HRP biosensor

The Osteryoung square-wave voltammetry (O-SWV) studies were done from a potential window of E = 100 mV to E = -800 mV at different square-wave frequencies; (a) 25 Hz,(b) 20 Hz, (c)10 Hz and (d) 5 Hz respectively using 2 steps in the square-wave, in solution containing 0.5 μM E2 and 0.1 M PBS pH 7.0.

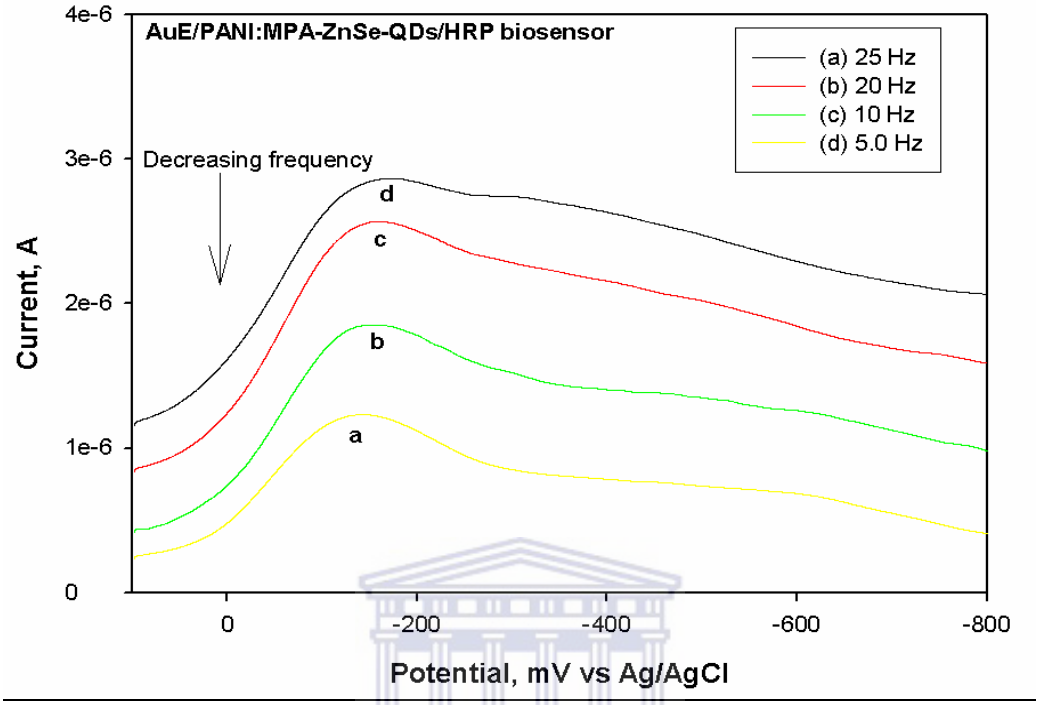

Figure 4-30: Osteryoung square-wave difference voltammograms representing the response of AuE/PANI:MPA-ZnSe-QDs/HRP biosensor towards 0.5 µM 17β-estradiol, in 0.1 M PBS, pH 7.0 at different frequencies (a) 25 Hz, scan rate (50 mV s^{-1}) (b) 20 Hz (40 mV s^{-1}), (c) 10 Hz (20 mV s^{-1}) and (d) 5.0 Hz (20 mV s^{-1}).

From Figure 4-30, it was observed that the frequency of 5.0 Hz, gave good well pronounced current peak at potentials E_{pc} = -198 mV with peak current; i_{pc} = 0.836 µA , which was closely related to the peak potential obtained from cyclic voltametric technique for 17β-estradiol in 4.1.2.4. This frequency was also slow enough to monitor the catalytic conversion of E2 by HRP immobilised onto the AuE/PANI:MPA-ZnSe-QDs/HRP biosensor. The frequency of 5.0 Hz was defined as the appropriate frequency and was used in all the studies involving the determination of E2 by Osteryoung square-wave and differential-pulse voltammetry.

4.1.2.6 Detection of 17β-estradiol and catalytic activity of the AuE/PANI:MPA-ZnSe-QDs/HRP biosensor

Cyclic voltammetry (CV) and differential-pulse voltammetry (DPV) techniques were used to monitor the AuE/PANI:MPA-ZnSe-QDs/HRP biosensor responses to different concentrations of 17β-estradiol**.** All the CV s and DPV measurements in this section were carried out under a partial oxygen atmosphere, by degassing the PBS for about 10 min with a purge of argon gas, after which the solution was allowed to stabilise for a further 10 min. The degassing process of the phosphate buffer solution was done only once before the first measurement for the biosensor and had been specified where applicable. The electrolyte solution used in this part of the study was 0.1 M PBS, pH 7.0 at 25 ^{o}C. The responses of the biosensor to 17β-estradiol (E2) substrate were monitored and recorded at a potential window between E = -600 mV and E = 700 mV. The scan rate used in this study was 20 mV s^{-1}; chosen on the bases described in previous section 4.1.2.

Figure 4-31, shows the responses that were obtained for the biosensor AuE/PANI:MPA-ZnSe-QDs/HRP towards different concentrations of 17β-estradiol (E2) from a concentration of 0.0 μM to a concentration of 2.5 μM of E2.

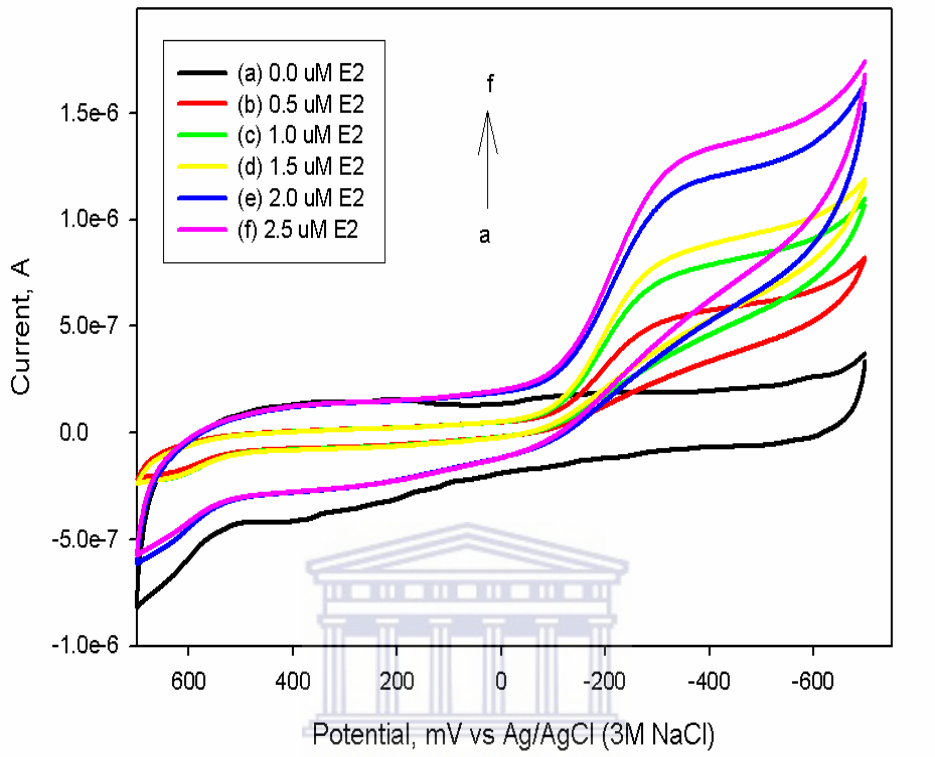

Figure 4-31: Cyclic voltammetry responses of AuE/PANI:MPA-ZnSe-QDs/HRP biosensor to different concentrations of 17β-estradiol (a) 0.0 µM, (b) 0.5 µM, (c) 1.0 µM (d) 1.5 µM, (e) 2.0 µM, and (f) 2.5 µM and under aerobic conditions in 0.1 M PBS; pH 7.2 at a scan rate of 20 mV s^{-1}.

From Figure 4-31, it was observed that, after the first addition of 17β-estradiol concentration equivalent to a volume of 0.2 µL corresponding to 0.5 µM E2 to 0.1 M PBS, followed by scanning the potential from negative direction (-Ve potential) to positive direction (+Ve potential), a peak at potential: E_{pc} = -200 mV was observed. The peak was postulated to be due to the current response generated by the electron transfer reaction occurring between of the enzyme HRP immobilised on the outside of the biosensor surface with substrate 17β-estradiol. According to Wash and co-workers [41], for alcohol oxidation by monooxygenase peroxidase the compound I preferable of HRP (Fe^{5+}), reacts with the first alcohols (in this case 17β-estradiol), a second addition of the

alcohol displaces the water molecule to readily bind the Fe^{4+} and then reduction occurs [49]. Thus reduction current peaks indicated by cyclic voltammograms in Figure 4-31 with a slight shift in potential towards positive potential as the substrate concentration is increased, might have been generated due to the conversion of Fe^{4+} oxidation state of HRP enzyme to Fe^{3+} by first E2 addition and continuously, the conversion had been declared to occur according to reaction mechanism summarised below [41]:

$HRP\text{-}Fe^{3+} + H_2O + O_2 \rightarrow HRP\text{-}Fe^{5+}(H_2O) + 2e^-$ (2e- redox step)

$HRP\text{-}Fe^{5+} + 2e^- + RCH_2OH \rightarrow HRP\text{-}Fe^{3+} + RCH_2C{=}O$, E = -205mV (conversion of E2)

Where RCH_2OH was assumed to be 17β-estradiol and $RCH_2C{=}O$ was assumed to be the oxidised product of estradiol, these abbreviations and assumptions only apply to this part of the context. The catalytic conversion of E2 was clearly a reduction reaction further supported by appearance of series of single reduction peaks as observed in the cyclic voltammograms. As the concentrations of the substrate 17β-estradiol were increases, the catalytic current signals proportionally increased and occurred at the approximate potential E_{pc} = -205 mV. The biosensor gave good response up to a maximum concentration level of 2.5 μM of E2.

The reproducibility studies were also done by preparing the three exact same biosensors and the biosensors were then utilised for quantitave determination of 17β-estradiol. The AuE/PANI:MPA-ZnSe-QDs biosensors fabricated showed a good stable reduction peaks for different concentrations of 17β-estradiol. The percentage error on the current responses generated for each of the biosensors was 1.5 % and correlation co-efficient of the biosensor measurements was R^2 = 0.831 done for at least at 2 concentration measurements, indicating the results were reproducible.

The Figure 4-33, indicates the differential-pulse voltammetry (DPV) responses (a more sensitive voltametric technique than cyclic voltammetry) obtained for the biosensor AuE/PANI:MPA-ZnSe-QDs/HRP, for determination of different concentrations of 17β-estradiol. For the DPV studies, the potential was scanned in one direction cathodically,

from positive potential E = 200 mV to negative potential: E = -600 mV, for the purpose of monitoring only the reduction peaks as discussed previously, that the catalytic reaction caused by biosensor response to 17β-estradiol was a reduction reaction. The scan rate used for this study was 20 mV s^{-1}, chosen on the bases discussed in section 4.1.2.1.

The DPV responses of AuE/PANI:MPA-ZnSe-QDs/HRP biosensor towards 17β-estradiol were demonstrated under two solution conditions i.e. anaerobic and aerobic conditions. The oxygen free environment was achieved by degassing phosphate buffer solution for about 15 min, thereafter a blanket of argon gas was kept on top of the solution for the whole duration of the experiment.

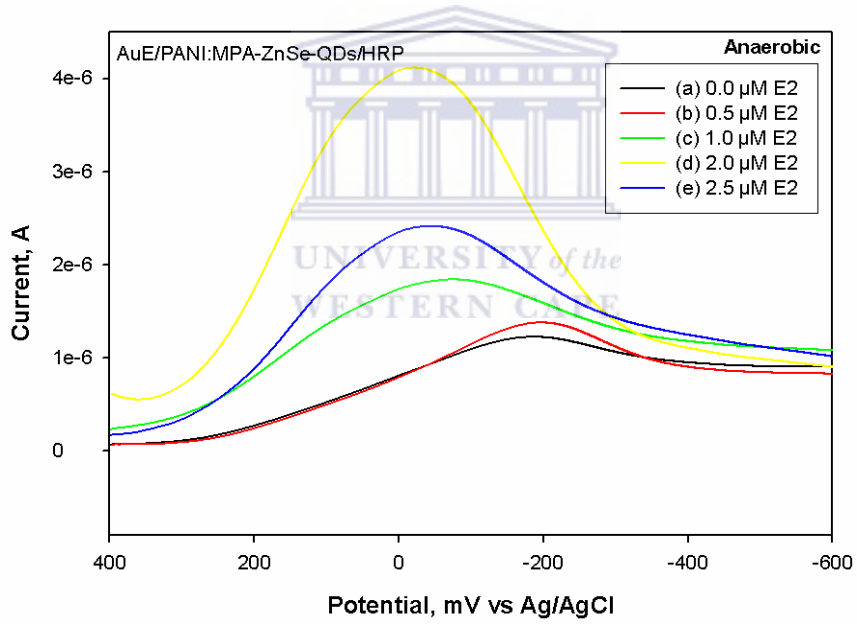

Figure 4-32: Differential-pulse voltammetry responses of AuE/PANI:MPA-ZnSe-QDs /HRP biosensor to different concentrations of 17β-estradiol (a) 0.0 µM, (b) 0.5 µM, (c) 1.0 µM (d) 2.0 µM, and (e) 3.0 µM, in 0.1 M PBS; pH 7.0 at a scan rate of 20 mV s^{-1}, anaerobic conditions.

In Figure 4-32, the differential-pulse voltammograms of AuE/PANI:MPA-ZnSe-QDs/HRP biosensor under anaerobic condition, showed a catalytic current peak which

appeared at a potential E_{pc} = -208 mV before any addition of a substrate, however after the first addition of 2 μL (0.5 μM) of E2 a shift in the potential was observed towards the positive potential as indicated by (c) in Figure 4-32, where a peak potential shifted to E_{pc} = -10 mV as the catalytic current increased simultaneously, the shift in the potential must have been caused by the fact that after the first addition of the analyte E2, the unstable state of HRP-Fe^{4+} of HRP (IV) hemi active site, being reduced to HRP-Fe^{3+} thus the shift in potential from E_{pc} = -208 mV to E_{pc} = -10 mV to more positive potential. The fourth addition of total volume 10 μL (2.5 μM) E2 in the 0.1 M PBS, caused the catalytic current peak to decrease , which was an indication of the HRP-Fe(IV) active site being saturated by high substrate concentrations [57].

For DPV biosensor responses under aerobic conditions, presented by Figure 4-33, the 0.1 M PBS was degassed for 15 min before running any DPV, there after, the gas inlet was let open allowing a continuous flow of oxygen into the electrochemical cell.

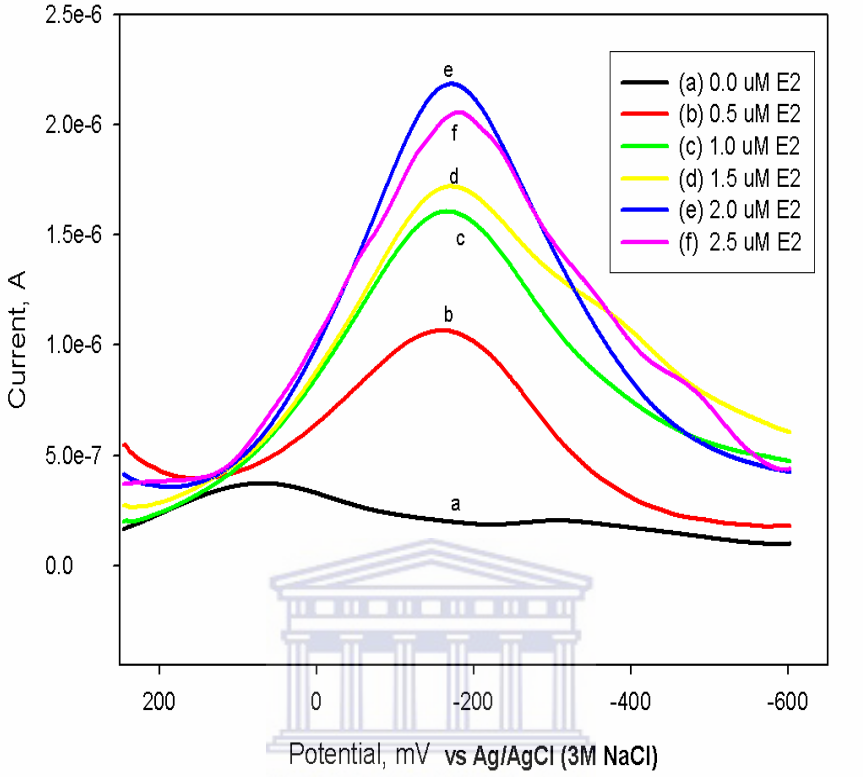

Figure 4-33: Differential-pulse voltammetry responses of AuE/PANI:MPA-ZnSe-QDs/HRP biosensor to different concentrations of 17β-estradiol (a) 0.0 µM, (b) 0.5 µM, (c) 1.0 µM (d) 1.5 µM, (e) 2.0 µM, and (f) 2.5 µM and (g) 3.0 µM, in 0.1 M PBS; pH 7.0 at a scan rate of 20 mV s^{-1}, aerobic conditions.

In Figure 4-33, the DPV responses showed well pronounced good reduction catalytic current peaks at potential E_{pc} = -205 mV, that had a minimal shift in the potential to more positive potential, compared to electrochemistry of the same biosensor when the responses to 17β-estradiol concentrations were monitored under anaerobic conditions. The catalytic current peaks generated in the DPV were proportional to the concentration of 17β-estradiol added in 0.1 M PBS. However after an addition 2.0 µM of E2 t in 0.1 M PBS, a decrease in the catalytic current was observed. The DPV responses of the biosensor AuE/PANI:MPA-ZnSe-QDs/HRP biosensor towards 17β-estradiol concentrations, indicated that the catalytic reaction occurred by the summarised reaction

in Figure 4-34. This catalytic reaction was postulated to be occurring via a single electron transfer between two intermediate oxidation states of horseradish peroxidase; HRP-Fe^{2+} and HRP-Fe^{3+}.The only possibility was that reaction was characterized by fast electron transfer kinetics due to the absence on of a huge shift in the potential as the concentration of the substrate:17β-estradiol was increased. A devised electron transfer reactions mechanism associated with the catalytic conversion of 17β-estradiol by the electrode AuE/PANI:MPA-ZnSe-QDs/HRP (i.e. biosensor) was shown in Figure 4-34.

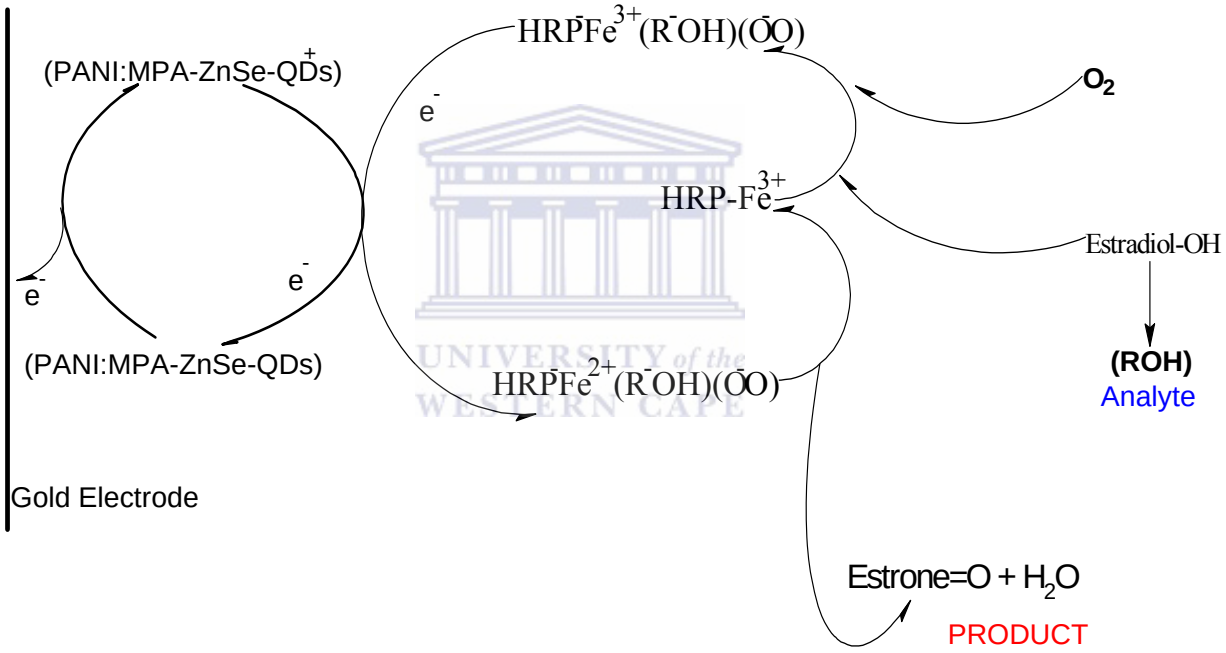

Figure 4-34: Electron transfer mechanism for catalytic conversion of 17β-estradiol by AuE/PANI:MPA-ZnSe-QDs/HRP biosensor.

The ROH represented 17β-estradiol (E2) and the R=O was the oxidised form of E2. In this mechanism, one clearly identifies that the catalytic conversion of E2 by HRP required the molecular oxygen (O_2),

HRP-Fe^{3+} + $2e^-$ + ROH + O_2 ➔ HRP-Fe^{2+} + RC=O, E = -205 mV (conversion of E2).

This reaction is a reaction abstracted from the catalytic reaction of HRP enzyme with alcohol compound reported by Walsh and co-workers [41]. The reaction showed that the oxygen is required to facilitate an adequate catalytic conversion of an alcohol compound by HRP to its catalytic product, which was similar to the investigation on this study, thus the best representation of catalytic reactions of the biosensor AuE/PANI:MPA-ZnSe-QDs/HRP towards the alcoholic derivative 17β-estradiol was that which was monitored under aerobic conditions.

The CV and DPV studies for the biosensor AuE/PANI:MPA-ZnSe-QDs/HRP responses to 17β-estradiol (E2) under aerobic conditions was further interpreted by devising a calibration curve and linearity curve shown in Figure 4-35 and Figure 4-36 respectively.

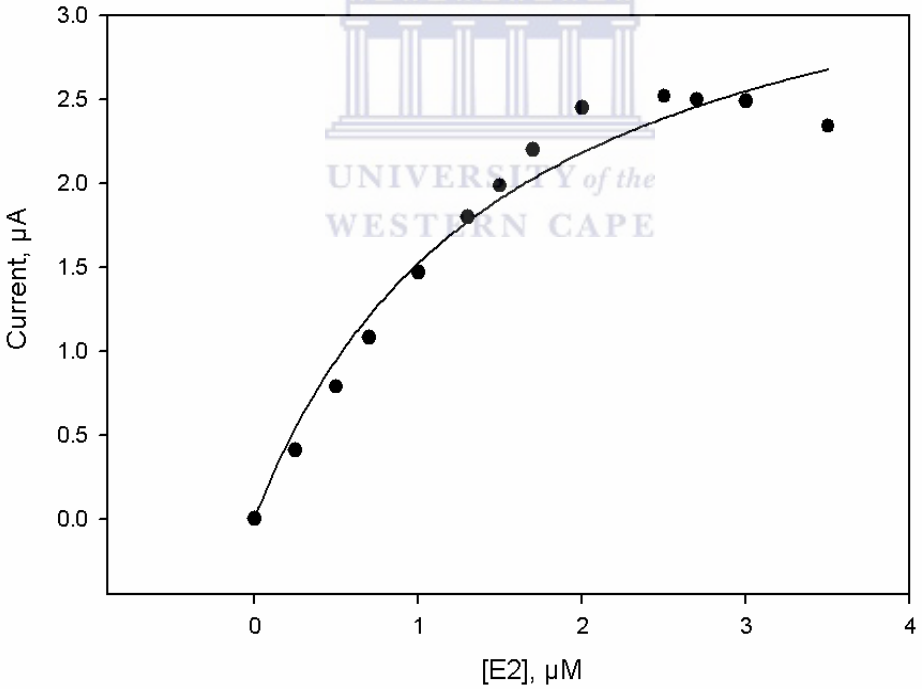

Figure 4-35: Calibration curve of AuE/PANI:MPA-ZnSe-QDs/HRP biosensor showing catalytic current responses of the biosensor to different concentration of 17β-estradiol.

The Figure 4-35 shows the linear calibration curve obtained for the biosensor AuE/PANI:MPA-ZnSe-QDs/HRP for responses towards E2 concentrations.

The interpretation of the hyperbolic calibration curve obtained for the biosensor AuE/PANI:MPA ZnSe-QDs/HRP was explained by use of Michaelis Menten model for enzyme to substrate catalytic kinetic reactions [41, 57]. The relationship is given by equation [41, 57]:

$$i_p = \frac{i_{max}[17\beta - estradiol]}{[17\beta - estradiol] + K_m^{app}} \quad \text{Equation 4.1-5}$$

Where i_p = peak currents, i_{max} = maximum current found to be 2.5 x 10^{-6} M, [17β-estradiol] = concentrations of 17β-estradiol and K_m^{app} Michaelis- Menten constant. The Michaelis Menten constant describes the efficiency and the activity of the enzyme to catalyse a specific substrate. For the biosensor the catalytic reaction of E2 by AuE/PANI:MPA-ZnSe-QDs/HRP biosensor fitted well with the Michaelis Menten behaviour and the K_m^{app} was found to be 0.073 mM. The value of the Michaelis Menten constant was a reasonable low indicating at least a good catalytic activity of the HRP to concentration of 17β-estradiol.

The linearity and sensitivity of the biosensor to different concentrations of E2 was estimated using SIGMA@ 8 software, from the linearity plots of catalytic peak current for different substrate (i.e. E2) concentrations.

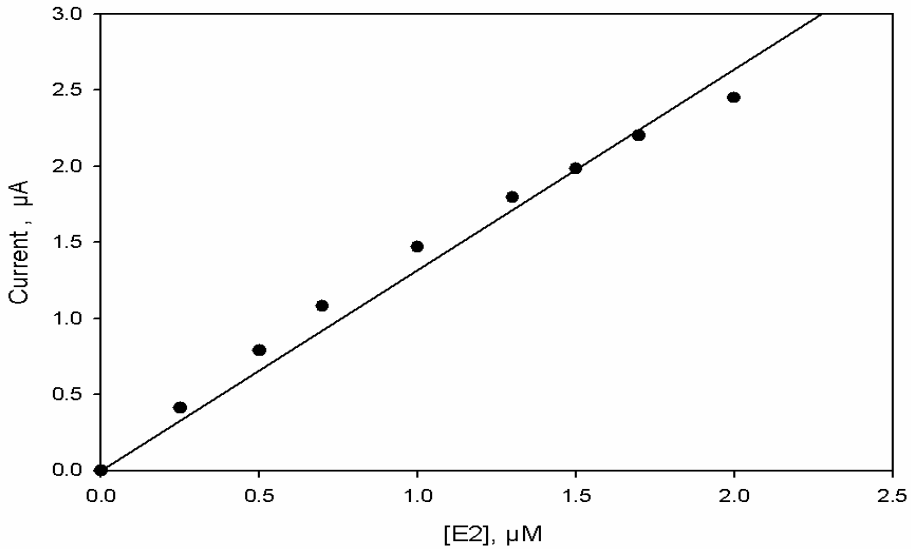

Figure 4-36: Linear calibration curve of AuE/PANI:MPA-ZnSe-QDs/HRP biosensor.

The co-relation coefficient for the plots was found to be; $R^2 = 0.989$. The linearity of the biosensor was found to be between 0.6 µM and 1.6 µM. On the other hand using 3σ the sensitivity of the biosensor was found to be 1.223 µA/µM, with the detection limit of 2.05×10^{-8} g L^{-1}.

4.1.2.7 The amperometric studies of AuE/PANI:MPA-ZnSe-QDs/HRP biosensor for the detection of 17β-estradiol

The amperometry is a time base voltametric techniques which utilises a single potential at which the reduction or oxidation occurs and usually more sensitive than CV, DPV and SWV. The amperometry also gives the indication of the response time of the biosensor to the addition different concentrations of the analyte. The amperometric responses were recorded at a potential of E = -205 mV, proven in the previous section to be peak potential around which E2 gets converted to its associated product by HRP enzyme immobilised onto the biosensor platform, this study was done at a frequency of 0.5 Hz.

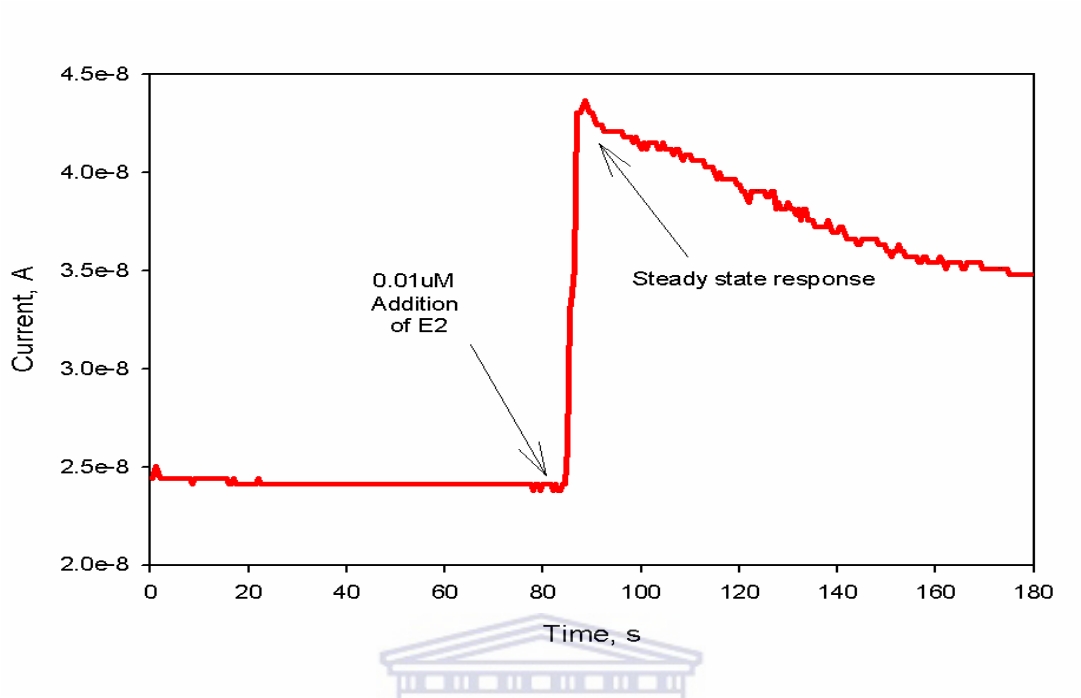

Figure 4-37: Steady state amperometric response of AuE/PANI:MPA-ZnSe-QDs/HRP biosensor towards 17β-estradiol.

For amperometric studies; shown in Figure 4-37, only a single amplified catalytic current response for the biosensor AuE/PANI:MPA-ZnSe-QDs/HRP towards addition of 0.5 µM E2 was observed. Thereafter the current signal de-amplified for an additional concentration of 0.5 µM of E2 into the 0.1 M PBS. The explanation to this observation could be possibly, that the enzyme got inhibited or the active site of the enzyme got saturated resulting in the enzyme loosing its activity. However, the response time of the biosensor was found to be 3s. The amperometric responses also indicated that the biosensor was sensitive to only a single concentration within its linearity range.

4.1.2.8 Stability studies of AuE/PANI:MPA-ZnSe-QDs/HRP biosensor

The study was done to investigate the effect of re-using the AuE/PANI:MPA-ZnSe-QDs/HRP biosensor over for more than once. A freshly prepared biosensor was used to measure at least five concentrations of 17β-estradiol for about 3 times using the same biosensor over more than once. After each measurement the biosensor was washed to remove any traces of species that might have adhered on the biosensor surface. Square-wave voltammetry were recorded at a potential window between: E = 300 mV to E = -600 mV, scanning from positive to negative in 0.1 M PBS at different concentrations of E2 at scan rate 20 mV s^{-1}. The study was shown in the next figure, labelled Figure 4-38.

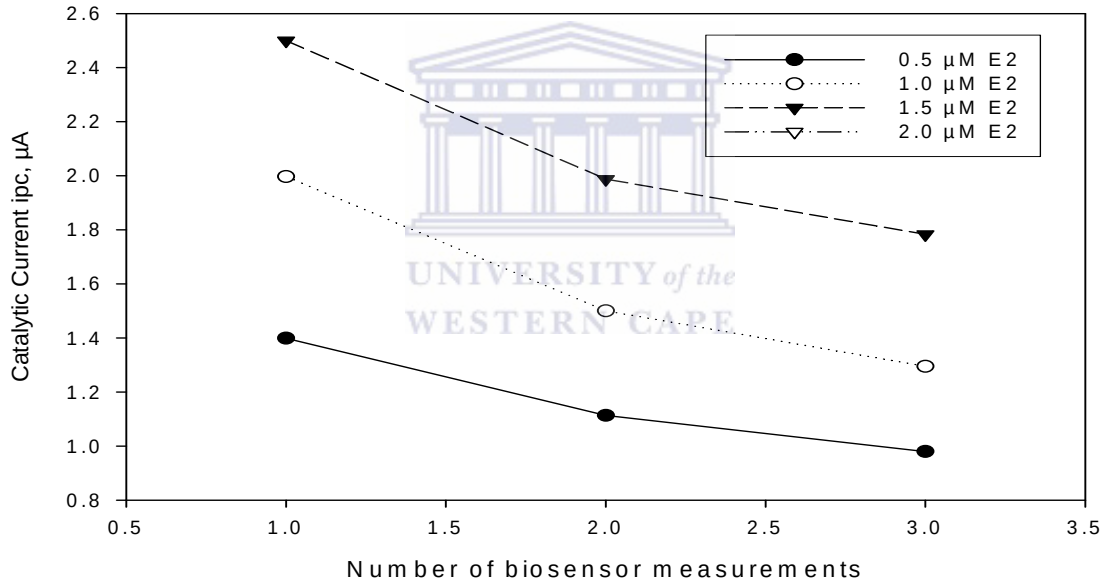

Figure 4-38: Stability studies of AuE/PANI:MPA-ZnSe-QDs/HRP biosensor surface and the effect of re-using the biosensor for more than once on its electrochemical properties.

In Figure 4-38, the triangular doted curves represents use at once, the unfilled white dots represents used twice and the black dots represent used three tomes. The calibration curves obtained for the study were listed in the additional figures at the end of this chapter.

The AuE/PANI:MPA-ZnSe-QDs/HRP biosensor catalytic peak current responses in Figure 4-38, clearly indicated that the number of times the biosensor was used played a major role on the catalytic current responses obtained for the biosensor, indicating a loss of catalytic activity of the biosensor as the biosensor is used more than once. The results indicated that the biosensor could be used for only once in order to attain the maximum accuracy of the catalytic current measurements towards different concentrations of E2. The estimation was done only on the concentration levels of E2 falling inside the linear range of the biosensor. The percentage decrease in the catalytic current between the first two measurements was about 50% was acceptable with standard deviation of 3σ and with an error of 1.233%, but in the case of the third measurement the percentage decrease was greater that 73% with error of 3.8% indicating the catalytic responses were outlined and inaccurate. This might have been caused by the fact that during E2 catalytic current measurements of the biosensor towards E2, the products formed during the catalytic reaction were insoluble and adsorbed on the biosensor surface making the enzyme immobilised onto the biosensor platform loosing its activity or the decrease in the catalytic activity might have been caused by de-sorption of the enzyme HRP from the biosensor surface [73].

4.1.3 Detection of similar estrogenic endocrine disrupting compounds 17α-ethnyl estradiol and estrone using the biosensor AuE/PANI:MPA-ZnSe-QDs/HRP

The study was performed to establish whether the developed biosensor AuE/PANI:MPA-ZnSe-QDs/HRP could work for other similar estrogenic endocrine disruptors similar to 17β-estradiol, which were EE2 and E1. 17α- ethnylestradiol (E2) is another type of estradiol which is used as a major ingredient to oral contraceptives consumed for birth control by woman. 17α-ethnylestradiol has the same structure as estradiol E2 but consists of ethnyl group at carbon 17 position of the estradiol back bone [3]

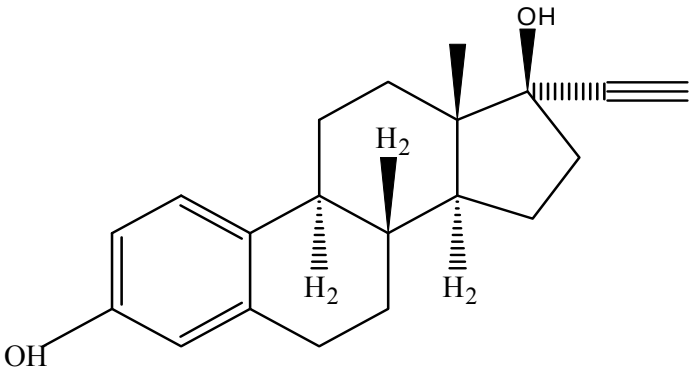

17-alpha ethnyl estradiol

Figure 4-39: Represents the structure of 17α-ethnylestradiol

The responses of the AuE/PANI:MPA-ZnSe-QDs/HRP biosensor to 17α-ethnylestradiol (EE2) were monitored and recorded at a potential window of E = -600 mV to E = 700 mV. The scan rate used in this study was 20 mV s^{-1}. For the first three micro molar concentration of EE2 the responses were shown in Figure 4-40.

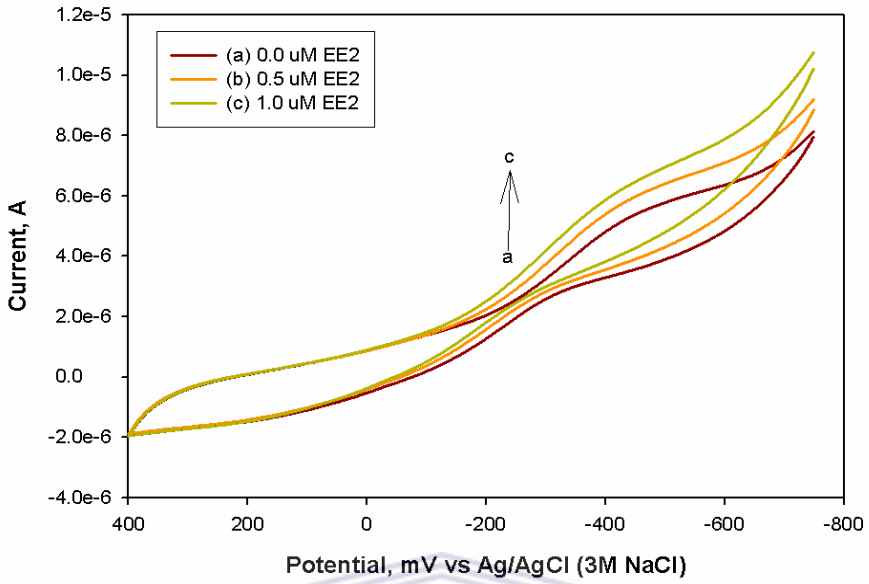

Figure 4-40: Cyclic voltammetry responses of AuE/PANI:MPA-ZnSe-QDs/HRP biosensor toward different concentrations of 17α-ethnylestraiol (EE2), in 0.1 M PBS, at a scan rate of 20 mV s^{-1}.

In Figure 4-40, a catalytic peak current at potential E_{pc}= -395 mV was observed at zero concentration of EE2, after an addition of 0.5 µM of EE2 to the PBS, minimal amplification in the catalytic current signal was observed at same potential, this was also observed for 1.0 µM total concentration of EE2 added to the phosphate buffer solution. Although a change in the catalytic current signal generated after each addition of different concentrations of EE2 in the PBS was observed for the biosensor AuE/PANI:MPA-ZnSe-QDs/HRP, the peak potential was totally different to the peak potential observed for the same biosensor when the substrate E2 was used. For EE2, the peak potential at which the catalytic reaction occurred was E_{pc} = 208 mV as opposed to the recently reported potential for EE2 which was E_{pc} = -395 mV.

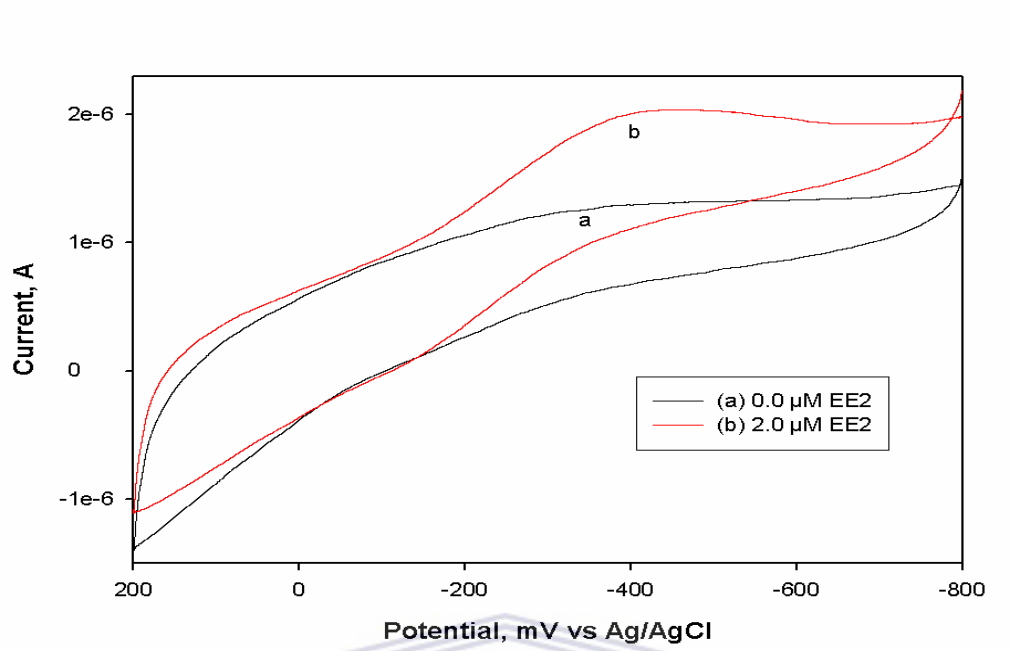

Figure 4-41: Cyclic voltammetry responses of AuE/PANI:MPA-ZnSe-QDs/HRP biosensor towards different concentrations of 17α-ethnylestraiol (EE2), (a) 0.0 µM EE2, (b) 2.0 µM EE2, in 0.1 M PBS, pH 7.0, scan rate 20 mV s^{-1}.

For the second set of cyclic voltammograms shown in Figure 4-41, using high concentrations of the substrate EE2, corresponding to the addition of 2.0 µM of EE2; the cyclic voltammetric studies showed a catalytic current peak at peak potential: $E_{pc} \approx 400$ mV. When the concentration of EE2 was increased to 2.5 µM, same catalytic peak current response was attained. This observation indicated that the biosensor had a capability of responding to concentration of EE2 up to a maximum of 2.0 µM.

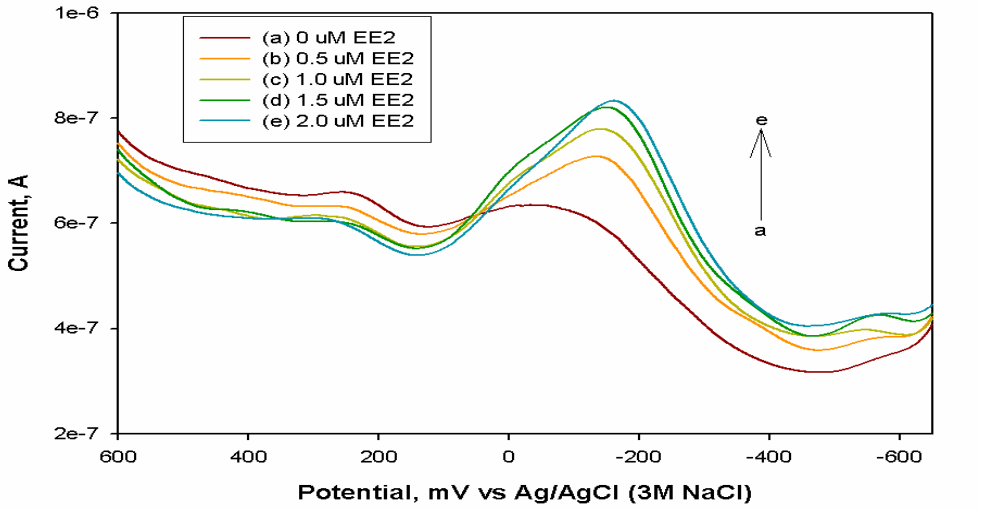

Figure 4-42: Osteryoung square-wave responses of the biosensor AuE/PANI:MPA-ZnSe-QDs/HRP toward different concentrations of EE2.

For the Osteryoung square-wave voltammetry the potentials corresponding to reduction catalytic current peak shifted by 100 mV to a peak potential of E_{pc} = -210 mV.

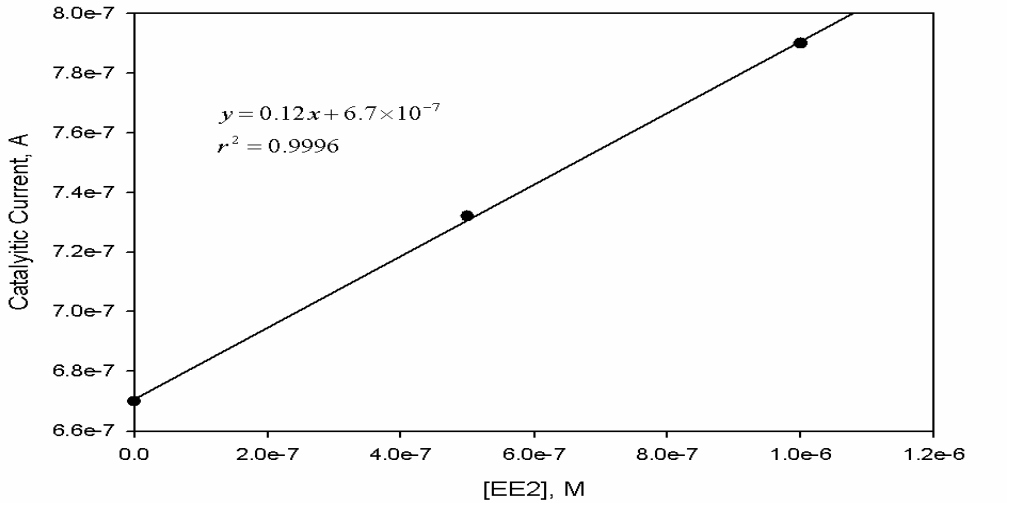

Figure 4-43: Linear calibration curve of AuE/PANI:MPA-ZnSe-QDs/HRP biosensor , illustrating the catalytic current responses of the biosensor towards concentrations of EE2.

In order to study the susceptibility of the HRP to catalyse the EE2, Michaelis Menten model was used to determining the kinetic parameter k_m^{app} the Michaelis Menten equation was normalised and a simplified form shown by $\frac{1}{i_{pc}} = \frac{1}{i_{max}} + \frac{k_m^{app}}{i_{max}[EE2]}$ Equation 4.1-6:

$$\frac{1}{i_{pc}} = \frac{1}{i_{max}} + \frac{k_m^{app}}{i_{max}[EE2]} \quad \text{Equation 4.1-6}$$

Where i_{pc} = current, i_{max} = 2.5 x 10^{-6} A, maximum current, [EE2] = concentration of 17α-ethnylestradiol and K_m^{app} Michaelis- Menten constant. The plot of the modified Michaelis Menten equation was shown in Figure 4-44 .

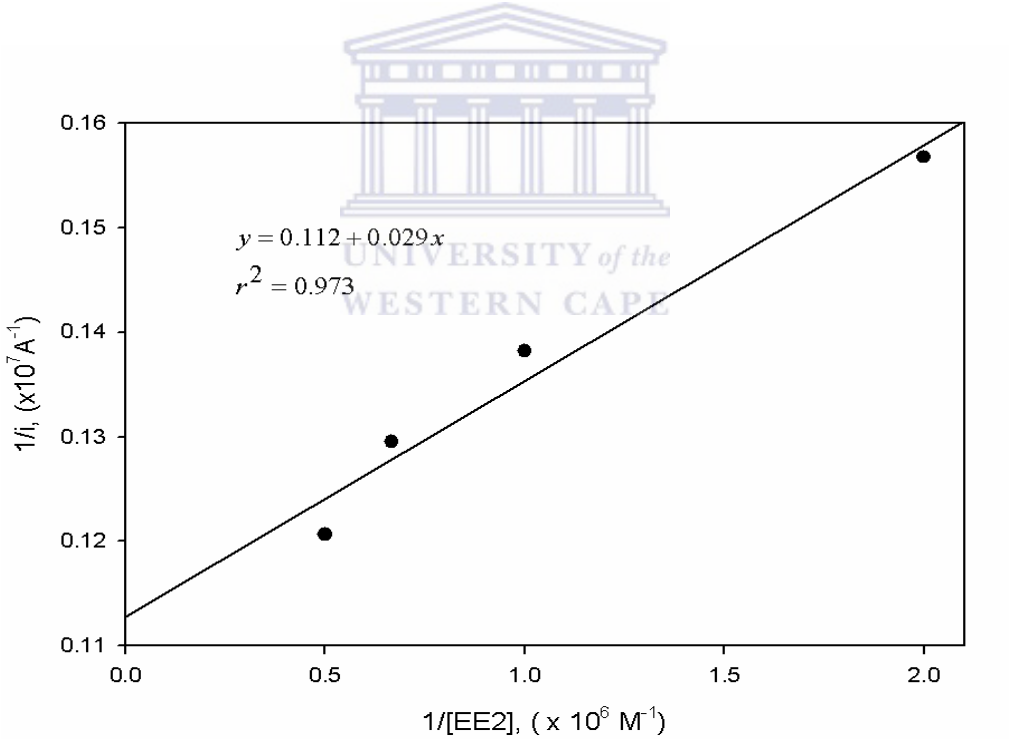

Figure 4-44: Michaelis Menten normalised model for AuE/PANI:MPA-ZnSe-QDs/HRP biosensor towards concentrations of EE2 for calculation of K_m^{app} and i_{max}.

Using the normalised Michaelis Menten approximation shown in Figure 4-44, the Michaelis Menten constant K_m^{app} was estimated to be 0.023 mM indicating a lower

catalytic activity of the biosensor towards the substrate EE2 compared to the previously obtained K_m^{app} for E2 which was 0.073 mM.

The biosensor AuE/PANI:MPA-ZnSe-QDs/HRP was again used for investigating its catalytic activity towards different concentrations of estrone (E1) and the electrochemistry was studied using Osteryoung square-wave voltammetry. The Osteryoung square-wave voltammograms were recorded at a potential range between E = 600 mV and E = -600 mV scanning reductively, at a scan rate of 20 mV s^{-1}. The obtained Osteryoung square-wave voltammograms were shown in Figure 4-45.

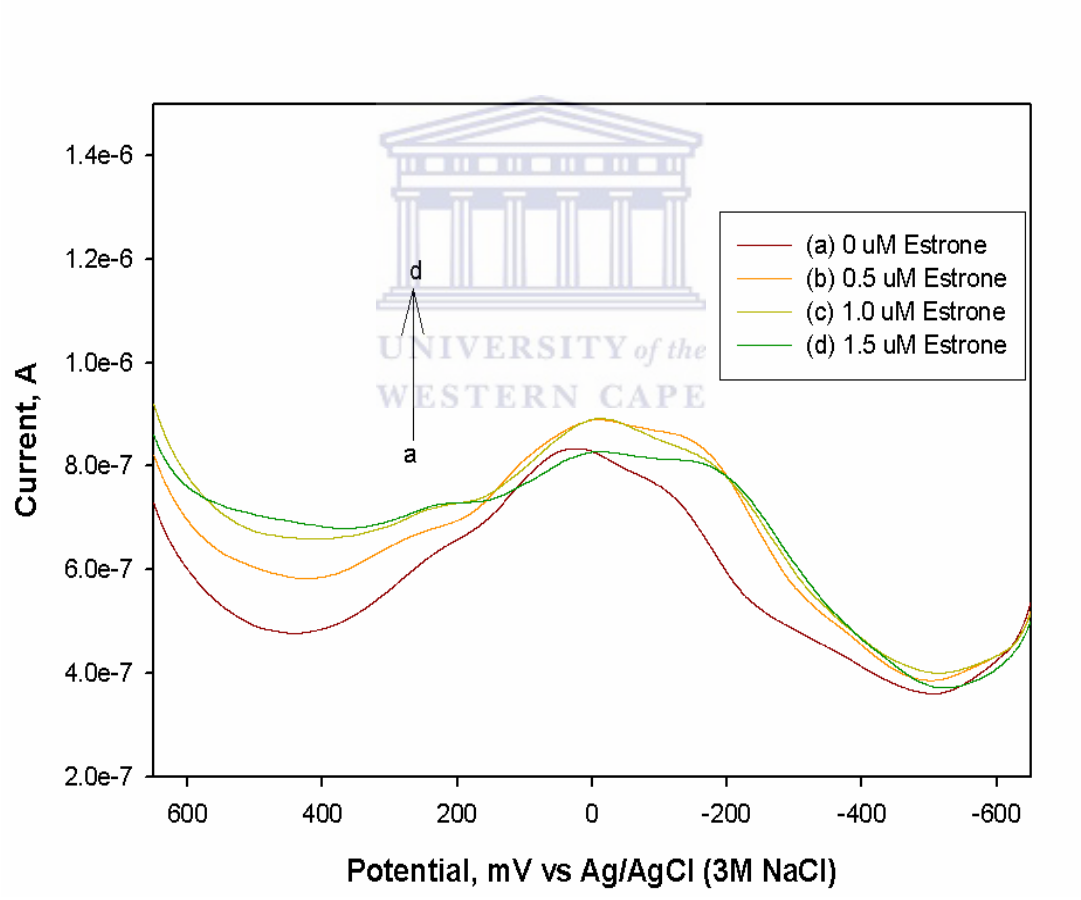

Figure 4-45: Responses of AuE/PANI:MPA-ZnSe-QDs/HRP biosensor towards different concentrations of estrone (E1).

The biosensor AuE/PANI: MPA ZnSe-QDs/ HRP gave no interpretable catalytic current responses towards different concentrations of E1 in the square-wave voltammetry, which indicated that the fabricated biosensor might be catalytically inactive towards E1. Thus this must have been due to biosensor being selective to alcohols since E1 (Estrone)-is a ketone and (E2, EE2) are alcohols. The HRP enzyme is well known to induce alcohols and peroxide [41, 57].

Table 4-2: The table shows the catalytic kinetic parameters obtained for the biosensor AuE/PANI:MPA-ZnSe-QDs towards different substrates used in this study.

Substrate	K_m^{app} **(mM)**	i_{max} **(µA)**	**Detection limit (g/mL)**	**Linear Range (µM)**
17 β Estradiol	0.073	2.5×10^{-6}	2.05×10^{-8}	0.25 - 1.7
17 α Ethnylestradiol	0.023	8.9×10^{-7}	$5.4\ 83x\ 10^{-5}$	0.20-1.0
Estrone	-	-	-	-

Although the biosensor AuE/PANI:MPA-ZnSe-QDs/HRP could be used to detect both E2 and EE2 estradiol derivatives effectively, the responses where distinguishable from each other with detection of E2 occurring at E_{pc} = -203mV and the detection of EE2 occurring at around E_{pc} = -390 mV. For future application of the biosensor the presence of these compounds can be identified by the peak potential at which the catalytic reaction occurs.

4.1.4 Interference studies of the biosensor AuE/PANI:MPA-ZnSe-QDs/HRP with H_2O_2

The studies were performed for the purpose of investigating the effect of interferences on the detection of 17β-estradiol, which can only result due the presence of other potential substrates of HRP enzyme. In the study the effect of one very powerful type of HRP enzyme substrate H_2O_2 was studied. The cyclic voltammograms were recorded at a potential window between E = -600 mV and E = 400 mV, defined in this study as the potential range at which the 17β-estradiol detection by biosensor AuE/PANI:MPA-ZnSe-QDs/HRP occurs. The study was performed using a conventional three electrode system under the same conditions described in paragraph 4.1.2.6, the electrolyte solution contained 0.1 M PBS and 1.5µM 17β-estradiol and varying the concentrations of H_2O_2 as shown in Figure 4-46.

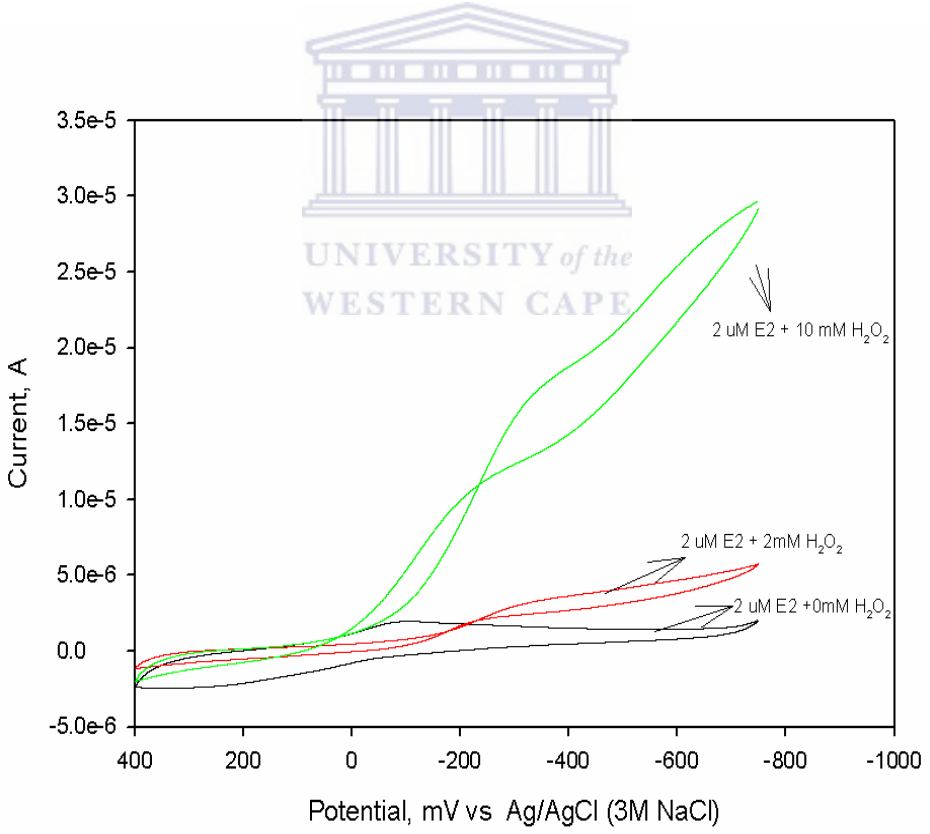

Figure 4-46: Cyclic voltammetry responses of AuE/PANI:MPA-ZnSe-QDs/HRP biosensor in the presence of; only 17β-estradiol, 17β-estradiol and 2 mM H_2O_2, lastly; 17β-estradiol and 2 mM H_2O_2, in 0.1 M PBS at a scan rate of 20 mV s^{-1}.

The crossing of the voltammograms as shown in Figure 4-46, could have been due to the presence of more than one electro-active species in the phosphate buffer solution, where these electro-active species reacted with each other chemically and electrochemically (17β-estradiol and hydrogen peroxide) causing cross-reaction in the electrolyte solution This explanation was proved by the absence of crossing voltammograms on the first black lined voltammogram in the same Figure 4-46, where no other substrate was present in the electrolyte solution except for 17β-estradiol. Thus for future applications of the biosensor AuE/ PANI:MPA-ZnSe-QDs/HRP interferences by hydrogen peroxide could be easily picked up by the catalytic current response exactly the same as the observed cyclic voltammograms.

However, the responses observed also indicated that the use of AuE/PANI:MPA-ZnSe-QDs /HRP for E2 could only be limited by very large H_2O_2 concentrations, from the preceding figure it was also observed that the H_2O_2 concentration levels detected by the biosensor were reclined at milli-molar level, the first addition was 2 mM of H_2O_2 in the solution containing the PBS and 2 μM E2 substrate, showed a little effect on the catalytic peak currents generated, and when the concentration of H_2O_2 was increased to 10 mM the effect of hydrogen peroxide was persistent, meaning only large concentrations up to milli molar (10^{-3} M) far most larger that the linear range obtained for the biosensor: to concentrations of E2, could affect the detection of 17β-estradiol. If high levels of hydrogen peroxide are present in the solution thus, must be eliminated prior to E2 measurements. The binding buffer can be used for elimination of the interferences and binds most unwanted species that might interfere with detection of the required analyte. For application in detection of unknown composition of analyte solution, an approach of eliminating the interference with hydrogen peroxide for accurate determination of 17β-estradiol, which must be firstly proved by appearance voltammograms shown in the above. H_2O_2 could be to selectively decomposed to water, living out only the analyte concentration of 17β-estradiol possibly if all the H_2O_2 could be converted. The hydrogen peroxide could be easily decomposed to O_2 and water in the presence of catalysts prior to E2 measurements.

Decomposition reaction of hydrogen peroxide: H_2O_2 ➔ $H_2O + O_2$

This reaction is often catalysed by catalyst such as manganese, silver etc. Thus for future and real-time application of the biosensor the hydrogen peroxide as the potential substrate would not be a problem for determination of unknown composition of standard solution proven to consist concentrations of E2, because of the ability of being able to selectively decompose peroxide by the above procedure prior to E2 detection. The decomposition of hydrogen peroxide gives water and oxygen [102]. Another approach is to modify the enzyme to be specific only to E2 which is done by an advance study of genetic engineering of the HRP enzyme which would selectively binds only to E2, and the HRP enzyme has been successfully modified and applied in biosensing devices involving many other substrates [53-54].

RESULTS: PART 2

4.1.5 The second biosensor AuE/Cystm/MPA-ZnSe-QDs/CYP3A4.

4.1.5.1 Spectroscopy of AuE/Cystm/MPA-ZnSe-QDs/CYP3A4 biosensor by FT-IR

The FT-IR measurements were carried out using Fourier Transform Infrared spectroscopy (FT-IR). The Infrared spectroscopy is the modern widely used technique for identification of functional groups present within a molecule [98]. The identification of a particular compound depends on the amount of light absorbed to cause any vibration at any particular frequency, measured in cm^{-1}. Figure 4-47 shows the FT-IR spectra that was obtained for free MPA-ZnSe- quantum dots, CYP3A4 and the biosensor AuE/Cystm/MPA-ZnSe-QDs/CYP3A4 respectively, carried out using NaCl pellets on liquid samples.

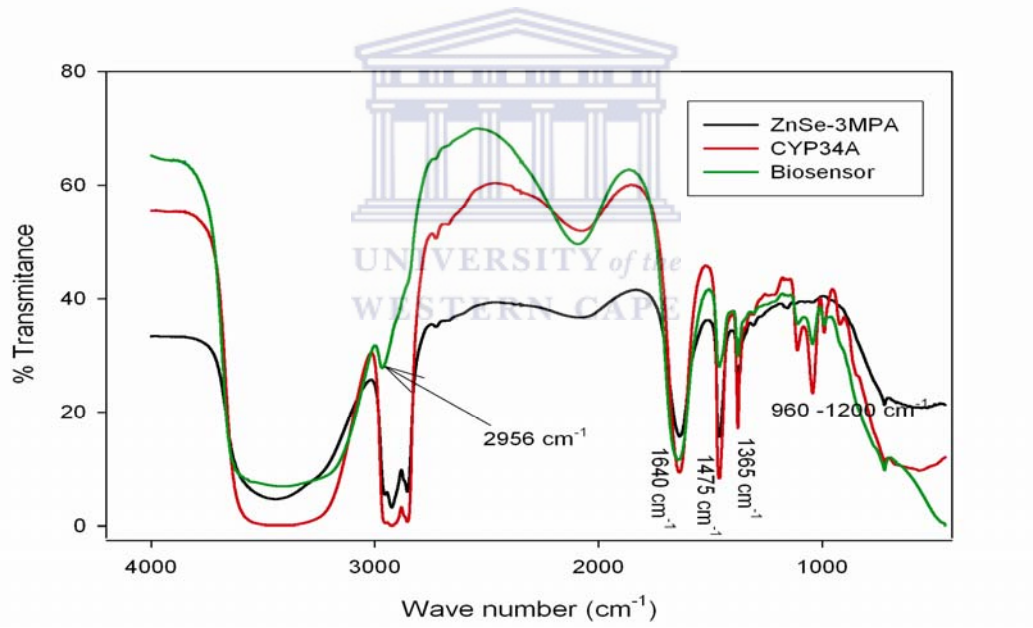

Figure 4-47: FT-IR studies of AuE/Cystm/MPA-ZnSe-QDs/CYP3A4 biosensor**.**

For the spectra of the first two, the ZnSe-3MPA or refered in the text as MPA-ZnSe-QDs (in black) and CYP34A, (in red) characterisc absorption split bands of nujol were observed at around 2850 – 3000 cm^{-1}. However, when the biosensor film; made of Cystm/MPA-ZnSe-QDs/CYP3A4 was fabricated and exposed to FT-IR spectra, a single new weak absorption band was observed at 2956.02 cm^{-1}. The band at 2956.02 cm^{-1} was

deduced to be the characteristic band of secondary amides. In this work, this band resulted from reaction of the free carboxylic group (-COOH) in MPA-ZnSe-QDs and the free amine group (-NH_2) in CYP34A according to the reaction in Figure 4-48:

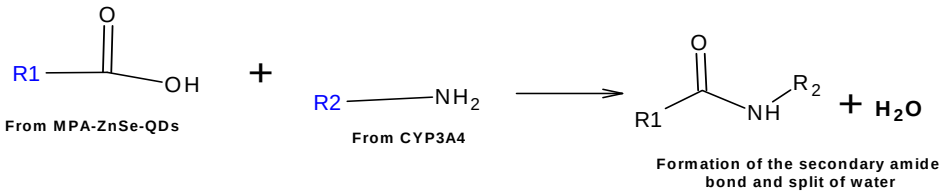

Figure 4-48: Represents a reaction of MPA-ZnSe-QDs with CYP3A4 amine groups

The validation of this observation then proved clearly that there was a strong interaction between the NH_2 groups from CYP3A4 and (COOH) from the 3-mercpto propionic acid capped ZnSe quantum dots, which was associated with the stability of the enzyme molecule onto the immobilised matrix. A common problem to biosensor is what, is called enzyme stripping which is due to the weekly bound bio-molecules onto the matrix. The best solution to this problem is; by preparing the enzyme biosensor in the stable environment or a stable immobilisation platform as possible so as to limit the problem of stripping and falling off the bio molecules or the enzyme from its solid support. It was then concluded that the platform used in construction of the biosensor AuE/Cystm/MPA-ZnSe-QDs/CYP3A4 was biocompatible and stable.

4.1.5.2 Microscopy of AuE/Cystm/MPA-ZnSe-QDs/CYP3A4 biosensor

The scanning electron microscopy was used to study and characterise the surface morphology of the (a) gold electrode before and after immobilisation by (b) cysteamine, (c) 3-mercaptopropionic acid capped ZnSe quantum dots and (d) CYP3A4 enzyme. Figure 4-49 represents the SEM images obtained during characterization of the different films deposited onto gold printed gold electrodes (SPGE).

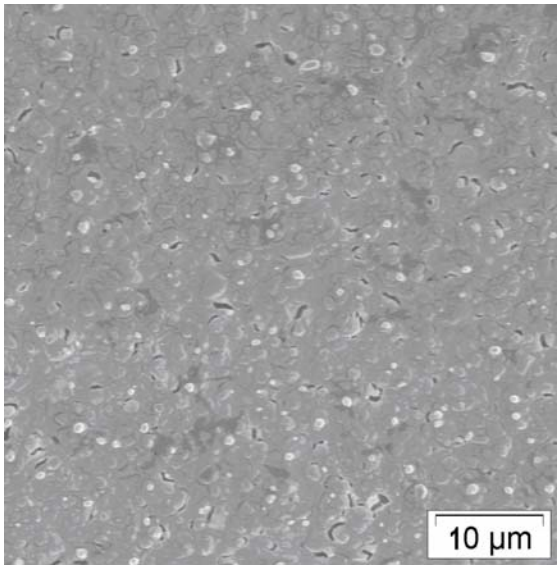

(a) Bare gold electrode

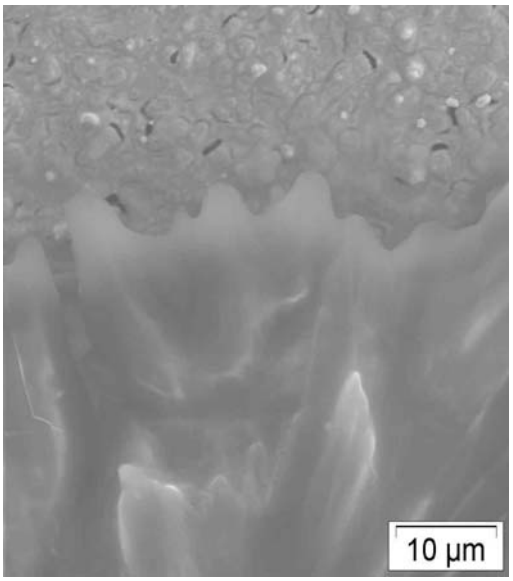

(b) AuE/cystm

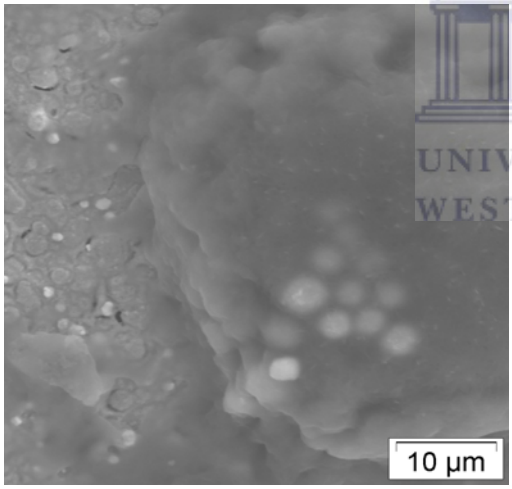

(c) AuE/Cystm/MPA-ZnSe-QDs

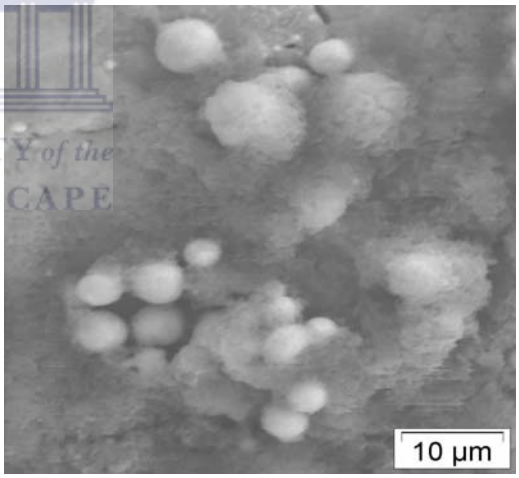

(d) AuE/Cystm/MPA-ZnSe-QDs/CYP3A4

Figure 4-49: (a)-(d) Represents the SEM of AuE bare, AuE/cystm, AuE/Cystm/MPA-ZnSe-QDs and AuE/Cystm/MPA-ZnSe-QDs/CYP3A4 biosensor respectively.

The SEM image Figure 4-49 (b) AuE/cystm: showed the morphology of the gold electrode after the immobilisation of a monolayer of cysteamine onto the gold surface. There was a clear distinguishable change in the morphology as compared to the bare gold electrode indicated by Figure 4-49 (a). This clearly indicated that the cysteamine

molecule formed a smooth layer by self assembling itself onto the rough gold surface sufficiently. This was also justified by appearance of some of the exposed or uncovered gold surface also shown in Figure 4-49 (b). The Figure 4-49 (b) and (c) also showed a distinguishable difference in their structural morphologies, Figure 4-49 (c) showed the morphology of the AuE/Cystm layer immobilised with MPA-ZnSe-QDs (i.e. AuE/Cystm/MPA-ZnSe-QDs film). The immobilisation of 3-mercaptopropionic acid capped zinc selenide quantum dots resulted in the quantum dots burring themselves within the cysteamine monolayer; with morphology of the MPA-ZnSe-QDs resembling a smooth surface and a huge growth in size of the formed dots (shown in white). At the same instance the cystymine molecules surrounded themselves around the quantum dots molecules (not particles) making the quantum dot molecules to grow huge in size. After the immobilisation of the CYP3A4 enzyme shown in Figure 4-49 (d), the surface morphology of the film changed from being smooth to rough, thus indicating the physical adsorption of the CYP3A4 enzyme on the MPA-ZnSe-QDs/Cystm modified gold electrode. These SEM studies done on the AuE/Cystm/MPA-ZnSe-QDs/CYP3A4 biosensor after each of the immobilisation steps, showed a clear distinguishable change in the morphologies after each immobilization step, which indicated that the immobilisation platform of the biosensor was sufficient. The obtained SEM images also clearly indicated that each of the immobilised material were able to sop up themselves physically onto the film previously bound to the electrode surface. Indicating that not only the covalent bounding of the films on top of each other occurred, but also the material or films immobilised onto the biosensor platform were able to enclose themselves within films previously mobilised on the electrode surface at the same time minimising the physical surface coverage of the gold electrode instead of forming a layer on top of each other, which would typically resulted in very thin layer onto the transducer surface, which in this case is gold electrode.

4.1.5.3 Catalytic activity of the AuE/Cystm/MPA-ZnSe/CYP3A4 towards 17β-estradiol

Cyclic voltammetry (CV) and square-wave voltammetry (SWV) were used to study the catalytic activity of the AuE/Cystm/MPA-ZnSe-QDs/CYP3A4 biosensor. All the cyclic voltammetry measurements were carried out under aerobic conditions at room temperature. The oxygen was necessary to complex the CYP3A4-Fe^{3+} (hemi stable active site of the enzyme CYP3A4) to Fe^{3+}-O_2 (oxygenated hemi active site of the enzyme CYP3A4) which is capable of undergoing catalytic redox reactions. The oxygenated iron centre of the CYP3A4 is known to be more active than unoxygenated Fe^{3+} centre, thus allowed for a rapid substrate reduction, and fast enzyme- substrate kinetics [67].

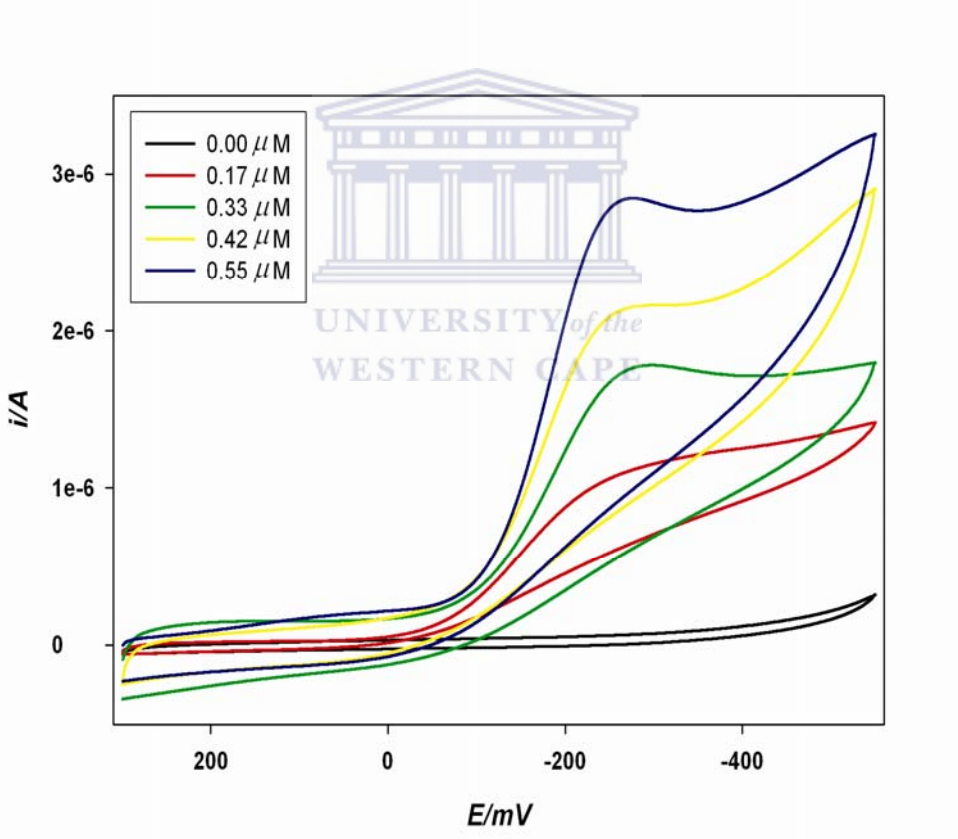

Figure 4-50: Cyclic Voltammograms representing the response of AuE/Cystm/MPA-ZnSe-QDs/CYP3A4 biosensor towards different concentrations of 17β Estradiol, in 0.1 M PBS, pH 7.4, scan rate 10 mV s^{-1}.

The response of the biosensor to 17β-estradiol substrate was studied at a potential window of E = 300 mV to E = -550 mV which has been reported by many CYP3A4 assays to be the most reliable working range for CYP3A4 enzymes [72]. The first biosensor measurements were carried out in 0.1 M PBS un-degassed solution, with no substrate concentration, there was no oxidation or reduction peak observed, as shown by Figure 4-50**:** When the first 2 μL increment of 17β-estradiol was added into the 0.1 M PBS electrolyte, there was an appearance of reduction peak that occurred at a potential of E_{pc} = -290 mV, the peak was a resultant of the reduction 17β-estradiol by CYP3A4 enzyme on the biosensor. Similar response was observed when the concentration of the substrate was increased followed by increase in catalytic current response. The catalytic reduction of 17β-estradiol was than found to be irreversible, because of absence of oxidation peak. Figure 4-50: shows Oysteryoung square-wave voltammograms of the biosensor response, proportional to the amount of 17β-estradiol added to 0.1 M PBS solution as the standard solution for the biosensor.

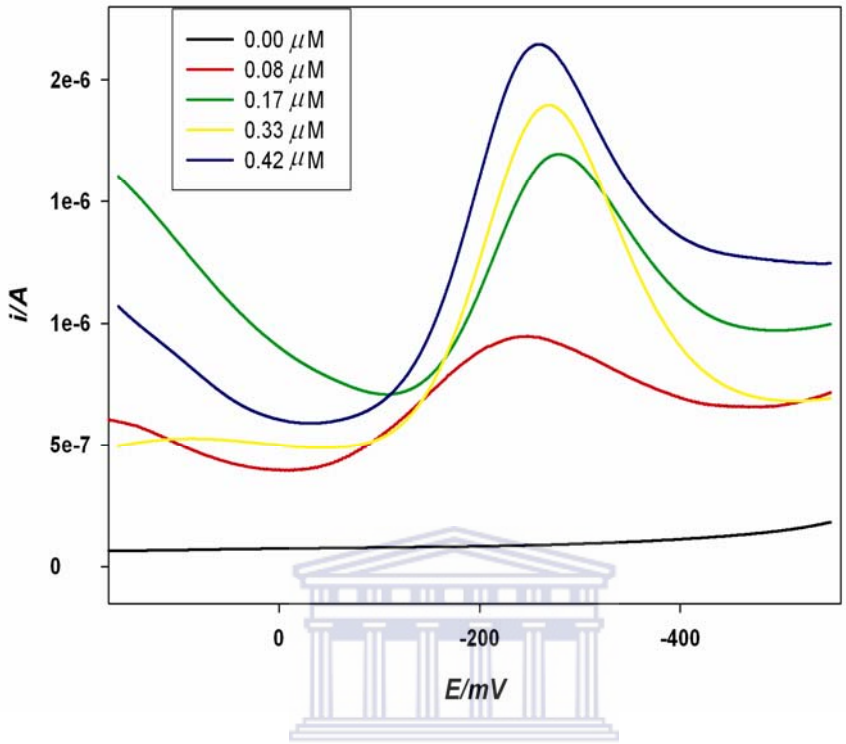

Figure 4-51: Oysteryoung square-wave voltammograms representing the responses of AuE/Cystm/MPA-ZnSe-QDs/CYP3A4 biosensor towards different concentrations of 17β estradiol (E2) in 0.1 M PBS, pH 7.4, scan rate 10 mV s^{-1}.

The cyclic and square-wave voltammograms for AuE/Cystm/MPA-ZnSe-QDs/CYP3A4 biosensor indicated a good catalytic activity of the biosensor towards the substrate 17β-estradiol as shown in Figure 4-51. A reduction peak was observed at a potential of about E_{pc} = -290 mV with a shift in potential towards the negative potentials as concentrations of substrate E2 were increased. The shift in potential towards the negative potential indicated that the HRP-Fe^{3+} active centre of the enzyme immobilised onto the biosensor was simultaneously becoming more susceptive to reduction, as the substrate E2 was being hydroxylated to form a hydroxyl-E2 product [66].

The calibration curve of the biosensor responses towards different concentrations of 17β estradiol was complied. The calibration curve indicated a linear current response of concentrations of 17β estradiol from 4.0x 10^{-8} M to 2.2x10^{-7} M, after which the biosensor showed a constant current response with increasing concentrations of 17β-estradiol (E2). This scenario was discussed to be, on the bases that there might have been an accumulation of substrate molecules onto the phosphate buffer solution, resulting in the CYP3A4 enzyme saturation, meaning the enzyme could no longer induce any more substrate closer to its active site. The following Figure 4-52 shows calibration curve representing the responses of AuE/Cystm/MPA-ZnSe-QDs/CYP3A4 biosensor towards 17β estradiol.

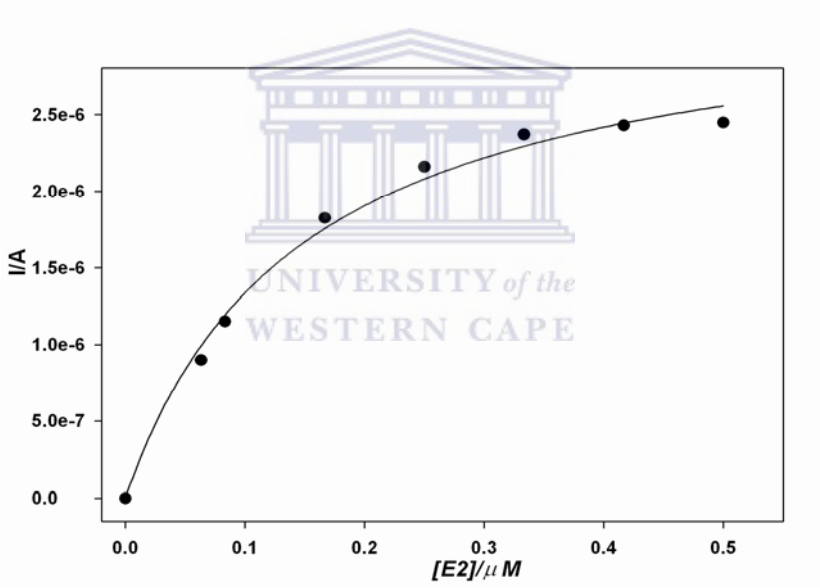

Figure 4-52: Calibration curve of AuE/Cystm/MPA/CYP3A4 biosensor representing the responses of the biosensor towards different concentrations 17β-estradiol.

The calibration curve for AuE/Cystm/MPA-ZnSe-QDs/CYP3A4 biosensor fitted well with Michaelis- Menten equation:

$$i_p = \frac{i_{max}[17\beta - estradiol]}{[17\beta - estradiol] + K_m^{app}} \quad \text{Equation 4.1-5}$$

Where i = current, i_{max} = maximum current, [17β-estradiol] = concentration of 17β-estradiol and K_m^{app} is the Michaelis- Menten constant. The Michaelis-Menten equation describes the kinetics of the enzyme- substrate, and the efficiency of the enzyme to its associated substrate [41, 57, 103]. The K_m^{app} for this study was found to be 0.056 µM. The previous developed biosensor AuE/PANI:MPA-ZnSe-QDs/HRP indicated much less Michaelis Menten constant thus, the latter biosensor AuE/Cystm/MPA-ZnSe-QDs/CYP3A4 gave a better Michaelis Menten constant, which indicated that CYP3A4 enzyme was immobilised on the biocompatible micro environment, with higher enzymic activity towards 17β-estradiol. The Figure 4-53 illustrates a simplified reaction mechanism which was suggested to be occurring during the catalytic electron transfer reaction between 17β-estradiol, and AuE/Cystm/MPA-ZnSe-QDs/CYP3A4 biosensor surface.

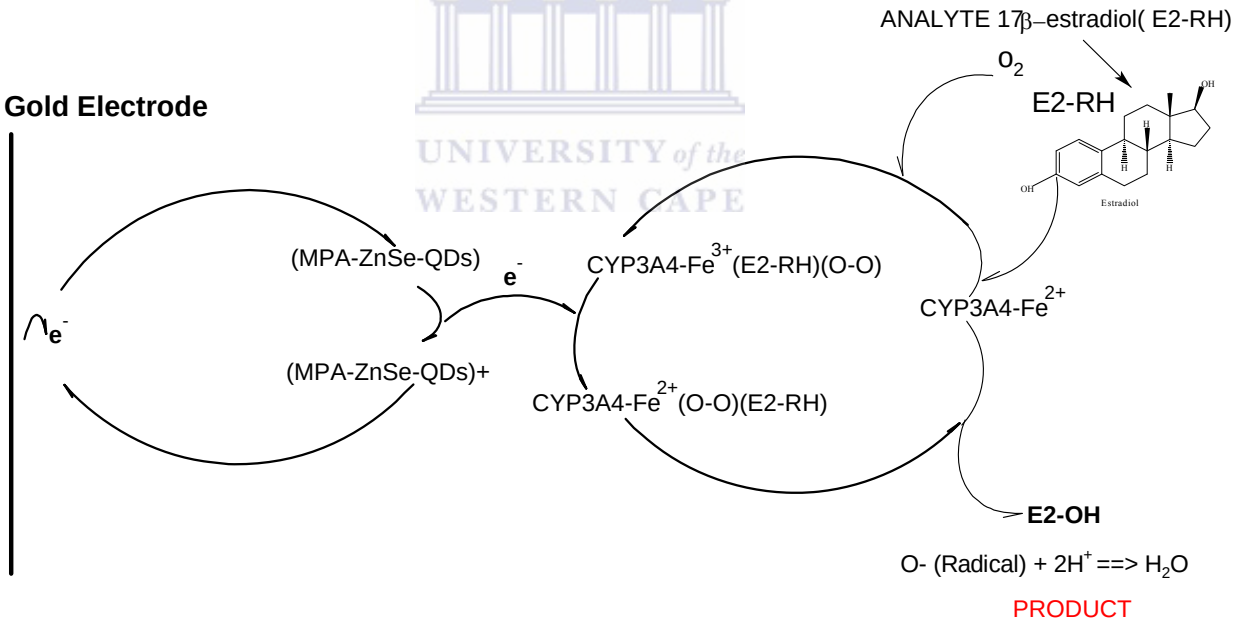

Figure 4-53: Reaction mechanism for E2 catalytic conversion at biosensor electrode.

Where E2-RH was 17β-estradiol, E2 OH wa the hydroxylated 17β-estradiol, o was an oxygen radical, $2H^+$ was the two hydrogen atoms and O_2 was oxygen. The catalytic reaction deduced to be proceededing by: a hemi centre of CYP3A4 referred to in the figure as CYP3A4-Fe^{3+}. The mechanism was that the resting state of the enzyme (i.e. CYP3A4-Fe^{3+}) selectively binds to the first available substrate which in the case was E2-

RH. The binding of the substrate E2-RH to the enzymes induces its active site causing a conversion from high spin state to low spin state which has relatively low binding energy. The CYP3A4-Fe^{3+}(E2-RH) then binds to the oxygen, to form CYP3A4-Fe^{3+}(E2-RH)(O-O), the binding of the enzyme immobilised onto the biosensor with the oxygen facilitates monooxygenation of the substrate, where the molecular oxygen attached at the enzymes active site of the cytochrome P450-3A4 splits into with one oxygen participating in oxygenation of the E2-RH to E2-ROH and the other oxygen atom splitting into a very reactive radical which binds with hydrogen atoms present in the phosphate buffer solution to form water. The second and third, and firth E2-RH substrate interaction with the biosensor surface generated the catalytic current as indicated by cyclic and differential-pulse voltammograms in Figure 4-51 and Figure 4-50.

4.1.5.4 The sensitivity of the AuE/Cystm/MPA-ZnSe-QDs/CYP3A4 biosensor

The sensitivity of the AuE/Cystm/MPA-ZnSe-QDs/CYP3A4 biosensor was obtained by using a standard deviation linear calibration curve plotted by Sigma Plot 8 software.

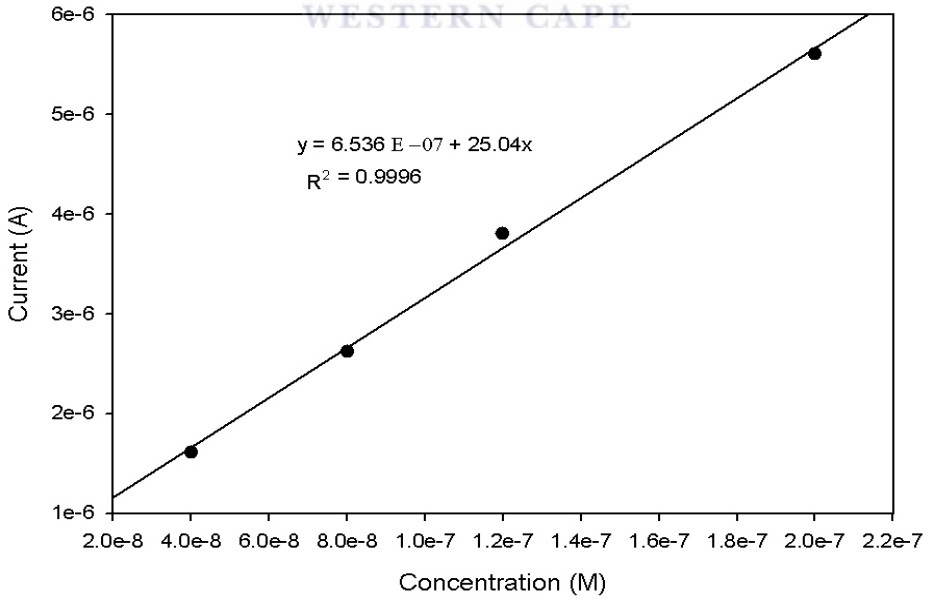

Figure 4-54: Linearity and sensitivity of AuE/Cystm/MPA-ZnSe-QDs/CYP3A4.

The sensitivity of the AuE/Cystm/MPA-ZnSe-QDs/CYP3A4 biosensor was found to be 25.04 μA/μM, which was interpolated by the slope of the linear range plot versus the (change in concentration of 17β-etsradiol) shown in Figure 4-54.

4.1.5.5 The amperometric studies of AuE/Cystm/MPA-ZnSe-QDs/CYP3A4 for the detection of 17β-estradiol

The study was done to determine the steady state response time of the biosensor AuE/Cystm/MPA-ZnSe-QDs/CYP3A4 to concentrations of E2**.** The amperometric responses were recorded at a potential of E = -290 mV, at a frequency 0.5 Hz, shown in Figure 4-55.

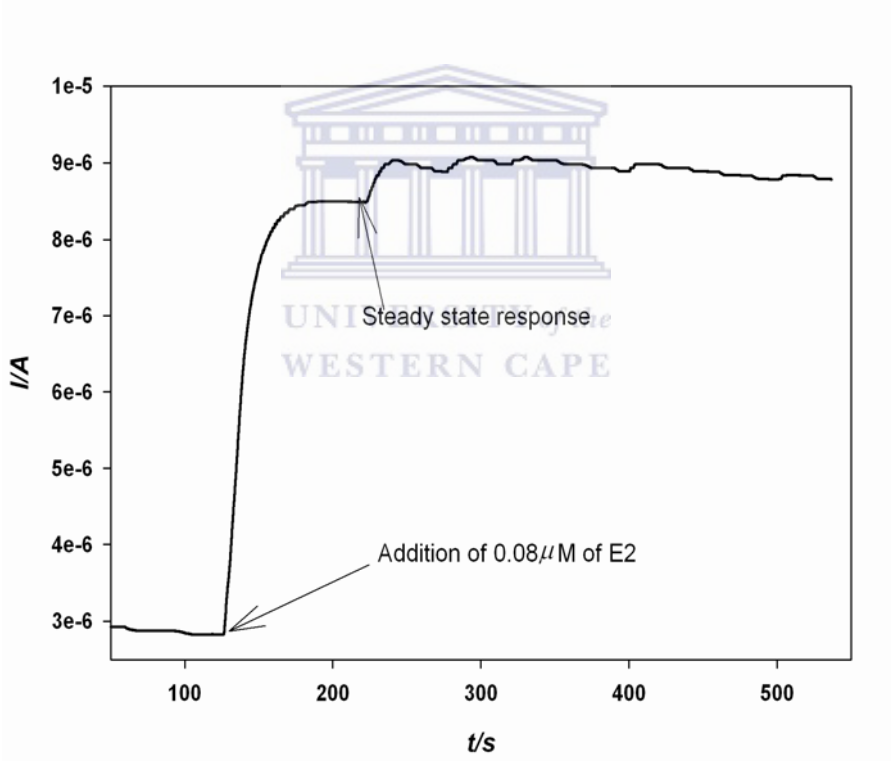

Figure 4-55: Steady state amperometric response of AuE/Cyst/MPA/CYP3A4 biosensor towards 17β –estradiol.

The response time of the biosensor after addition of 0.08 μM E2 was found to be 3 seconds deduced from the results obtained from the steady state amperommetry (Figure 4-55). Thus roughly 6 measurements of E2 concentrations could be measured within 10

min, excluding the time required to prepare and assemble the biosensor. Table 4-3 gives the summary and catalytic kinetic parameters obtained for the electrochemical enzyme biosensor developed during this study.

Table 4-3: Represents the catalytic kinetic parameters of the developed biosensors for the detection of 17β-estradiol substrate.

Biosensor	K_m^{app} **(mM)**	i_{max} **(µA)**	**Detection limit (g/L)**	**Linear Range (µM)**
AuE/PANI:MPA-ZnSe-QDs/HRP	0.073	2.5×10^{-6}	2.05×10^{-8}	0.25 - 1.7
AuE/Cystm/MPA-ZnSe-QDs/CYP3A4	0.056	2.3×10^{-6}	2.8×10^{-8}	0.04 - 0.2

The parameters indicated that the biosensor AuE/Cystm/MPA-ZnSe-QDs/CYP3A4 gave better catalytic activity toward 17β-estradiol based on kinetic catalytic parameters reported in table 4 such as K_m^{app} = 0.056< 0.073 obtained for AuE/PANI:MPA-ZnSe-QDs/HRP, indicating that the biosensor AuE/Cystm/MPA-ZnSe-QDs/CYP3A4 was a better biosensor suitable for detection of 17β-estradiol. The CY3A4 is involved in real metabolism of steroids including 17β-estradiol listed in [65, 104] as one of its major substrate.

LIST OF APPENDIX

LIST OF APPENDIXES

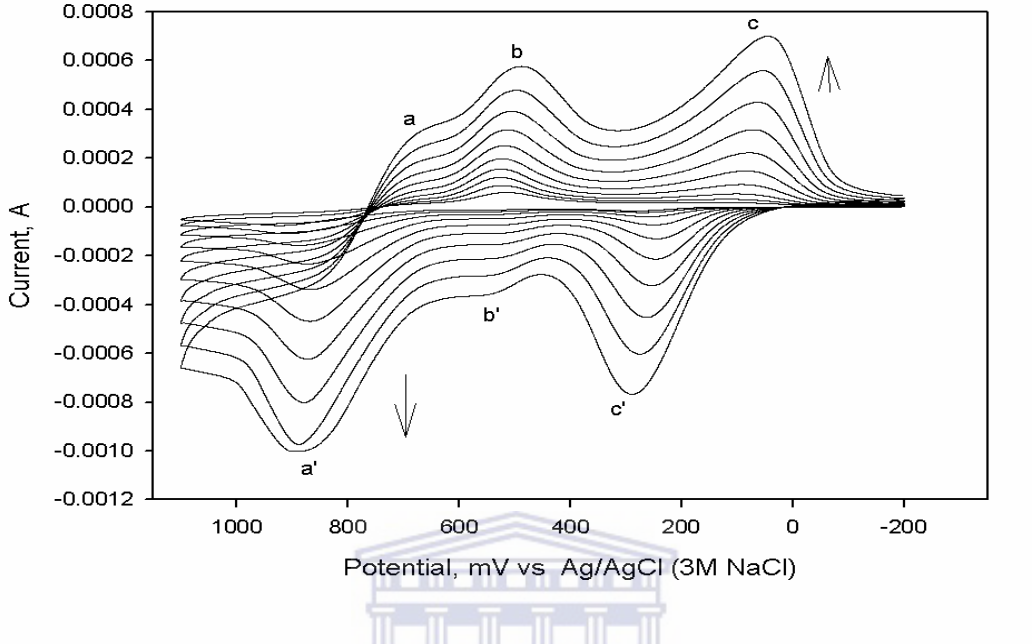

Figure 4-56: Electro-deposition of PANI onto a gold disk electrode in 1 M HCl and 92 µL aniline monomer at a pH 0.4, scan rate 100 mV s^{-1}.

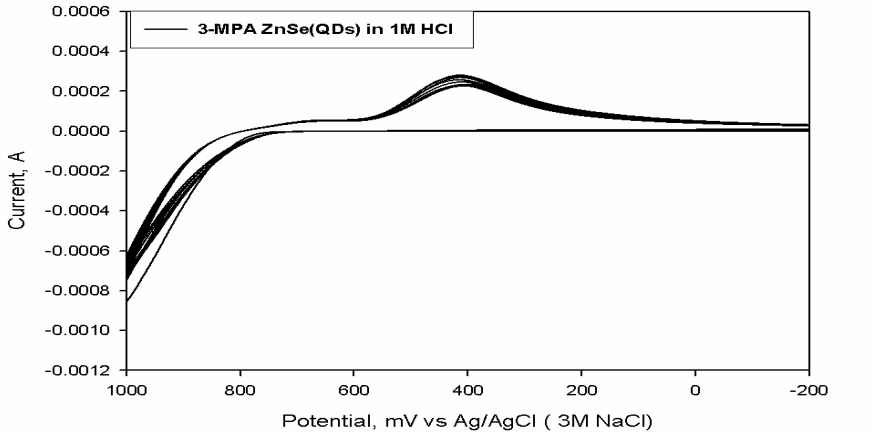

Figure 4-57: Cyclic voltammograms representing the electro-deposition of MPA-ZnSe-QDs film onto gold electrode in 1 M HCl , pH 0.4, at a potential window between E = 1100mV and E = -200 mV, scan rate of 100 mV s^{-1}.

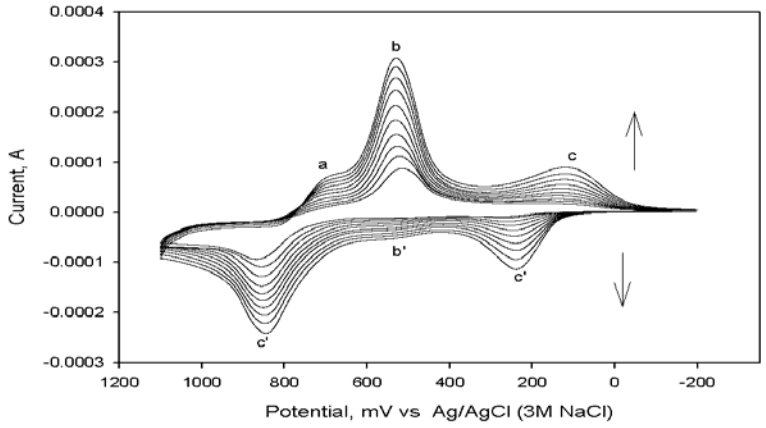

Figure 4-58: Cyclic voltammograms representing the electro-deposition of PANI:MPA-ZnSe-QDs film onto gold electrode in 1 M HCl , pH 0.4, at a potential window between E = 1100 mV and E = -200 mV, scan rate of 100 mV s^{-1}., for aniline to MPA-ZnSe-QDs ratio of (2:1).

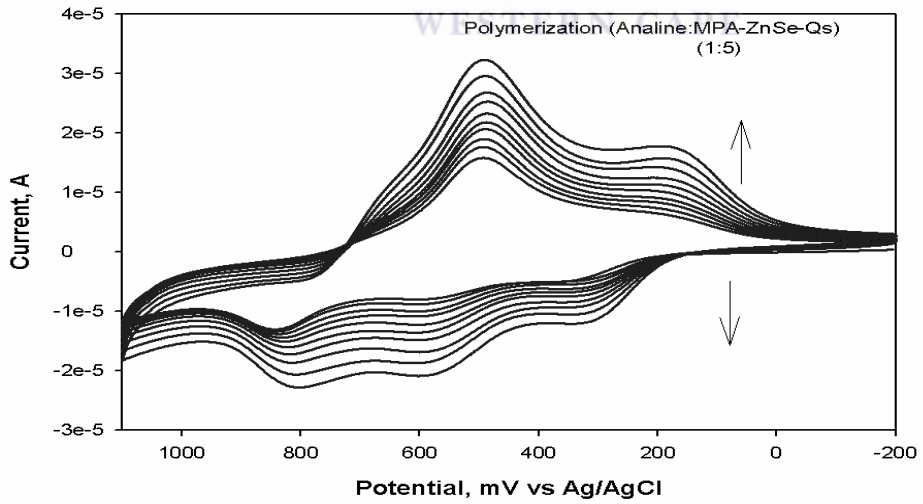

Figure 4-59: Cyclic voltammograms representing the electro-deposition of PANI:MPA-ZnSe-QDs film onto gold electrode in 1 M HCl , at a potential window between E = 1100 mV and E = -200 mV, scan rate of 100 mV s^{-1}, for aniline to MPA-ZnSe-QDs ratio of (1:5).

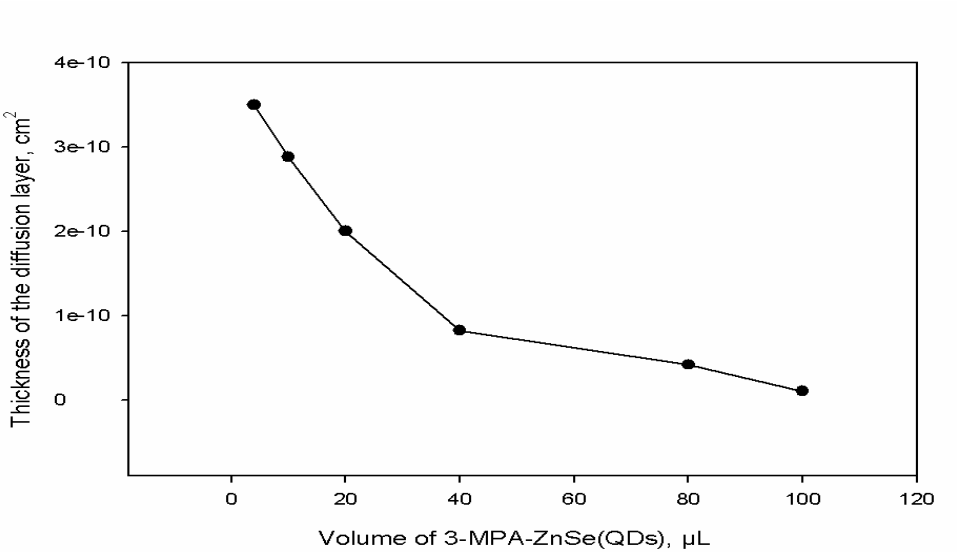

Figure 4-60: Effect of the volume of MPA-ZnSe-QDs on the thickness of PANI:MPA-ZnSe-QDs film deposited onto a gold electrode when volume of analine was kept constant; 92 µL.

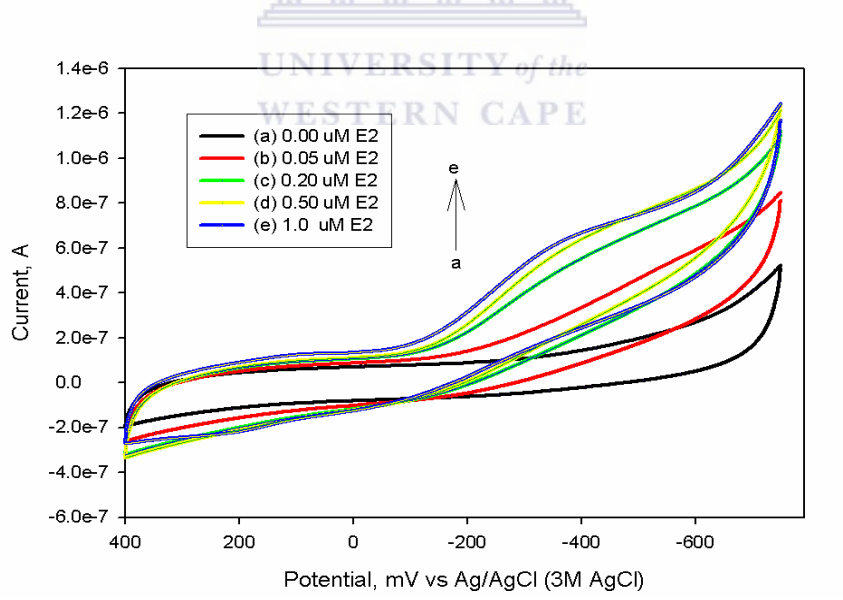

Figure 4-61: Cyclic voltammograms representing the reproduced AuE/PANI:MPA-ZnSe-QDs/HRP biosensor and determination of 17β-estradiol concentrations in 0.1 M PBS, pH 7.0, at a potential window between E = 400 mV and E = -800 mV at scan rate of 20 mV s^{-1}, aerobic conditions.

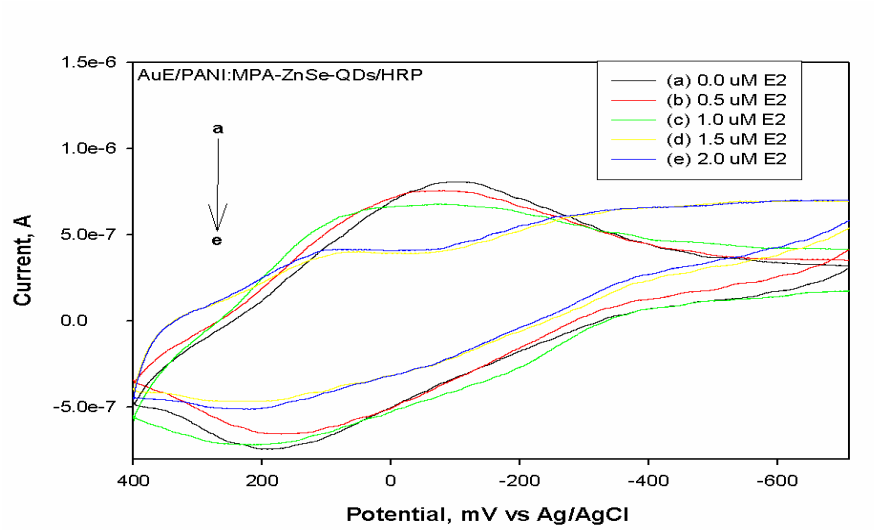

Figure 4-62: Cyclic voltammetry responses of AuE/PANI:MPA-ZnSe-QDs/HRP biosensor to different concentrations of 17β-estradiol (a) 0.0 µM, (b) 0.5 µM, (c) 1.0 µM (d) 1.5 µM, and (e) 2.0 µM, in 0.1 M PBS; pH 7.0 at a scan rate of 20 mV s^{-1} at anaerobic conditions.

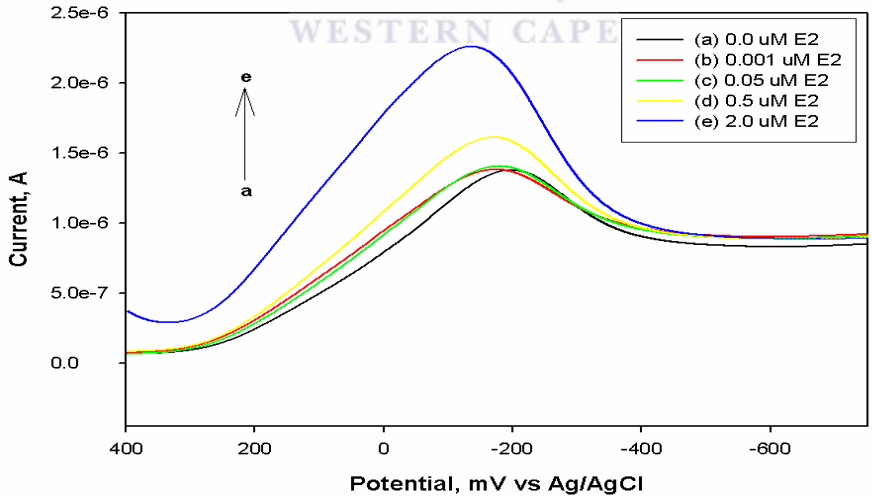

Figure 4-63: Osteryoung square-wave voltammetry responses of AuE/PANI:MPA-ZnSe-QDs/HRP biosensor to different concentrations of 17β-estradiol; (a) 0.0 µM, (b) 0.001 µM, (c) 0.05 µM (d) 0.5 µM, and (e) 2 µM, in 0.1 M PBS; pH 7.0 at a scan rate of 20 mV s^{-1} at aerobic conditions.

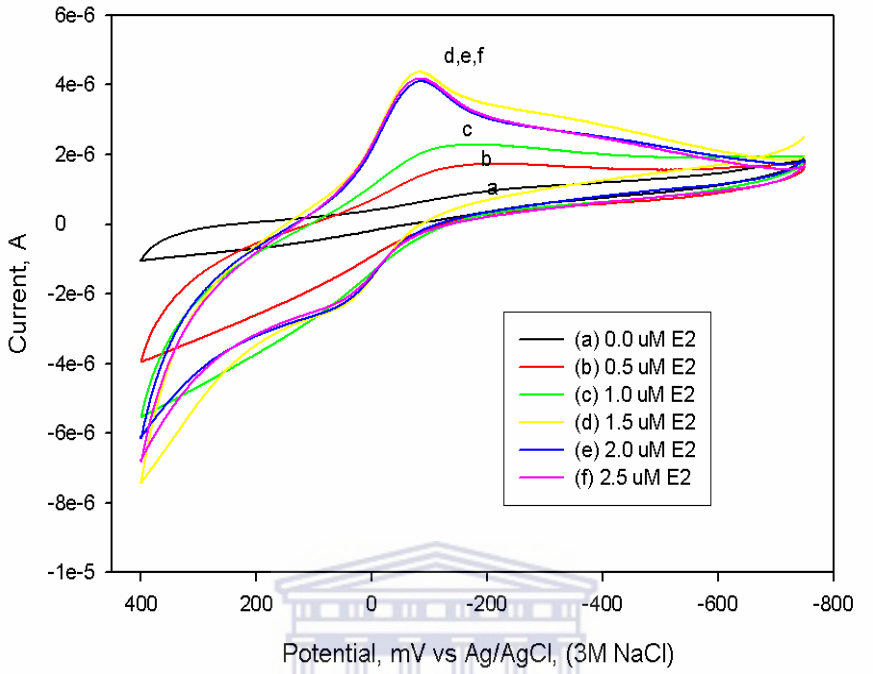

Figure 4-64: Cyclic voltammograms responses of AuE/PANI:MPA-ZnSe-QDs/HRP biosensor to different concentrations of 17β-estradiol in 0.1 M PBS, pH 7.0, at a potential window between E = 400 mV and E = -800 mV at scan rate of 20 mV s^{-1}, after being used more than once, under aerobic conditions.

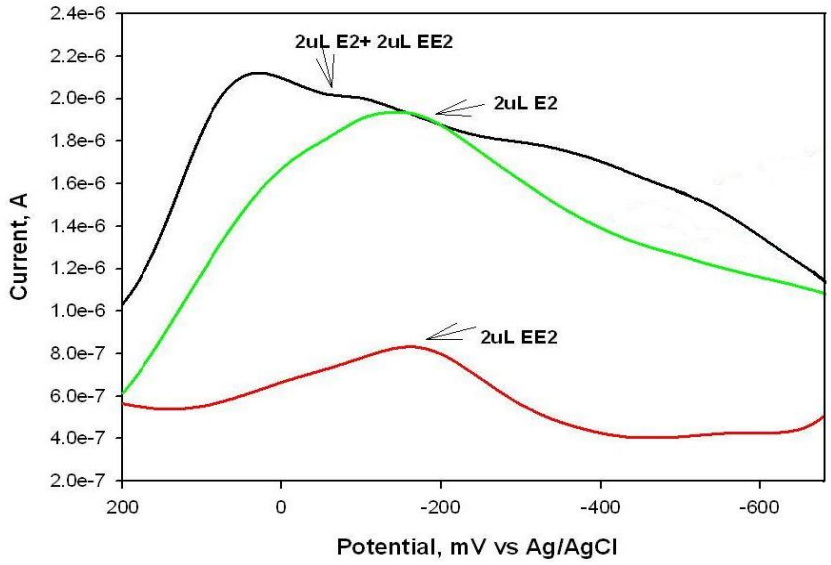

Figure 4-65: Difference Osteryoung square-wave voltammogrrammes representing the response of AuE/PANI:MPA-ZnSe-QDs/HRP biosensor to mixed substrates concentrations of E2, EE2 and EE2 + E2 in 0.1 M PBS, pH 7, and a frequency of 10 Hz or scan rate of 20 mV s^{-1}, under aerobic conditions.

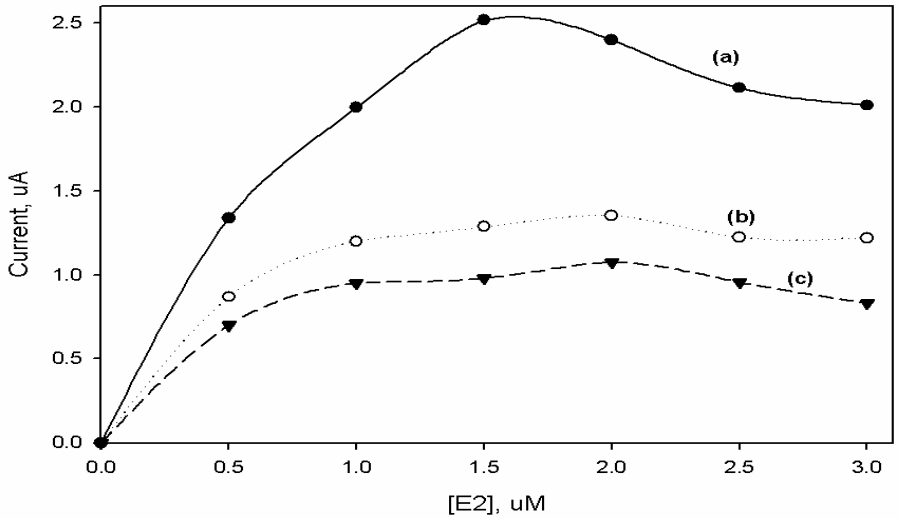

Figure 4-66: Calibration curves representing the stability of AuE/PANI:MPA-ZnSe-QDs/HRP biosensor after: (a) 1st measurement, (b) 2nd measurement and (c) 3rd measurement at different concentrations of 17β-estradiol.

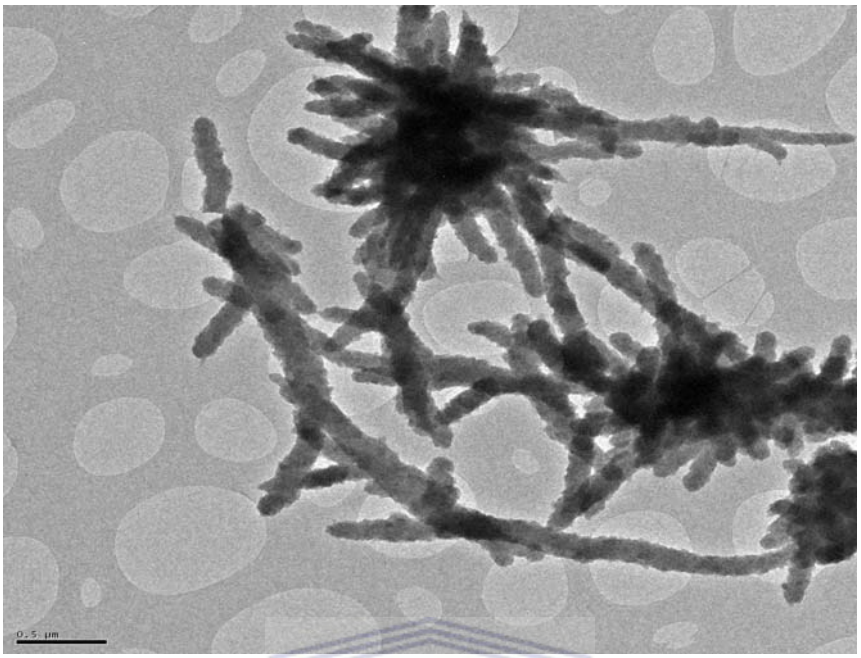

Figure 4-67: The TEM image of PANI.

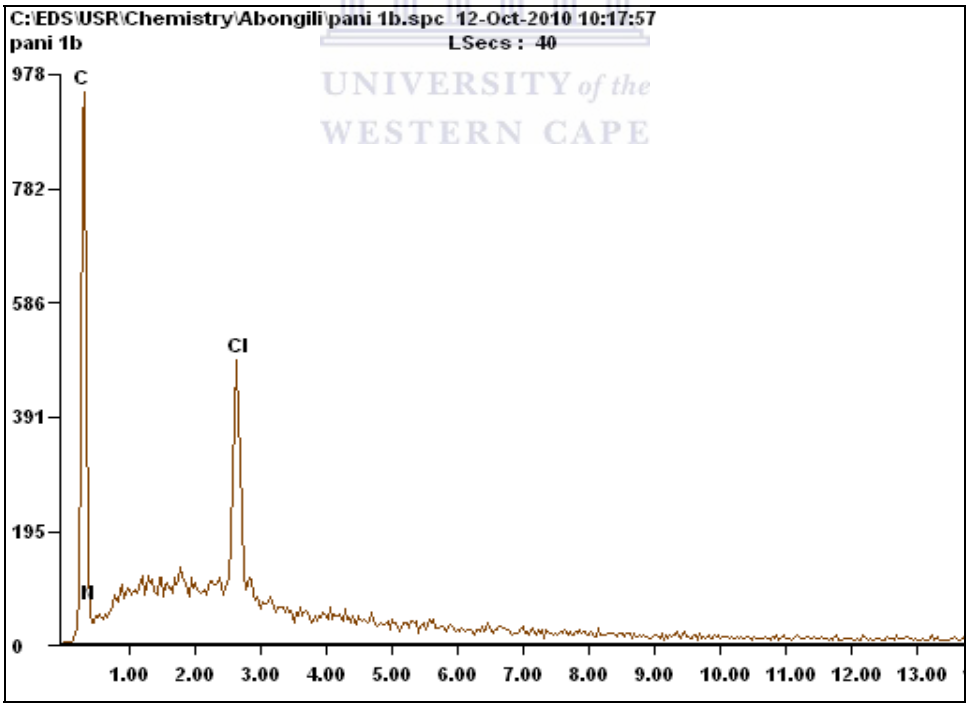

Figure 4-68: Original EDAX spectra of PANI.

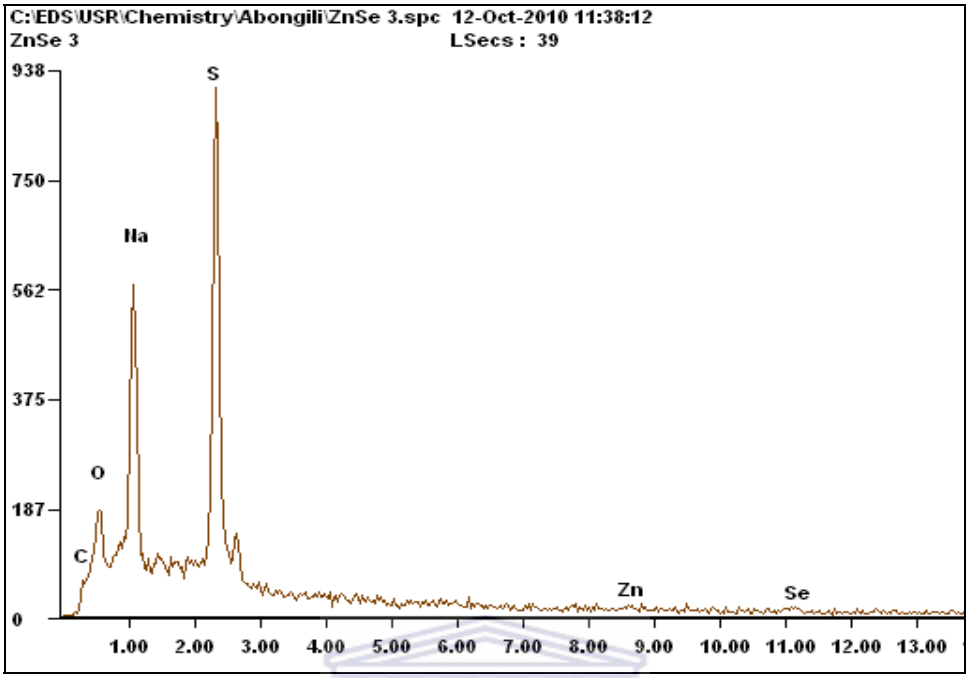

Figure 4-69: Original EDAX spectra of MPA-ZnSe-QDs.

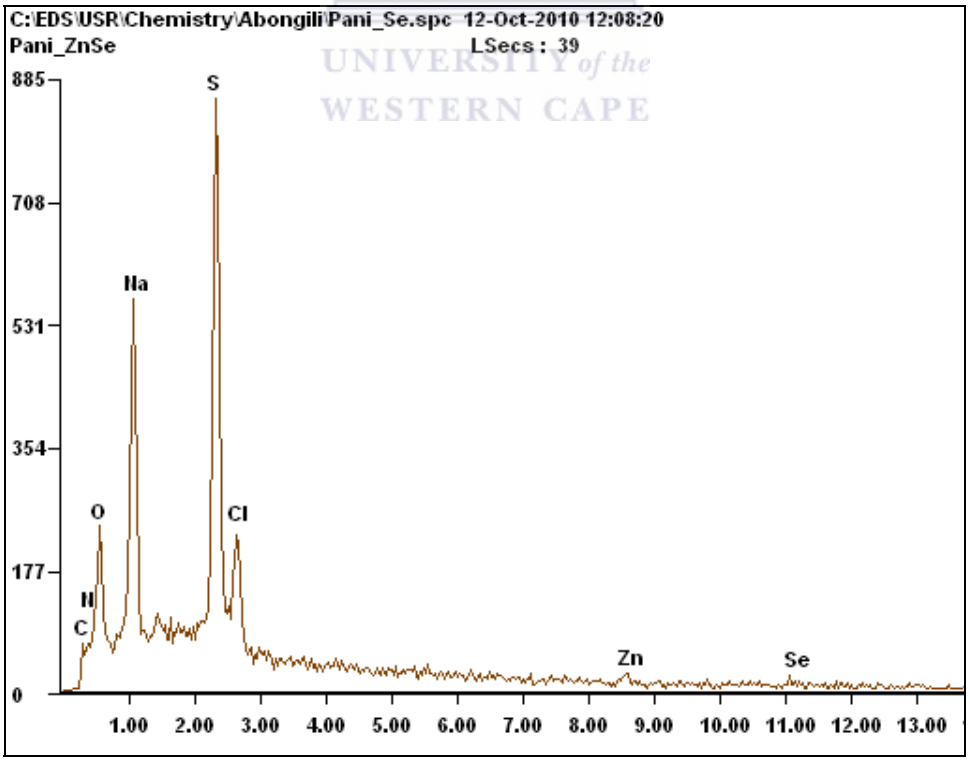

Figure 4-70: Original EDAX spectra of PANI:MPA-ZnSe-QDs.

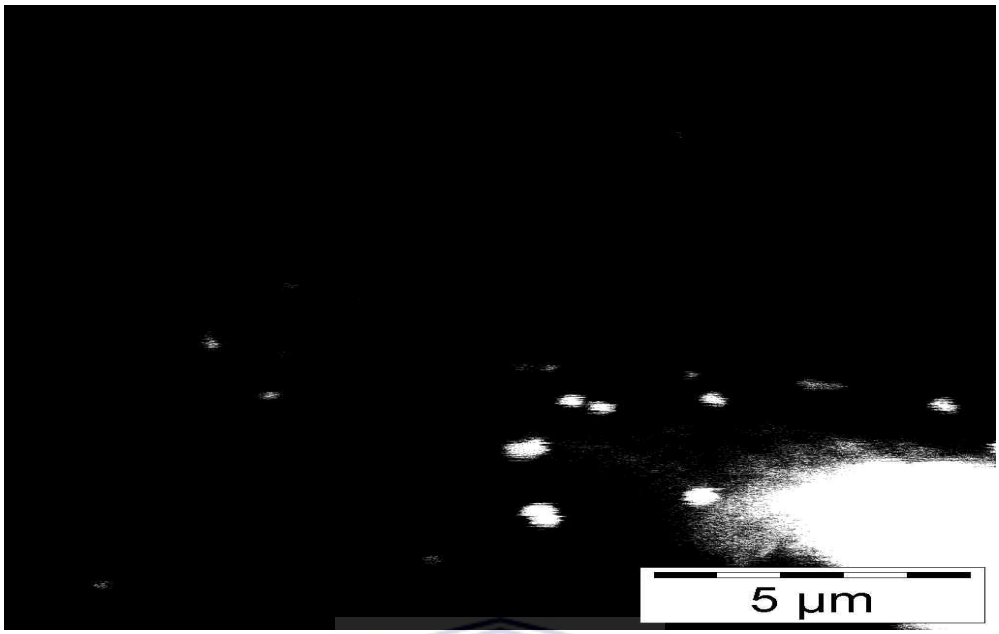

Figure 4-71: The SEM image of MPA-ZnSe-QDs that exhibited charging.

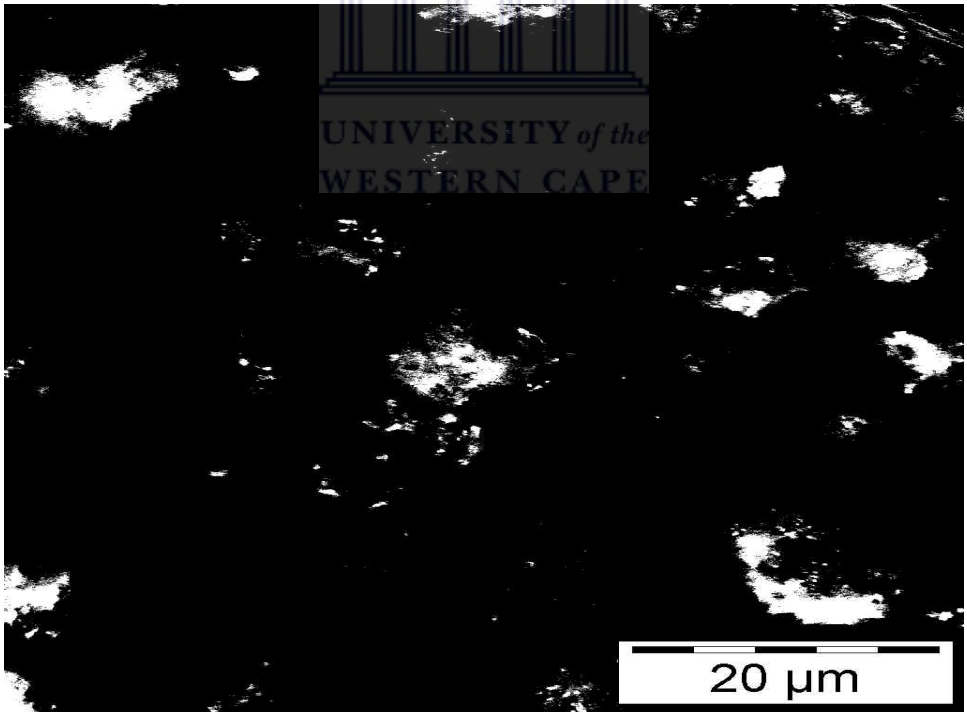

Figure 4-72: The SEM image of PANI:MPA-ZnSe-QDs which exhibited charging.

CONCLUSION

CHAPTER 5

5.1 CONCLUSION

Two electrochemical enzyme biosensors were successfully developed for quantitative detection of 17β-estradiol using two different enzyme horseradish peroxidase and cytochrome P450-3A4. The biosensor immobilised with horseradish peroxidase, catalysed the oxidation E2 to unknown ketone product, but the biosensor fabricated using Cytochrome P450-3A4 induced the conversion of E2 to tri-alcohol estradiol. The difference in the mechanisms of the reactions by these two enzymes indicated that although these two enzymes showed similarity in their structure of the active site, with both of them being hemi monooxygenases, they are ordinary specific to the type of reactions they catalyse making them to exhibit slightly different electronic catalytic properties as it was observed in the study. However the difference in the active site of cytochrome P450 and peroxidase is the amino acid derivatives present closely to their active site which is; for HRP the enzyme has histidine (*His*) – aspirate acid (*Asp*) amino acid derivative attached as a fifth ligand at the Fe^{3+} resting state iron centre where in the case of CYP3A4 the fifth ligand is the thiol ligand derived amino acid also known as cystein. These amino acids are responsible for binding to substrate thus the catalytic electron transfer behaviour of these enzymes would expectedly differ. The biosensor fabricated using HRP showed reasonable catalytic activity towards concentrations both E2 and EE2 indicating some capability of the enzyme to also catalyse EE2, although this was the case the HRP immobilised into the biosensor could be genetically engineered to detect specifically one type of estradiol or any other desired substrate, the HRP is a very good enzymes which shows tremendous environmental stability [58] . This enzyme had been also successfully used in most enzyme linked immuno absorbent assay (ELISAs) for estradiol meaning this enzyme is indeed very useful to E2 detection and shows accuracy and activity; however ELISA kit, is time consuming and not so economical, thus the biosensor developed could be a potential economical way to detect E2 sufficiently and accurately. The generic expression of the enzyme CYP3A4 in *Escherichia Coli* (*E. Coli*)

is genetic engineering of the cytochrome P450 in *E coli* to modify the enzyme such that it could only catalyse the reactions of CYP3A4 occurring naturally only outside the endoplasmic reticulum which includes biosynthesis of steroids such as 17β-estradiol in study, but would unable to catalyse other reactions as this enzyme has many substrate of which mostly are metabolised in the liver, thus changing the environmental conditions of the enzyme and inducing its active site allows the enzyme to only respond to stimuli associated with a specific type of analyte under certain conditions. The biosensor constructed using CYP3A4 expressed in *E.Coli* showed exceptional good catalytic activity toward E2 with Michaelis Menten constant of 0.056 mM indicating the CYP3A4 enzyme was mobilised on the most stable biocompatible environment, which also indicated that the enzyme had higher affinity for the substrate E2 compared to HRP on second biosensing system which has Michaelis Menten constant of 0.073 mM.

CHAPTER 6

6.1 BIBLIOGRAPHY

1. Jensen, E. V., Jacobson, H. I., Walf, A. A., and Frye, C. A. (2010) Estrogen action: A historic perspective on the implications of considering alternative approaches, *Physiology & Behavior 99*, 151-162.
2. Adama, M., Sesay, David, C., and Cullen. (2001) Detection of hormone mimics in water using a miniaturized SPR sensor, *Environmental Monitoring and Assessment 70*, 83–92.
3. Alda, M. L. d., and Barceló, D. (2000) Determination of steroid sex hormones and related synthetic compounds considered as endocrine disrupters in water by liquid chromatography-diode array detection- mass spectrometry, *Journal of Chromatography 892*, 391-406.
4. Campbell, C. G., Boglin, S. E., Green, F. B., grayson, A., Wozei, E., and Stringfellow, W. T. (2006) Biologically directed environmental monitoring fate and transport of estrogenic endocrine disrupting compounds in water: A review, *Chemosphere 65*, 1265-1280.
5. Saaristo, M., Craft, J. A., Lehtonen, K. K., and Lindström, K. (2010) An endocrine disrupting chemical changes courtship and parental care in the sand goby, *Aquatic Toxicology 97*, 285-292.
6. Schilirò, T., Pignata, C., Rovere, R., Fea, E., and Gilli, G. (2009) The endocrine disrupting activity of surface waters and of wastewater treatment plant effluents in relation to chlorination, *Chemosphere 75*, 335-340.
7. Shappell, N. W., Hyndman, K. M., Bartell, S. E., and Schoenfuss, H. L. (2010) Comparative biological effects and potency of 17[alpha]- and 17[beta]-estradiol in fathead minnows, *Aquatic Toxicology 100*, 1-8.
8. Kumara, P., and Singh, K. (2009) ZnSe quantum dots: Synthesis, characterization and PL properties, *Journal of Optoelectronic and Biomedical Materials Wurtzite 1*, 59 - 69.

9. Singh, K. P., Kang, W. K., and Hee-Woo, R. (2009) Quantum dot doped solid polymer electrolyte for device application, *Electrochemistry Communications 11*, 1247–1250.
10. Yang, L., Yang, J., Liu, X., Zhang, Y., Wang, Y., Fan, H., Wang, D., and Lang, J. (2008) Low-temperature synthesis and characterization of ZnO quantum dots, *Journal of Alloys and Compounds 463*, 92–95.
11. Walling, M. A., and Novak, J. A. (2009) Quantum Dots for Live Cell and In Vivo Imaging, *Journal of Molecular Science 10*, 441-491.
12. Ndangili, P. M., Arotiba, O. A., Baker, P. G. L., and Iwuoha, E. I. (2010) A potential masking approach in the detection of dopamine on 3-mercaptopropionic acid capped ZnSe quantum dots modified gold electrode in the presence of interferences, *Journal of Electroanalytical Chemistry 643*, 77–81.
13. Suo, B., Su, X., Wu, J., Chen, D., Wang, A., and Guo, Z. (2010) Poly (vinyl alcohol) thin film filled with CdSe-ZnS quantum dots: Fabrication, characterization and optical properties, *Materials Chemistry and Physics 119*, 237-242.
14. Algar, W. R., Tavares, A. J., and Krull, U. J. (2010) Beyond labels: A review of the application of quantum dots as integrated components of assays, bioprobes, and biosensors utilizing optical transduction, *Analytica Chimica Acta 673*, 1-25.
15. Zhang, F., Li, C., Li, X., Wang, X., Wan, Q., Xian, Y., and Yamamoto, K. (2006) ZnS quantum dots derived reagentless uric acid biosensor, *Talanta 68*, 1353-1358.
16. Zhao, J., Chen, G., Zhu, L., and Li, G. (2010) Graphene quantum dots-based platform for the fabrication of electrochemical biosensors, *Electrochemistry Communications,* doi: 10.1016/j.elecom.2010.11.005
17. Saeeda Jaffar, Nam, K. T., Khademhosseini, A., Xing, J., Langer, R. S., and Belcher, A. M. (2004) Layer-by-Layer surface modification and patterned plectrostatic deposition of quantum dots, *Nano letters 4*, 1421-1425.
18. Li, H., Liu, S., Dai, Z., Bao, J., and Yang, X. (2009) Applications of nanomaterials in electrochemical enzyme biosensors, *Sensors 9*, 8547-8561.

19. Li, X., Zhou, Y., Zheng, Z., and Xiuliyue. (2009) Glucose biosensor based on nanocomposite films of CdTe quantum dots and Glucose Oxidase, *American Chemical. Society 25*, 6580-6586.
20. Gerard, M., Chaubey, A., and Malhotra, B. D. (2002) Application of conducting polymers to biosensors, *Biosensors and Bioelectronics 17*, 345-359.
21. Dao, D. P., Mei, N. L., Qun, L. H., and Bing, L. N. (2007) Application of meso-2,3-dimercaptosuccinic acid self-assembled gold electrode for voltammetric determination of copper, *Crotica Chemica Acta 80*, 61-66.
22. Karolien DeWael, Hans Buschopa, Lina De Smet, and Adriaensa, A. (2008) Immobilization of cytochrome c on cysteamine-modified gold electrodes with EDC as coupling agent, *Talanta 76*, 309-313.
23. Li, J., and Al-Azzawi, F. (2009) Mechanism of androgen receptor action, *Maturitas 63*, 142-148.
24. USEPA. http://www.epa.gov/endocrine/#eds.
25. Chang, H.-S., Choo, K.-H., Lee, B., and Choi, S.-J. (2009) The methods of identification, analysis, and removal of endocrine disrupting compounds (EDCs) in water, *Journal of Hazardous Materials 172*, 1-12.
26. Alda, M. J. L. d., and Barceló, D. (2000) Determination of steroid sex hormones and related synthetic compounds considered as endocrine disrupters in water by liquid chromatography-diode array detection- mass spectrometry, *Journal of Chromatography 892*, 391-406.
27. Kretzschmar, G., Papke, A., Zierau, O., Möller, F. J., Medjakovic, S., Jungbauer, A., and Vollmer, G. (2010) Estradiol regulates aryl hydrocarbon receptor expression in the rat uterus, *Molecular and Cellular Endocrinology 321*, 253-257.
28. Fishman, J., Bradlow, H. L., and Gallagher, T. F. (1960) Oxidative metabolism of estradiol, *Journal of Bilogical Chemistry 235*, 3104-3107.
29. Cardoso, C. C., Ricardo, V. P., Frussa-Filho, R., Porto, C. S., and Abdalla, F. M. F. (2010) Effects of 17[beta]-estradiol on expression of muscarinic acetylcholine receptor subtypes and estrogen receptor [alpha] in rat hippocampus, *European Journal of Pharmacology 634*, 192-200.

30. Kumar, S., Lata, K., Mukhopadhyay, S., and Mukherjee, T. K. (2010) Role of estrogen receptors in pro-oxidative and anti-oxidative actions of estrogens: A perspective, *Biochimica et Biophysica Acta 10*, 1127-1135.

31. Preedy, J. R. K., and Aiteken, E. H. (1961) The determination of estrone, estradiol-17P, and estriol in urine and plasma with column partition Chromatography, *The Journal of Biological Chemistry 236*,1300-1309

32. Hui-Bin, W., Jin-Ming, L., Dan-Ning, W., Li-Xia, Z., Zhen-Jia, L., and Xi-Tang, Y. (2007) Detection of 17β-Estradiol in river water and human, urine by highly sensitive chemiluminescence enzyme immunoassay, *Chinese Journal of Analalytical Chemistry 35*, 320–324.

33. Nekvapil, T., Borkavcava, I., and Smutha, M. (2009) Estrogenic profile of the Svratks, *Acta. Brono 78*, 313-317.

34. Gulevskaya, S. A., Lobastova, T. G., and Donova, M. V. (2010) Hydroxylation of 3[alpha]- and 3[beta]-hydroxy steroids in position 7 by a fungus of Gibberella zeae VKM F-2600, *Journal of Biotechnology 150*, 461-461.

35. Holland, H. L., and Weber, H. K. (2000) Enzymatic hydroxylation reactions, *Current Opinion in Biotechnology 11*, 547-553.

36. Koshimura, M., Utsukihara, T., Hara, A., Mizobuchi, S., Horiuchi, C. A., and Kuniyoshi, M. (2010) Hydroxylation of steroid compounds by Gelasinospora retispora, *Journal of Molecular Catalysis B: Enzymatic 67*, 72-77.

37. Li, A., and Bigelow, J. C. (2010) The 7-hydroxylation of dehydroepiandrosterone in rat brain, *Steroids 75*, 404-410.

38. Ze-Nefng, C., Yani, S., Zhao-Qian, L., Lian-Sheng, W., Ou-Yang, and Sheng, D. (2000) Role of Cytochrome P450 in estradiol metabolism in vitro, *Acta Pharmacology22*, 148-154.

39. Alistair, G. C., Renwick, oon, C. Y., Chambers, S. u. M., and Brown, C. (1981) Estradiol-17P Dehydrogenase from chicken liver, *The Journal of Biological Chemistry 256*, 1981-1887.

40. Jung, E.-M., Choi, K.-C., Yu, F. H., and Jeung, E.-B. (2010) Effects of 17[beta]-estradiol and xenoestrogens on mouse embryonic stem cells, *Toxicology in Vitro 24*, 1538-1545.

41. Walsh, C. (1979) *Enzymic Reaction Mechanisms,* Chapter 1-20, W H Freeman and Company, San Franscico.

42. Wójtowicz, T., Lebida, K., and Mozrzymas, J. W. (2008) 17[beta]-estradiol affects GABAergic transmission in developing hippocampus, *Brain Research* 1241, 7-17.

43. Deborde, M., Rabouan, S., Gallard, H., and Legube, B. (2004) Aqueous Chlorination kinetics of same endocrine disruptors, *Environmebtal. Science and Technology 38*, 5577-5583.

44. Wu H, Ramsay C., Ozaeta, P (2002) Serum estradiol quantified by isotope dilutiongas-chromatography/mass spectroscopy, *Clinical Chemistry 48*, 364-366.

45. Chen, H.-C., Kuo, H.-W., and Ding, W.-H. (2009) Determination of estrogenic compounds in wastewater using liquid chromatography-tandem mass spectrometry with electrospray and atmospheric pressure photoionization following desalting extraction, *Chemosphere 74*, 508-514.

46. Sook, B. G., Suhyeong, C., and Byung-Gee, K. (2005) A novel electrochemical detection method for aptamer biosensors, *Biosensors and Bioelectronics 21 21*, 863–870.

47. Song, J., Yang, J., and Hu, X. (2008) Electrochemical determination of estradiol using a poly(L-serine) film-modified electrode, *Journal of Applied Electrochemestry 38*, 833–836.

48. Yang, S. M., Chen, Z., Li, Y., Jiang, X., and Lin, X. (2005) A novel reagentless biosensor based on self-assembled HRP and nile blue premixed with poly(styrenesulfonate) architectures, *Chinese Chemical Letters 16*, 983-986.

49. Xu, X., Liu, S., and Ju, H. (2003) A Novel Hydrogen Peroxide sensor via the direct electrochemistry of horseradish peroxidase immobilized on colloidal gold modified screen-printed electrode, *Sensors 3*, 350-360.

50. Clark, L., and Lyons, C. J. (1962) Electrode systems for continuous monitoring in cardiovascular surgery, *Annals of the New York Academy of Sciences 102*, 29-45.
51. Deng, C., Chen, J., Nie, Z., and Si, S. (2010) A sensitive and stable biosensor based on the direct electrochemistry of glucose oxidase assembled layer-by-layer at the multiwall carbon nanotube-modified electrode, *Biosensors and Bioelectronics 26*, 213-219.
52. Lee, A.-C., Liu, G., Heng, C.-K., Tan, S.-N., Lim, T.-M., and Lin, Y. (2008) Sensitive electrochemical detection of horseradish peroxidase at disposable screen-printed carbon electrode, *Electroanalysis 20*, 2040-2046.
53. Liu, Y., Peng, D., Huang, L., Wang, Y., Chang, C., Ihsan, A., Tao, Y., Yang, B., and Yuan, Z. (2010) Application of a modified enzyme-linked immunosorbent assay for 3-amino-2-oxazolidinone residue in aquatic animals, *Analytica Chimica Acta 664*, 151-157.
54. Lee, J. Y., Shin, H. Y., Kang, S. W., Park, C., and Kim, S. W. (2011) Application of an enzyme-based biofuel cell containing a bioelectrode modified with deoxyribonucleic acid-wrapped single-walled carbon nanotubes to serum, *Enzyme and Microbial Technology 48*, 80-84.
55. http://www.wisegeek.com/what-are-enzymes.htm.
56. http://www.google.co.za/imgres?imgurl=http://isbibbio.wikispaces.com/file/view/enzymes. Isibibbio Overview of enzymes.
57. Fersht, A. (1985) Enzyme Structure and Mechanism, *Book Chapter*,
58. Nigel, C., and Veitch. (2004) Horseradish peroxidase: a modern view of a classic enzyme, *Photochemistry 65*, 249–259.
59. Ebarvia, B. S., and Sevilla, F. (2005) Piezoelectric quartz sensor for caffeine based on molecularly imprinted polymethacrylic acid, *Sensors and Actuators 107*, 782–790.
60. Lee, Y.-M., Kwon, O.-Y., Yoon, Y.-J., and Ryu, K. (2006) Immobilization of horseradish peroxidase on multi-wall carbon nanotubes and its electrochemical properties, *Biotechnology Letters 28*, 39–43.

61. Ahirwal, G. K., and Mitra, C. (2009) Direct electrochemistry of horseradish peroxidase-gold, nanoparticles conjugate, *Sensors 9*, 881-894.
62. Guo, Y., Guadalupe, A.R. (1997) Direct electrochemistry of horseradish peroxidase adsorbed on glassy carbon electrode from organic solution, *Chemical Communications*, 1437-1438.
63. Veitch, N. C. (2004) Horseradish peroxidase: a modern view of a classic enzyme *Photochemistry 65*, 249–259.
64. Kim, H.-J., Piao, M.-H., Choi, S.-H., Shin, C.-H., and Lee, Y.-T. (2008) Development of amperometric hydrogen peroxide sensor based on horseradish peroxidase-immobilized Poly(Thiophene-co-EpoxyThiophene), *Sensors 8*, 4110-4118.
65. Dianne, K., Hammond, Zhu, B. t., Wang, M. Y., and Ricci, M. J. (1997) Cytochrome P450 metabolism of estradiol in hamster liver and kidney, *Toxicology and Applied Pharmacology 145*, 54-60.
66. Bellec, G., Dréano, Y., Bail, J.-P., Ménez, J.-F., and Berthou, F. (1997) Cytochrome P450 hydroxylation of carbon atoms of the alkyl chain of symmetrical N-nitrosodialkylamines by human liver microsomes, *Mutation Research/Fundamental and Molecular Mechanisms of Mutagenesis 377*, 199-209.
67. Enclopedia. http://en.wikipedia.org/wiki/Cytochrome_P450.
68. Shet, M. S., Fisher, C. W., Holmans, P. L., and Estabrook, R. W. (1993) Human Cytochrome P450 3A4: Enzymatic properties of a purified recombinant fusion protein containing NADPH-P450 reductase, *Journal of Pharmacology 90*, 11748-11752.
69. Guengerich, F.P. *Cytochrome P450,* Plenum Press, New York (1995) p. 473–535..
70. Johnston, J. B., Ouellet, H., Podust, L. M., and Ortiz de Montellano, P. R. Structural control of cytochrome P450-catalyzed [omega]-hydroxylation, *Archives of Biochemistry and Biophysics,* doi:10.1016/j.abb.2010.08.011

71. Marijunath, S., Charles, W., Fisher, Holmans, P. L., and EstaBrook, R. Human cytochrome P450 3A4, enzymic properties of purified recombinant fusion protein containing NADPH-P450 reductase, *Product Academy USA 90*, 11748-11752.

72. Hendricks, N. R., Waryo, T. T., Arotiba, O., Jaheed, N., Baker, P. G. L., and Iwuoha, E. I. (2009) Microsomal cytochrome P450-3A4 nanobiosensor for the determination of 2,4 Dichlorophenol-An endocrine disruptor compound, *Electrochemica Acta 54*, 1925-1931.

73. Mattram, C. (1990) Electrode material for electrosynthesis, *Chemical. Review 90*, 837-865.

74. Yu, W. W., Chang, E., Drezek, R., and Colvin, V. L. (2006) Water-soluble quantum dots for biomedical applications, *Biochemical and Biophysical Research Communications 348*, 781–786.

75. Pushpendra, K., and Kedar, S. (2009) Wurtzite ZnSe quantum dots: synthesis, characterization and PL properties, *Journal of Optoelectronic and Biomedical Materials 1*, 59 - 69.

76. Nikesh, V. V., and Mahamuni, S. (2001) Highly photoluminescent ZnSe/ZnS quantum dots, *Semicondiconductor Science and Technology 16*, 687–690.

77. Li, H., Shih, W. Y., and Shih, W.-H. (2007) Non-heavy-metal ZnS quantum dots with bright blue photoluminescence by a one-step aqueous synthesis, *Nanotechnology 18*, 205-604.

78. Jun, Y.-w., Koo, J.-E., and Cheon, J. (2000) One-step synthesis of size tuned zinc selenide quantum dots via a temperature controlled molecular precursor approach, *Chemical Communications. 14*, 1243–1244.

79. Chuan-Liang, F., Xinhua, Z., Martin, S., Anne-Marie, C., Jean-Pierre, M., and Wolfgang, K. (2007) Graded-Bandgap quantum-dot-modified nanotubes: a sensitive biosensor for enhanced detection of DNA hybridization, *Advanced Material. 19*, 1933–1936.

80. Lin, K.-F., Cheng, H.-M., Hsu, H.-C., Lin, L.-J., and Hsieh, W.-F. (2005) Band gap variation of size-controlled ZnO quantum dots synthesized by sol–gel method, *Chemical Physics Letters 409,* 208–211.

81. Pruneanu, S., Veress, E., Marian, I., and Oniciu, L. (1999) Characterization of polyaniline by cyclic voltammetry and UV-Vis absorption spectroscopy, *Journal of Materials Science 34*, 2733-2739.

82. Muñoz, E., Colina, Á., Heras, A., Ruiz, V., Palmero, S., and López-Palacios, J. (2006) Electropolymerization and characterization of polyaniline films using a spectroelectrochemical flow cell, *Analytica Chimica Acta 573-574*, 20-25.

83. Chen, H.-S., Huang, H.-C., and Chen, C.-M. (2004) Quantum dots/conductive polymer nanocomposite, *NSTI-Nanotech 3*, 34-36

84. Goodman, M. D., Xu, J., Wang, J., and Lin, Z. (2009) Semiconductor conjugated polymer-quantum dot nanocomposites at the air/water interface and their photovoltaic performance, *Journal of Chemical Mater 21*, 934–938.

85. Wang, X., JifangWu, Li, F., and Li, H. (2008) Synthesis of water-soluble CdSe quantum dots by ligand exchange with p-sulfonatocalix(n)arene (n = 4, 6) as fluorescent probes for amino acids, *Nanotechnology 19*, 205-501.

86. Mathebe, N. G. R., Morrin, A., and Iwuoha, E. I. (2004) Electrochemistry and scanning electron microscopy of polyaniline/peroxidase-based biosensor, *Talanta 64*, 115-120.

87. Oedzene, M., and Karagozler. (1999) Electrochemical preparation and sensor properties of conducting polyaniline films, *Turkish Journal Chemistry 23*, 89-98.

88. Sharma, A., Sharma, R. (2004) Polymer nanocomposite: structure, synthesis, *NSTI-Nanotech 3*, 834-837.

89. Jamadade, V. S., Dhawale, D. S., and Lokhande, C. D. (2010) Studies on electrosynthesized leucoemeraldine, emeraldine and pernigraniline forms of polyaniline films and their supercapacitive behavior, *Synthetic Metals 160*, 955-960.

90. Goodman, D. M., Jun, X., Jun, W., and Zhiqun, L. (2009) Semiconductor conjugated Polymer-Quantum Dot nanocomposites at the Air/Water Interface and Their Photovoltaic Performance, *Chemical. Matter 21*, 934-938.

91. Bledzki, A. K., Mamun, A. A., Jaszkiewicz, A., and Erdmann, K. (2010) Polypropylene composites with enzyme modified abaca fibre, *Composites Science and Technology 70*, 854-860.

92. Ravindran, S., Chaudhary, S., Colburn, B., Ozkan, M., and Ozkan, C. S. (2003) Covalent coupling of quantum dots to multiwalled carbon nanotubes for electronic device applications, *Nano letters 3*, 447-453.

93. Tomczaka, N., czewski, D. J., Hana, M., and Vancsoa, G. J. (2009) Designer polymer–quantum dot architectures, *Progress in Polymer Science 34*, 393–430.

94. Zanello, P. (2003) *Inorganic Electrochemistry, Theory, Practice and Application*, Royal Society of Chemistry, Chapter 1-4, Cambridge.

95. University of Tennessee, *Introduction to SEM and TEM,* http://web.utk.edu/~prack/MSE%20300/SEM.pdf

96. Goldstein, J., Newbury, D. E., Joy, D. C., Echlin, P., Lyman, C. E., and Lifshin, E.(2003), *Scanning electron microscopy and x-ray microanalysis*, Plenum, New York..

97. Clark, B. J., Frost, T., and Russell, M. A. (1993) U*V spectroscopy: techniques, instrumentation, data handling*, Chapman and Hall, London.

98. Pavia, Lamphan, and Kriz (2009) *Introduction to Spectroscopy* 4th ed, Brooks/Cole Cangage Learning, Carlifonia.

99. Barth, A. (2007) Infrared spectroscopy of proteins, *Biochimica et Biophysica Acta (BBA) - Bioenergetics 1767*, 1073-1101.

100. Terui, N., Fugetsu, B., and Tanaka, S. (2006) Voltammetric Behavior and Determination of 17b-estradiol at multi-wall carbon Nanotube-Nafion modified glassy carbon electrode, *Analytical Sciences 22*, 895-898.

101. Xi, Y., Jianzhang Zhou, Honghui Guo, Chengdong Cai, and Lin, Z. (2005) Enhanced photoluminescence in core-sheath CdS–PANI coaxial nanocables: A charge transfer mechanism, *Chemical Physics Letters 412*, 60-64.

102. Enclopedia. http://en.wikipedia.org/wiki/Hydrogen peroxide.

103. Iwuoha, E. I., Smyth, M. R., and Lyons, M. E. G. (1997) Organic phase enzyme electrodes: kinetics and analytical applications, *Biosensors and Bioelectronics 12*, 53-75.

104. Yu, A.-M., Fukamachi, K., Krausz, K. W., Cheung, C., and Gonzalez, F. J. (2005) Potential role for human cytochrome P450-3A4 in estradiol homeostasis, *Journal of Endocrinology 146*, 2911–2919.